ALMA MATER STUDIORUM
UNIVERSITÀ DI BOLOGNA

DOTTORATO DI RICERCA IN

SCIENZE E TECNOLOGIE DELLA SALUTE

Ciclo 37

Settore Concorsuale: 09/C2 - FISICA TECNICA E INGEGNERIA NUCLEARE

Settore Scientifico Disciplinare: ING-IND/18 - FISICA DEI REATTORI NUCLEARI

DESIGN, DEVELOPMENT, AND FUNCTIONAL CHARACTERIZATION OF COLD PLASMA SYSTEMS TO REDUCE AIRBORNE TRANSMISSION OF HOSPITAL ACQUIRED INFECTIONS & COVID-19

Presentata da: Pasquale Isabelli

Coordinatore Dottorato

Igor Diemberger

Supervisore

Vittorio Colombo

Co-supervisore

Vittorio Sambri

Esame finale anno 2025

To my family for always supporting
and respecting my ideas.

“Murphy's law doesn't mean that something bad will happen.
It means that whatever can happen, will happen.”

Joseph Cooper

Table of contents

Abstract

The recent emergence of novel viral diseases, such as the COVID-19 pandemic caused by SARS-CoV-2, underscored the critical need for improved indoor air quality management. Airborne transmission has been a primary mode of COVID-19 spread, significantly contributing to its profound social and economic impacts. Additionally, airborne transmission is a significant factor in the spread of health acquired infections (HAIs), another problem that has a huge economic impact on the healthcare system and society, considering the substantial number of people involved.

This thesis explores novel strategies to increase the number of systems that improve indoor air quality. In particular, the technology chosen to achieve this goal and provide an alternative or synergistic solution to traditional air treatment methods is cold atmospheric plasma (CAP). CAP comprises various reactive species, including charged particles, radicals, and UV, capable of interacting with biological systems. Specific components within CAP, such as reactive oxygen and nitrogen species (RONS), exhibit strong antimicrobial properties. These RONS act upon microorganisms through various mechanisms, ultimately leading to their inactivation. In this context, this study focuses on designing and developing CAP sources for contrasting the spread of HAIs and SARS-CoV-2 viruses and verifying their antimicrobial efficacy.

This dissertation is divided into three main sections. The first (Chapter 1) presents a systematic review of CAP applications in virology, covering studies from 2000 to 2023. Following Preferred Reporting Items for Systematic Reviews and Meta-Analyses (PRISMA) guidelines, 110 articles were analyzed, with data collected on publication year, last author's country affiliation, CAP source type, targeted applications, and virus species studied. Results demonstrate CAP's effectiveness in inactivating a wide range of viruses, including both enveloped and non-enveloped, DNA and RNA viruses affecting humans, animals, and plants. CAP inactivates viruses through multiple mechanisms, including direct viral particle damage, replication disruption, and modulation of the host immune response.

The second section (Chapter 2) regards the design and characterization of a direct dielectric barrier discharge (DBD) plasma source developed for decontaminating bacterial and viral bioaerosols. Serving as a proof of concept for the project, this device was among the first CAP prototypes to undergo biological testing against the SARS-CoV-2 virus. The results demonstrated its efficacy in deactivating bacterial bioaerosols, achieving a Log Reduction of approximately 3.7, and completely inactivating the SARS-CoV-2 virus.

The third section (Chapters 3, 4, and 5) focuses on scaling up the proof of concept, resulting in the development of two distinct devices for decontaminating airborne pathogens. The first device, called Rotating DBD, is a tabletop unit designed for air treatment in various environments, including hospital rooms, residential spaces, and offices. The second device, called the InDuct plasma source, is intended for installation within ventilation ducts. Both were electrically characterized, and their gas-phase chemistry was evaluated using various diagnostic techniques. Finally, both devices demonstrated high efficacy against bioaerosols containing *Staphylococcus epidermidis*, achieving bacterial inactivation rates of over 99.9%.

Abbreviations

AIDS - Acquired immunodeficiency syndrome

BLAM - Blaustein Atomizer

CAP - Cold atmospheric plasma

CDC - Centers for Disease Control and Prevention

COVID-19 - Coronavirus disease 19

DBD - Dielectric Barrier Discharge

DBGD - Dielectric barrier grating discharge

DC - Direct current

DPBS - Dulbecco's Phosphate Buffered Saline

ECDC - European Centre for Disease Prevention and Control

FCV- Feline calicivirus

FDA - Food and Drug Administration

GDP - Gross domestic product

HAIs - Health acquired infections

HAV - Hepatitis A virus

HBV - Hepatitis B virus

HEPA - High-Efficiency Particulate Air

HIV - human immunodeficiency virus

HIV-1 Human Immunodeficiency Virus 1

HSV-1 - Herpes simplex virus type 1

HuNoV - Human Norovirus

HV - High voltage

HVAC - Heating, Ventilation, and Air Conditioning

IAQ - Indoor air quality

ICTV - International committee on taxonomy of viruses

IFM - International Monetary Fund

MBMS – Molecular beam mass spectrometry

MNV - Murine norovirus

MS - Mass spectrometry

NIOSH - National Institute for Occupational Safety and Health

OAS - Optical absorption spectroscopy

OES - Optical emission spectroscopy

OSHA - Occupational Safety and Health Administration

PMMA - Polymethylmethacrylate

PMMoV - Pepper mild mottle virus

PRRV - Porcine reproductive and respiratory virus

PTL - Plasma treated liquid

PVY - Potato virus Y

RH - Relative humidity

RDBD – Rotating dielectric barrier discharge

RNS - Reactive nitrogen species

RONS - Reactive oxygen and nitrogen species

ROS - Reactive oxygen species

RT-PCR - Reverse transcription polymerase chain reaction

SARS-CoV-2 - Severe acute respiratory syndrome coronavirus 2

SDBD - Surface Dielectric Barrier Discharge

SEM - Scanning Electron Microscope

TSA - Tryptone soy agar

UADL - Upper antimicrobial detection limit

UL - Underwriters Laboratories

UV - Ultraviolet

WHO - World Health Organization

Chapter 1

A novel approach for virus treatment: a systematic review of cold atmospheric plasma applications in virology

1.1 Introduction

The rapid and extensive global spread of the SARS-CoV-2 (severe acute respiratory syndrome coronavirus 2) virus in 2019 had profound consequences, causing a significant disruption lasting over two years. The ramifications of this event were considerable, affecting social, human, and economic spheres, and exerting a notable impact on the healthcare system and the global economy. The extent of the crisis has led to a surge in global interest in innovative and alternative strategies to fight the transmission of viruses. This chapter provides an overview of the diverse modes of viral transmission and the main stages of the viral life cycle, and it also introduces cold atmospheric plasma (CAP) as a promising tool for fighting viruses. CAP is a specific state of plasma that is typically generated at or near room temperature and at atmospheric pressure [1]. CAP comprises a reactive mix of free electrons, atoms, and molecules in neutral and excited states, including reactive oxygen and nitrogen species (RONS), UV radiations, and electric fields, which have several impactful effects on biological matter [1],[2]. All these components and, above all, RONS have antimicrobial properties [3], and they can effectively inactivate bacteria, viruses, fungi, and spores.

The properties of CAPs justify the significant number of studies that focus on utilizing CAPs for the inactivation of a range of pathogens, including viruses. The interaction between CAPs and viruses predating the emergence of SARS-CoV-2 has also been the subject of investigation [1],[2],[4]. The earliest article on the use of CAPs against viruses dates back to 2007. However, following the outbreak of the SARS-CoV-2 pandemic, there has been a notable surge in research works focusing on utilizing CAPs for viral inactivation. This chapter offers an overview of viral infections and their impact on human health, their transmission routes, and the methods currently employed to control the spread of viruses. Furthermore, this chapter assesses CAP as an alternative approach for viral inactivation and treatment of infections, presenting a systematic review of current knowledge on CAP application in virology. The discussion will extend to the fundamental properties of CAP, including its generation methods and current utilization in the state-of-the-art for contrasting the spread of viruses. Finally, the primary mechanisms underlying the interaction between CAP and viruses will be explored.

1.1.1 Fundamentals on viruses

Viruses are the most ubiquitous entities in the biosphere, and every living organism encounters millions of viral particles daily. A virus is a tiny infectious particle that depends on a host cell for replication. Its structure consists of genetic material, DNA or RNA, enclosed in

a proteinaceous capsid. While some viruses possess an additional lipid envelope, a defining characteristic of all viruses is their obligate intracellular parasitism [5],[6]. Viruses are infectious agents that exploit the host cell machinery to form viral replication complexes, reprogramming the cell to prioritize the production of viral progeny. The sole purpose of this process is to generate and spread new viral particles.

Viruses share certain basic characteristics, despite their considerable diversity. In general, the viral life cycle (Figure 1.1) can be divided into three stages: entry, genome replication, and exit [7]. The ability of the virus to selectively infect specific cell types is the initial entry stage. Specific receptors on the surface of the target (host) cells determine this specificity. Each cell has a unique pattern of protein receptors on its surface, and these receptors are used by the virus to target specific cells for infection. The entry process involves: - attachment, where the virus encounters and attaches to the cell surface; - penetration, where the virus enters the cytoplasm; - uncoating, where the virus sheds its capsid. Once uncoated, the naked viral genome is used for gene expression and replication. This is followed by the accumulation of viral proteins and genomic material, which combine to form progeny viral particles, which are then released into the extracellular space. The exit phase of the viral life cycle consists of this final step of virion assembly and release from the infected cell [7].

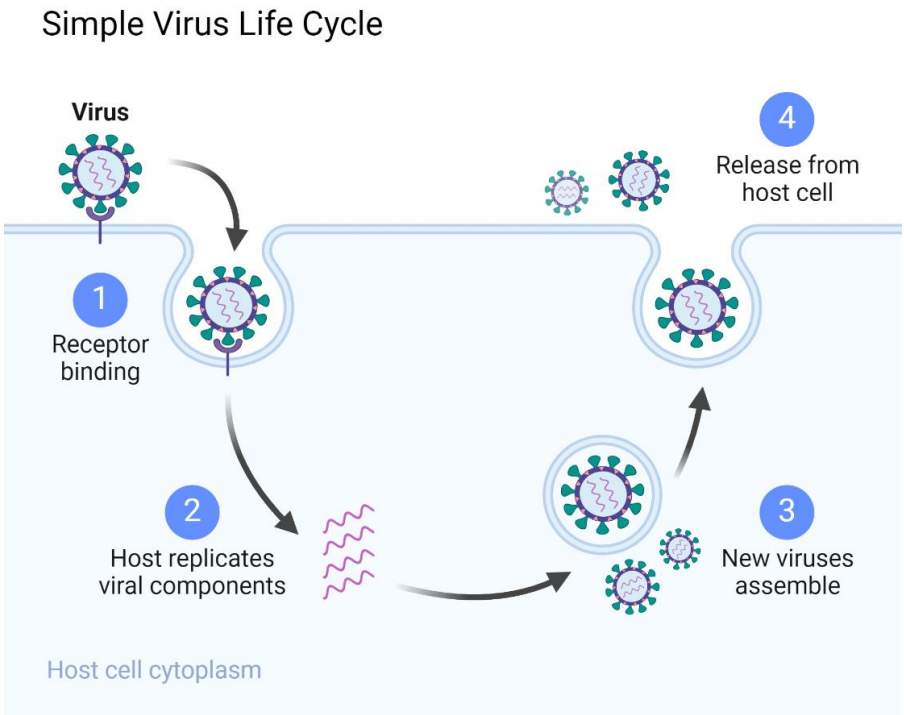

Figure 1.1 *– A simple virus life cycle divided into three stages: entry (attachment, penetration, uncoating), genome replication (gene expression and replication), and exit (virion assembly and release). Figure created using BioRender, adapted from [7]. (https://www. biorender.com/).*

1.1.2 Virus transmission routes and containment strategies

Evidence of viral infections can be traced back to some of the earliest documented human activities, although viruses have only been recognized as distinct biological entities for just over a century. Furthermore, long before viruses were formally identified, strategies to control viral diseases were employed. It was not until the 20th century that significant efforts were made to fully understand and control these ubiquitous pathogens [5]. Throughout history, there are many examples of how viral diseases have caused widespread devastation, claimed millions of lives, and left an indelible mark on human civilization. For example, influenza viruses have caused several pandemics. These include the Spanish flu (1918-1919) [8], the Asian flu (1957-1958)[9], and the H1N1 influenza pandemic (2009-2010) [10]. The human immunodeficiency virus (HIV) and acquired immunodeficiency syndrome (AIDS) have had a profound impact on global health since their discovery in the 1980s [11]. Another notable example is the Ebola virus disease, which caused a severe and often fatal outbreak in West Africa from 2014 to 2016 [12]. Most recently, the spread of the SARS-CoV-2 virus affected the world (2020 – 2022), causing millions of deaths and significant disruption to society, healthcare, and the global economy.

Viruses can be transmitted through various modes, such as direct and indirect means. Direct transmission (direct physical contact, respiratory droplets) refers to the transferer of the virus by direct contact or droplet spread. Viruses, for example, herpes simplex virus or human papillomavirus, are transmitted through direct physical contact (e.g., skin-to-skin contact, sexual intercourse, or kissing) [13]. In respiratory transmission, infectious agents (e.g., influenza and SARS-CoV-2) are spread from an infected person through coughing, sneezing, or via saliva and immediately enter the respiratory tract of another person.

Indirect transmission typically involves an intermediary between hosts. Unlike droplet transmission, which occurs directly from one person to another, airborne transmission of viruses is carried by aerosolized particles that remain suspended in the air for long periods and can travel long distances. This mode of transmission does not require close contact with an infected person and can be considered along the indirect modes. Other vehicles, such as food, water, or inanimate objects, can indirectly spread virions. For example, respiratory droplets containing potentially infectious microorganisms can contaminate inanimate objects or surfaces, transforming them into fomites (inanimate object surfaces that can spread infectious agents), which can serve as vehicles for transmission [14]. These are some of the primary modes of virus transmission; however, there are various alternative routes, such as fecal-oral or bloodborne

transmission. It is important to highlight that viruses employ different transmission mechanisms, some of which may co-occur [5],[13].

Viral diseases exert a substantial influence on the global economy and society. To effectively reduce viral transmission, emphasis must be placed on preventing and managing viral infections. Management typically involves administering antiviral drugs targeting the viruses themselves or the host cell factors [15] or employing medications that reduce symptoms while the immune system fights the virus. However, the emergence of antiviral resistance, a consequence of viral evolution, has decreased the efficacy of antiviral treatments. Mitigating antiviral resistance presents significant challenges in the therapeutic approach to viral infections. For this reason, preventing viral infections has become increasingly important.

Several prevention strategies include vaccination, immune system care, and good hygiene. Furthermore, individuals are consistently exposed to viruses, as highlighted previously, as these pathogens can be transmitted through various means. Consequently, it becomes imperative to implement preventive measures to inhibit the transmission and subsequent occurrence of viral infections.

A multifaceted approach utilizing disinfectants, chemical agents, and physical methods like filtration and ultraviolet (UV) radiation has been, and continues to be, a cornerstone in combating virus transmission. For instance, filtration plays a critical role in managing air quality within Heating, Ventilation, and Air Conditioning (HVAC) systems. These filters function by mechanically trapping microorganisms but not inactivating them[16]. While filtration offers a valuable tool, it does present certain limitations. The accumulation of captured microorganisms on the filter mesh can create a favorable environment for bacterial growth, necessitating frequent maintenance or replacement. Filters also increase the pressure drop within HVAC ducts, raising energy consumption. This requires the use of oversized fans to maintain airflow. Ultraviolet-C (UV-C) radiation represents another approach to virus mitigation. However, its effectiveness depends on sufficient pathogen exposure times, often incompatible with typical airflow rates within HVAC systems. Furthermore, UV-C operates on a line-of-sight principle, limiting its efficacy in complex duct networks. Finally, exposure to UV-C radiation can potentially induce skin irritation (erythema) and other adverse effects [16],[17].

The high number of health acquired infections (HAIs) that occur each year [18] and the emergence of new diseases that affect large populations, such as COVID-19 (as reported by the World Health Organization - WHO), highlights the limitations of current technologies. These outbreaks reveal gaps in prevention, demonstrating that existing tools are often insufficient to

fully contain or manage novel, rapidly spreading pathogens. The global response to these crises has led to the exploration of innovative containment strategies, including CAP technology.

1.1.3 Fundamentals on CAP

Plasma is a quasi-neutral ionized gas composed of electrons, positive and negative ions, photons, and reactive species, also referred to as the fourth state of matter, and more than 99% of the visible Universe is in the plasma state [1],[19]. The term "quasi-neutral" denotes a state of equilibrium between electrons and ions. In contrast, "ionized" refers to the existence of at least one electron that is not bound to an atom or molecule, which results in the conversion of atoms or molecules into ions with a positive charge. Free electric charges (electrons and ions) in plasma enable it to conduct electricity, interact internally with other particles, and respond strongly to magnetic fields [1],[20]. Additionally, plasma discharges can be artificially generated (laboratory-generated plasmas) by applying a sufficiently strong electric field to a neutral gas. This electric field induces what is known as electrical breakdown, a process whereby a non-conductive material, such as a gas, is transformed into a conductor [1],[21]. As in any gas, the temperature of the plasma is determined by the average energies of its particles, both neutral and charged, and their degrees of freedom, including translational, rotational, vibrational, and those related to electronic excitation. Consequently, plasmas are characterized as multi-component systems with multiple temperatures [1]. The nature of laboratory-generated plasmas is defined by the temperature difference between electrons (T_e) and heavy particles (T_h), which is strictly determined by the energy exchanges between these species. Indeed, energy is initially absorbed by electrons (the lightest species in the system) from the electric field. Subsequently, due to the significant mass difference between electrons and heavy particles, electrons lose only a small portion of their energy in collisions, leading to an electron temperature that is initially higher than that of the heavier species. Repeated collisions can equilibrate this temperature difference ($T_e \approx T_h$) via Joule heating. These plasmas are classified as equilibrium plasmas (or thermal plasmas) and are characterized by macroscopic temperatures typically higher than 1000 K. If equilibrium conditions cannot be reached for an insufficient time or quantity of energy, or if a cooling mechanism prevents the heating of the entire gas, the temperature of the electrons will typically exceed that of the heavy particles ($T_e >> T_h$), resulting in a non-equilibrium plasma (or a non-thermal plasma). However, at atmospheric pressure, because the density of electrons in the plasma discharge is very low compared to the density of heavy particles, the macroscopic temperature is almost equal to T_h. When the T_h is close to

room temperature and the pressure is maintained at atmospheric levels, these non-equilibrium plasmas are called CAPs [1]. This thesis will exclusively discuss and investigate cold plasmas operating at atmospheric pressure. CAP comprises a variety of reactive species, including charged particles, radicals, and UV, which are capable of interacting with biological systems. The specific components of CAP, including RONS, have been observed to exhibit notable antimicrobial properties. These reactive mix interact with microorganisms through various mechanisms, ultimately resulting in their inactivation [1],[2].

1.1.4 Factor influencing the interaction between CAP and viruses

Research conducted in recent years has shown promising results, demonstrating the efficacy of CAP in inactivating or reducing the viral load of a broad spectrum of viruses, including those affecting humans, animals, and plants [19],[22],[23]. However, each study in this field can be considered unique due to the use of different plasma sources (often lab-custom-made) and operating conditions (e.g. voltage, current, power), environmental conditions (such as temperature and relative humidity), inherent properties of the matrix (e.g. surfaces, liquids, bioaerosols, etc.) and the specific properties of the virus being studied.

1.1.4.1 Plasma sources

CAP treatment efficacy is demonstrably influenced by many factors, including the type of plasma source employed and the specific process parameters utilized. CAP can be generated through plasma sources based on different architectures, such as dielectric barrier discharge (DBD), surface dielectric barrier discharge (SDBD), plasma jet, or corona discharge. Additionally, parameters like average discharge power, gas composition, and treatment time can be manipulated to achieve desired outcomes [22],[23].

DBD configurations are characterized by the presence of at least one insulating material as a dielectric barrier, which prevents the transition to a thermal plasma discharge (arc-like discharge), stopping current and spark formation [1],[24],[25]. Typical dielectric materials employed in DBD plasma sources are glass, quartz, ceramics, and mica [24]. The space between the dielectric and the electrode, or between two dielectrics, is called the gas gap [24]. When one or both electrodes are powered, and the applied voltage is higher than the gas breakdown voltage, a discharge is initiated [26]. As the discharge begins, charged particles accumulate on the dielectric surface, creating a localized voltage drop. This voltage opposes the externally applied voltage, reducing the discharge current and extinguishing the discharge. In the next half

cycle of the applied power, the voltage rises again, reigniting the discharge. This cyclic process is repeated for each period of the applied voltage waveform [24]. Due to the capacitive nature of the discharge setup, an alternating or pulsed high voltage is necessary to sustain the plasma. Indeed, the dielectric material between electrodes works like a capacitor, which can store charge. A direct current (DC) voltage cannot sustain the plasma because it can not create the required oscillations in the electric field [26]. An alternating or pulsed voltage, on the other hand, continuously changes polarity. Typically, the gas gap ranges from 0.1 to 10 mm, allowing plasma to operate efficiently at atmospheric pressure with moderately high voltage levels (1-100 kV_{rms}) and a frequency of 500 Hz to 500 kHz [1],[24],[26]. At atmospheric pressure, DBDs are not uniform but filamentary. They are composed of a large number of high intensity streamers (micro-discharges) that connect electrodes, often moving between and interacting with each other [1],[27]. These current channels are very fast (1-10 ns), and the filament radius is about 100 μm [25].

Based on the general working principles, different arrangements can be realized. It is possible to identify two main categories: volume DBDs and surface DBDs.

In the volume DBDs, one (Figure 1.2-a) or both electrodes are covered by a dielectric material, and the plasma discharge is ignited in the gas gap, also known as the interelectrode gap (Figure 1.2-b).

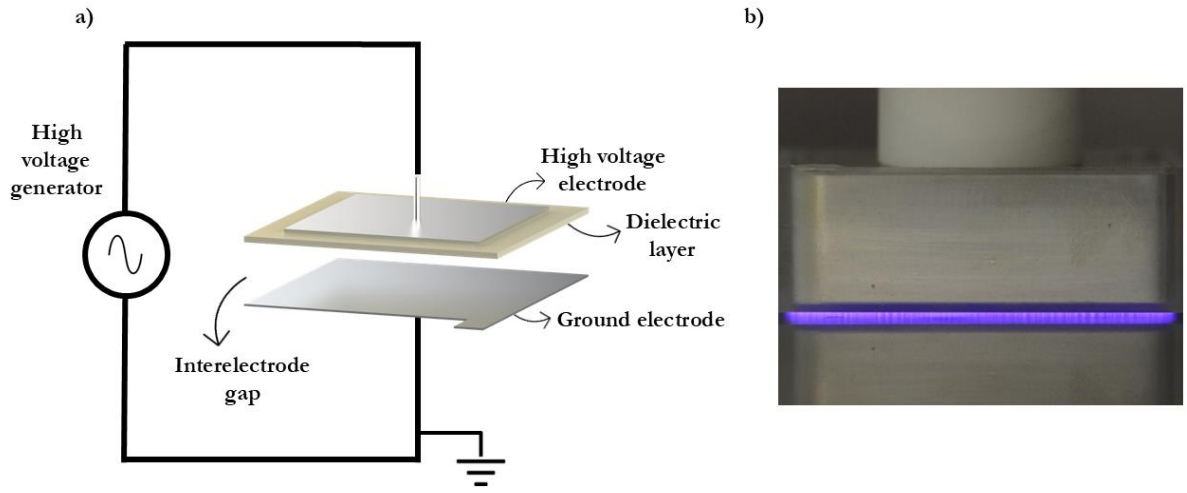

Figure 1.2 – a) *Schematic of a typical DBD with a single electrode covered by a dielectric layer;* ***b)*** *picture of a DBD. The DBD picture was acquired in the Laboratories of the Research Group for Industrial Applications of Plasmas (Alma Mater Studiorum – Università di Bologna, Italy).*

In surface DBDs (Figure 1.3-a), both the electrodes are in direct contact with the dielectric material, and plasma is generated on the edge of the ground electrode, which is often a mesh (Figure 1.3-b), in order to maximize the plasma generation surface [24],[26]. In this

configuration, a part of the plasma reactive agents, such as electrons, ions, and the electromagnetic field, remains localized close to the ground electrode, limiting their direct interaction with the treated substrates. As a result, the primary agents contributing to the treatment are long-lived reactive species like ozone.

The versatility of DBD configurations in terms of geometric design and operating condition settings is wide. Discharge conditions optimized in small-scale laboratory experiments can often be effectively scaled up for large industrial installations. In addition, efficient and cost-effective power supplies are readily available to support operations at high power levels.

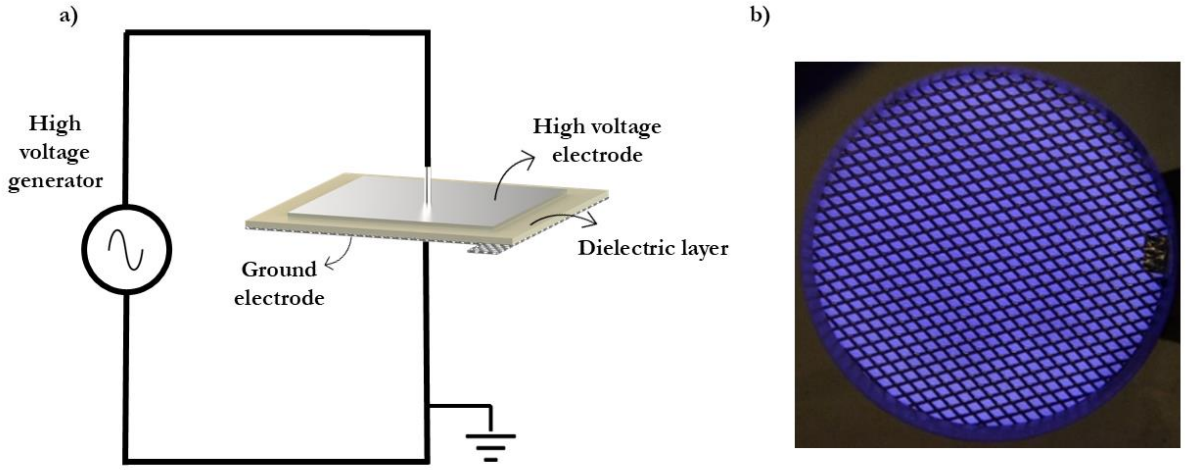

Figure 1.3 – a) *Schematic of a typical surface DBD;* ***b)*** *picture of a surface DBD with grounded mesh electrode. The surface DBD picture was acquired in the Laboratories of the Research Group for Industrial Applications of Plasmas (Alma Mater Studiorum – Università di Bologna, Italy).*

Corona plasma sources necessitate a high-voltage (HV) electrode, such as a pin (Figure 1.4-a), thin wire, or a sharp edge, to generate an electric field close to the electrode that is significantly stronger than the field in the surrounding gas and ignite the discharge [1]. The corona discharges are always non-uniform (Figure 1.4-b).

The most prevalent configuration for corona discharge employs a pin-to-plane arrangement, as illustrated in Figure 1.4-a. This configuration's simplicity and capacity to initiate discharge at atmospheric pressure contribute to its widespread adoption.

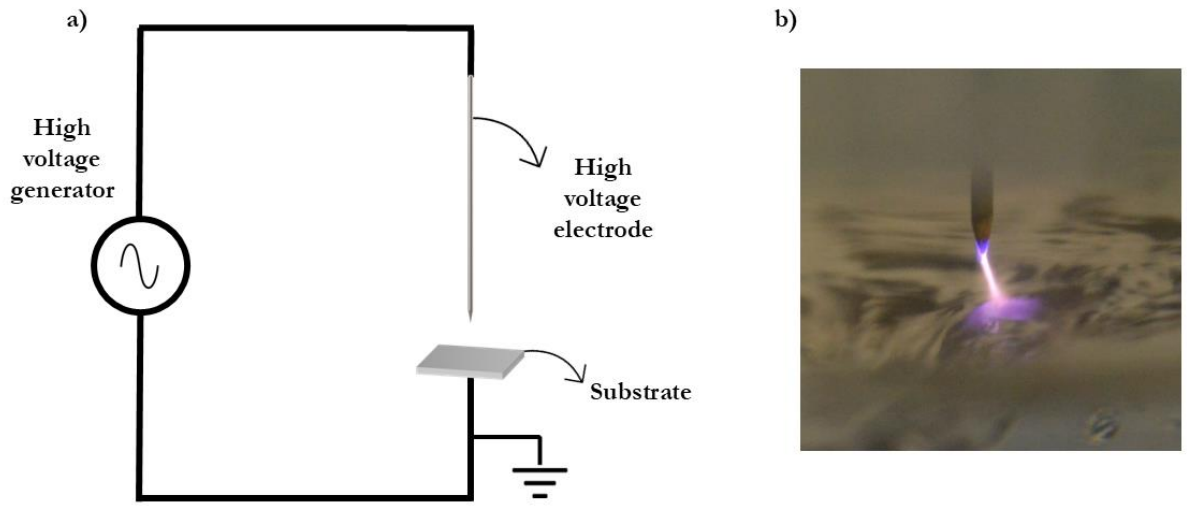

Figure 1.4 – a) *Schematic of a typical pin-to-plane corona plasma source;* ***b)*** *picture of a corona discharge on water. The picture was acquired in the Laboratories of the Research Group for Industrial Applications of Plasmas (Alma Mater Studiorum – Università di Bologna, Italy).*

Plasma jets are a distinct category of CAP sources known for producing a stream of chemically reactive species. There are many configurations of plasma jet sources, but they all have in common that a gas discharge is operated in an unsealed electrode assembly and is projected outside the electrode assembly into the environment. The expansion of the plasma is often due to the high flow rate of a carrier or working gas (noble gases such as helium and argon) [28]. Due to their ability to produce plasmas that are non-constrained or confined by electrode limitation, these plasma sources have gained significant attention. Many different plasma jet configurations exist, and one of the possible classifications is based on the electrode arrangement. Among the main configurations of plasma jets, the DBD jet (Figure 1.5) and the corona jet (Figure 1.6) are notable examples [2]. Figure 1.5-a shows a possible DBD jet architecture consisting of a dielectric tube with a centered HV pin electrode and a ground metal ring electrode on the outside of the tube. A cold plasma jet is created in the surrounding air when a working gas (helium, argon) flows through the dielectric tube, and a kHz HV generator is switched on (Figure 1.5-b). Typically, the plasma jets only employ a power of several watts, so the power density delivered to the plasma remains low, and the gas temperature is close to room temperature [29]. Moreover, the length of the plasma plume can reach several centimeters [29][30]. Finally, whether the substrate to be treated is far away or close to the nozzle, there is no risk of arcing due to the presence of the dielectric. These features make these plasma sources easy and practical.

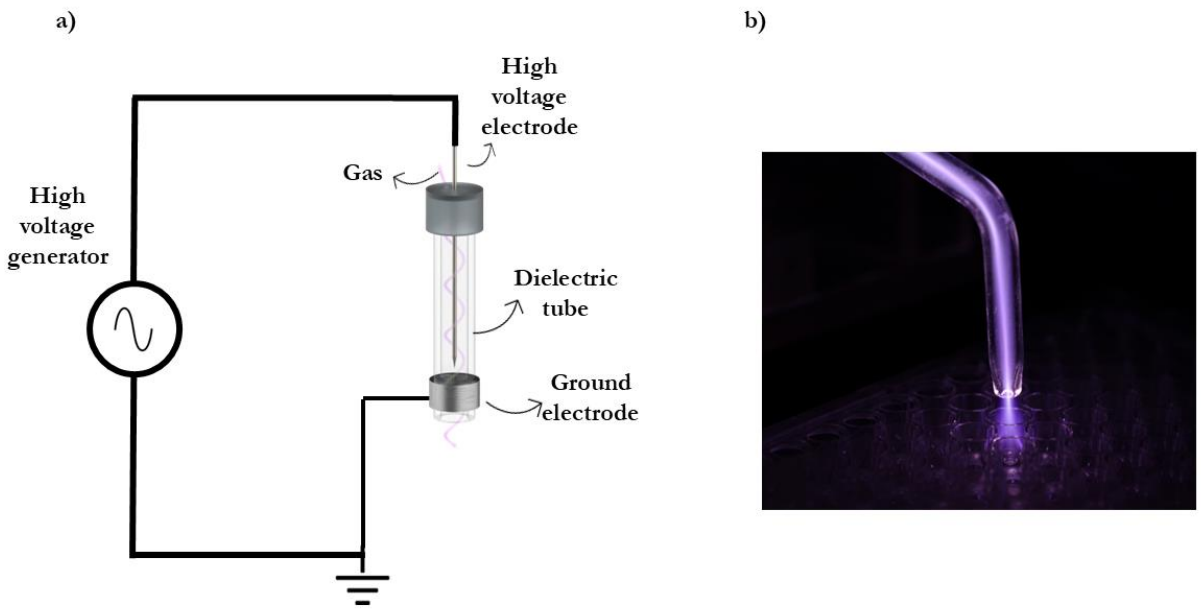

Figure 1.5 – a) *Schematic of a typical DBD plasma jet;* ***b)*** *picture of a plasma plume generated by a DBD plasma jet. The picture was acquired in the Laboratories of the Research Group for Industrial Applications of Plasmas (Alma Mater Studiorum – Università di Bologna, Italy).*

Figure 1.6-a shows a typical configuration of a corona jet. Compared to the previous configuration, there is no ground electrode ring outside the dielectric tube. In this case, the tube has the only role of guiding the gas flow, and so, in this configuration, there is a risk of arcing, making them unsuitable for biomedical applications.

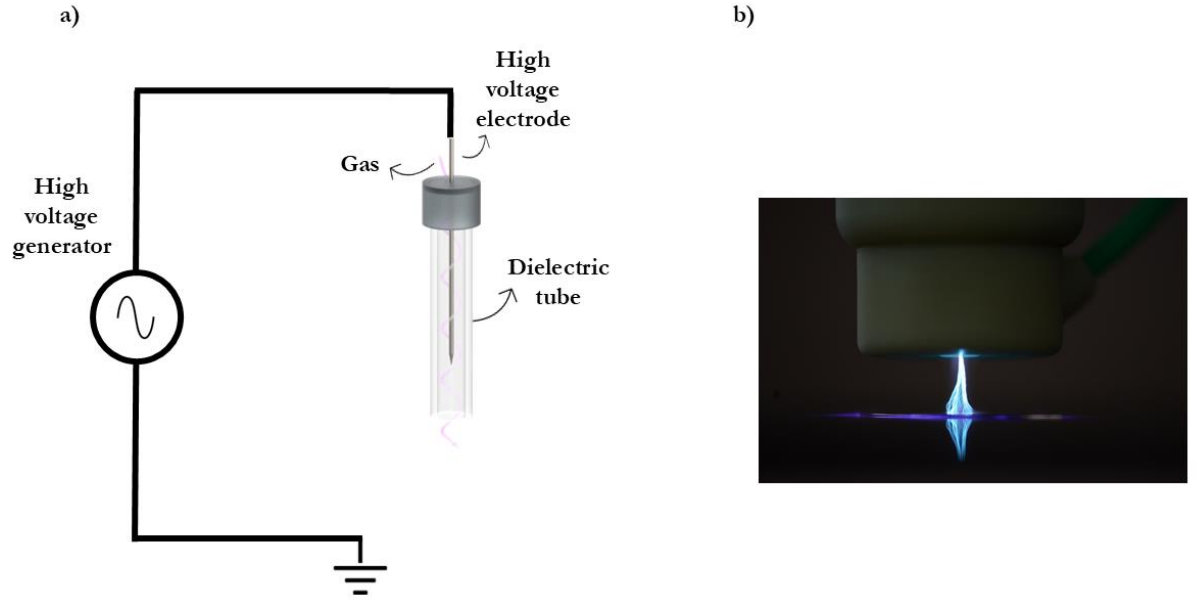

Figure 1.6 – a) *Schematic of a typical corona plasma jet;* ***b)*** *picture of a plasma plume generated by a corona plasma jet. The picture was acquired in the Laboratories of the Research Group for Industrial Applications of Plasmas (Alma Mater Studiorum – Università di Bologna, Italy).*

1.1.4.2 Operating conditions

Plasma operating conditions, such as voltage, frequency, and current, can influence the interaction between CAP and microorganisms, such as viruses and bacteria. Indeed, all these parameters influence the power dissipated in the plasma discharge. For example, it is known that the power of plasma is proportional to the voltage applied in the discharge zone. Basically, changing the input power means altering the composition of the plasma, and consequently, it influences the interaction between CAP and microorganisms as viruses[1],[23]. For example, with high power, the production of reactive species such as singlet oxygen, hydroxyl radicals, and nitrogen oxides (all species relevant to inactivation mechanisms, as will be shown in the results of the systematic review) can increase.

1.1.4.3 Environmental conditions

Environmental conditions are an important factor influencing plasma physics and chemistry. In particular, the formation of reactive species is particularly influenced by relative humidity (RH). Indeed, the production of reactive oxygen species (ROS) such as hydroxyl radicals, hydrogen peroxide, and ozone is affected by the presence of water vapor in the air. Furthermore, by reducing the surface resistance of the dielectric material (in the case of DBD plasma sources) through the adsorption of water molecules, water vapor can reduce the number of micro-discharges [23],[31]. Finally, high humidity in the discharge can lead to loss of electron energy due to electron-molecule collisions, and so this quenching effect can weaken the plasma [32].

Environmental temperature affects CAP, potentially altering plasma chemistry and efficiency in applications such as pollution control and sterilization by influencing electron collisions and species production [33],[34].

1.1.4.4 Treatment type

CAP can interact with microorganisms in different ways. It is also possible to distinguish three primary methods.

Direct treatment is when the contaminated matrix or microorganisms are directly exposed to plasma discharge, which includes all the antimicrobial components, such as long- and short-lived reactive species.

Conversely, indirect or remote treatment involves exposing the target or microorganisms to the post-discharge zone with a high concentration of long-lived reactive species. In this kind of treatment, the charged particles recombine before reaching the sample, so they do not play a significant role in microbial inactivation. In addition, short-lived reactive species are rarely able to reach the target.

An alternative strategy involves plasma-treated liquids (PTLs) as a medium for the interaction with microorganisms. In this type of treatment, different types of liquid can be treated using CAP in order to change the properties of the liquid itself, mainly by enriching it with reactive species. After plasma treatment, PTLs are used to interact with microorganisms.

1.1.4.5 Matrices typology

The effect of CAP treatments also extends to specific properties of the treated matrices, such as surfaces, liquids, and bioaerosols (tiny airborne particles that originate from living things containing microorganisms), which also play a significant role.

Different properties of the substrate surface, such as surface roughness, porosity, wettability, electrical conductivity, and chemical composition, can influence the interaction between CAP and microorganisms [23]. Rough or porous substrates can realize microenvironments that shield microorganisms from direct plasma exposure [35],[36]. The presence of the liquids on the substrate can increase the concentration of some species, such as hydrogen peroxide and ozone. Moreover, the chemical composition can affect how RONS interact with the surface [37]. Some materials can absorb some species like ozone. Conductive surfaces can impact the electric field used to ignite plasma discharge.

In the case of liquids or bioaerosols, the interaction with CAP is influenced by the liquid nature and/or the size and distribution of droplets forming bioaerosol. When CAP interacts with liquids, many reactive species generated in the gas phase can dissolve into the liquid [38]. Some liquids, especially those containing organic matter, can neutralize RONS reacting with them. Moreover, in the case of bioaerosols, the size of the particles is a significant factor in the interaction with CAP [39]. Smaller droplets have a larger surface-area-to-volume ratio, which allows RONS to interact more effectively with microorganisms contained in bioaerosol [40]. The distribution of the droplets should also be considered because some particles may be less exposed to RONS if the bioaerosols are unevenly distributed or clustered.

1.1.4.6 Viruses

The impact of different viruses on the interaction with CAP can differ depending on several factors related to the virus itself. The key characteristics of viruses that influence their response to CAPs are the same as those used in general viral classification. These include the type of nucleic acid in the virion (DNA or RNA), the presence or absence of a lipid envelope, as well as the size of the virion and its capsid [5].

The classification of viruses has been a subject of debate and controversy up to the present day. Several approaches to the classification of viruses have been proposed, which is a reflection of the complexity and diversity of these infectious agents [5]. The traditional system is based on “Order”, “Family”, “Genus” and “Species”. This system is adopted by the International Committee on Taxonomy of Viruses (ICTV) and the general criteria is viruses should be categorized according to their common characteristics and not according to the organisms or cells they infect or the diseases they cause. A second principle was to focus on the nucleic acid genome as the primary criterion for classifying. The standard method for assigning viruses to a particular family and ordering the various members in the family is the evaluation of the relationships between viruses through the analysis of the similarity of nucleic acid and how viral proteins are obtained from this [5]. Moreover, since the viral genome contains the complete instructions for virus replication, molecular virologists have long regarded it as the most important factor in virus classification. The Baltimore classification was added to the classical system. This classification places seven classes based on genome type, replication strategy, and mode of viral RNA synthesis [5].

1.2 Materials and Methods

The systematic research was conducted in adherence to the guidelines outlined by the Preferred Reporting Items for Systematic Reviews and Meta-Analyses (PRISMA) [41].

1.2.1 Documents identification

The research for pertinent literature was conducted using two prominent electronic databases, Scopus and Web Of Science. The research on the two databases was conducted using keywords related to the CAPs world, such as "cold atmospheric plasma" or "non-equilibrium plasma," in conjunction with keywords associated with the viruses, such as "virus" or "surrogate".

1.2.2 Inclusion criteria

The systematic review covered all original studies and reviews on the interaction between CAPs and viruses published in English since 1 January 2000.

1.2.3 Exclusion criteria

All publications made after December 31, 2023, were not considered. The review did not include the following: case reports, editorials, letters to the editor, short/rapid reports, highlights, symposia, abstracts, and preprints.

1.2.4 Selection criteria and data extraction

The obtained research results were screened based on evaluating titles and abstracts. Records that appeared potentially relevant were retrieved in full-text format for a comprehensive assessment, thereby determining their definitive inclusion in this review. Reviews were taken separately. Data on the year of publication, the last author's country affiliation, the type of CAP source, and virus species were all extracted. The analysis of the identified articles revealed a distribution across six pre-defined categories:

- **Fundamentals**: basic studies on the interaction between plasma and viruses.
- **Surfaces**: use of CAPs to decontaminate surfaces from viruses.
- **Liquids**: use of CAPs to decontaminate liquids from viruses.
- **PTLs:** use plasma-treated liquids as an intermediate medium to inactivate viruses.
- **Bioaerosols**: use of plasma to inactivate virus-containing bioaerosols.
- **Reviews**: an overview of current thinking on the topic.

1.3 Results

1.3.1 Number and geographic distribution of articles on CAP and viruses

A total number of 1543 documents were identified. Among these publications, 526 were duplicated studies and excluded. The remaining 1017 publications were scrutinized and screened based on study selection criteria. A final total of 110 publications was included: 80 original articles (72.7%) and 30 reviews (27.3%) (Figure 1.7). A comprehensive list of all identified documents is provided as a supplementary table in Appendix 1. Since 2007, the number of documents has grown exponentially (Figure 1.8). Moreover, a rapid increase is evident from 2019; this observation is logically supported by the COVID-19 pandemic that

broke out in 2019, which led to a strong global scientific effort to develop mitigation measures for the spread of SARS-CoV-2. As a result, there has been a significant increase in studies in the cold plasma community that focused on employing CAPs for viral inactivation. The global distribution of research (Figure 1.9) reveals the United States as the leading contributor, accounting for 24.5 % of the publications. China and South Korea follow at 11.8% and 9.1%, respectively, and Germany and Japan are grouped at approximately 7.3% each. Italy closes the group of top contributors with 5.5% of the publications. All remaining countries contributed less than 5 % to the literature.

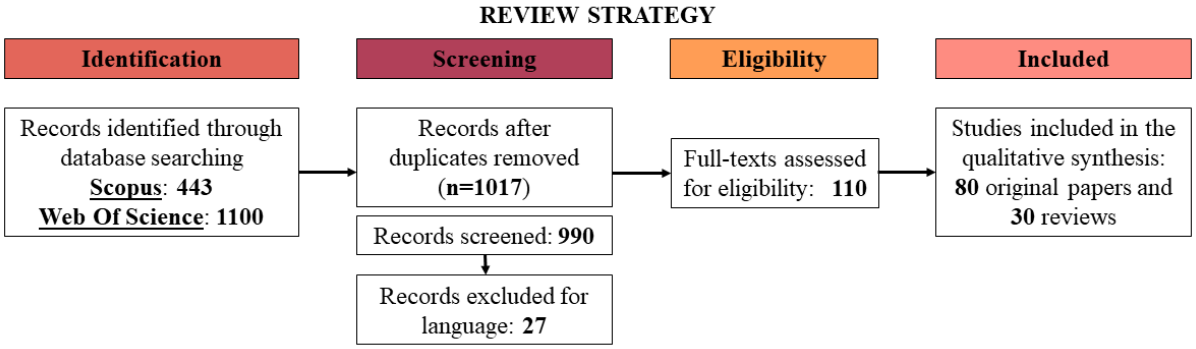

Figure 1.7 *– Flow diagram of studies screened, assessed for eligibility, and included in the systematic review.*

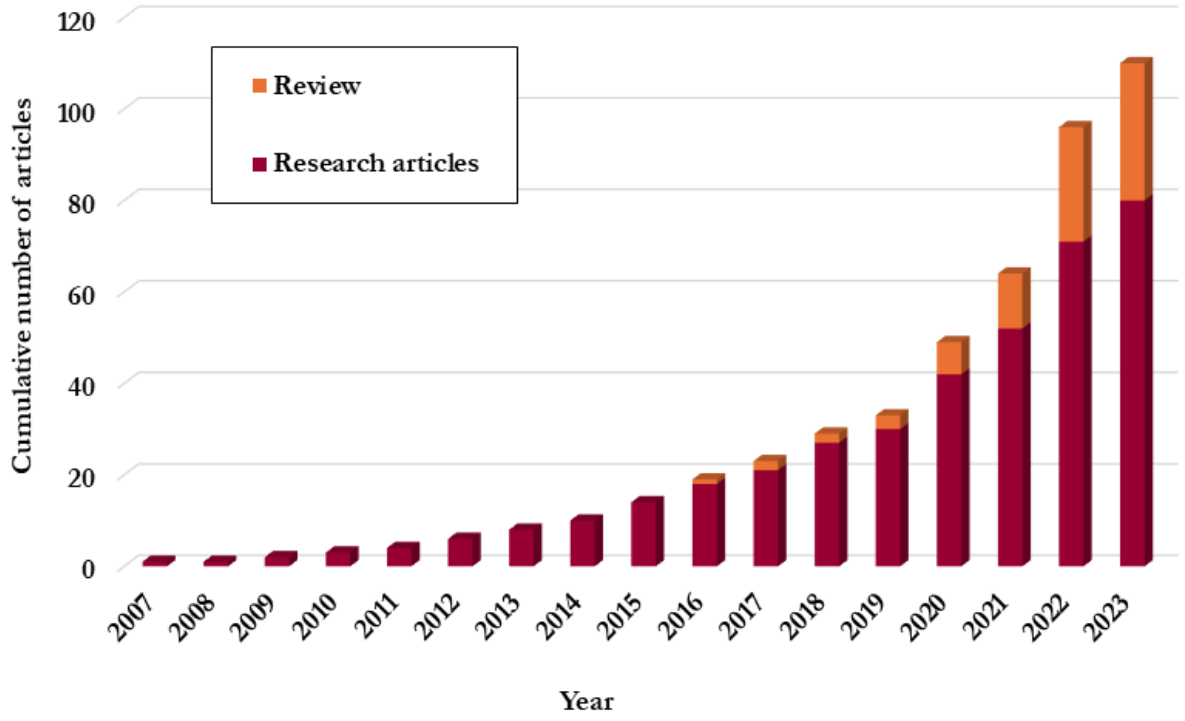

Figure 1.8 *– Cumulative published articles on CAP technology for virus treatments.*

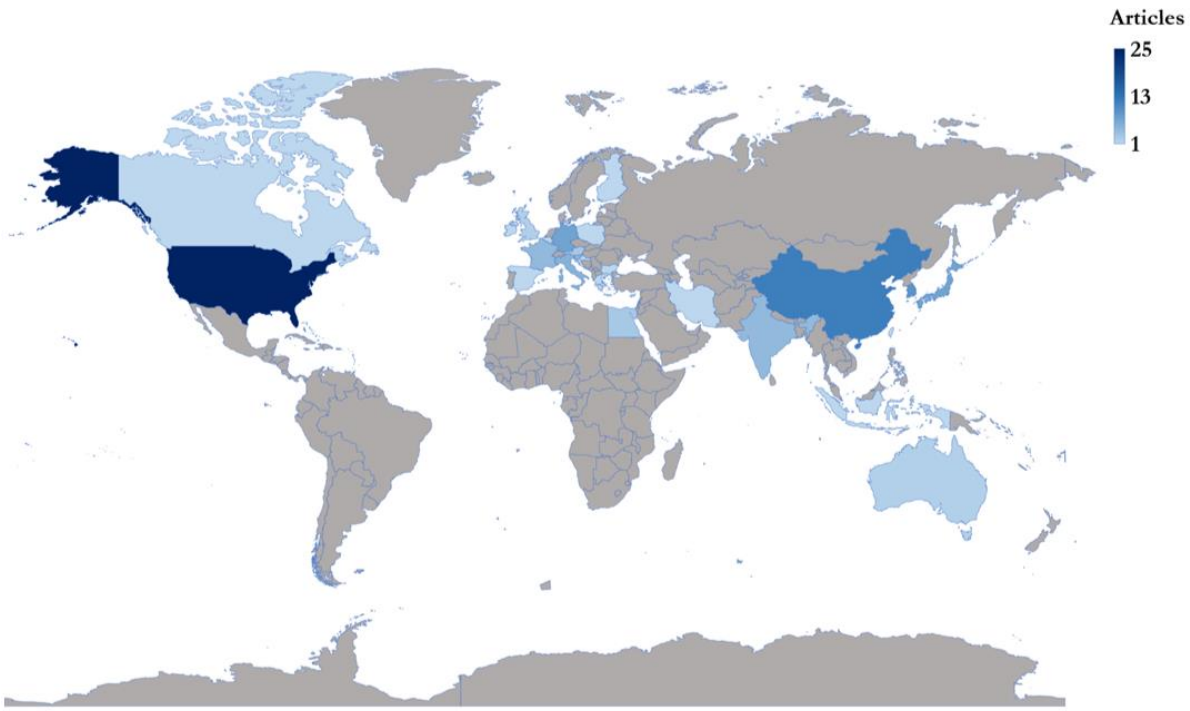

Figure 1.9 *– Geographical distribution of identified articles.*

1.3.2 Quantitative analysis of articles distribution across the six pre-defined categories

As illustrated in Figures 1.10 and 1.11, a substantial portion of the studies (28.2 %) are under the category of fundamental research. These investigations aim to elucidate the fundamental mechanisms governing the interaction between CAPs and viruses. Excluding review articles (27.3 %), the second most prevalent category focuses on the decontamination of surfaces from viruses, with 21.8 % of the publications. A notably smaller proportion (11.8 %) is dedicated to the inactivation of viruses within aerosols, an area closely associated with airborne transmission. This emphasizes the critical need for a more significant study of this very relevant topic. Studies investigating the decontamination of liquids containing viruses using CAPs, as well as those exploring the use of plasma-treated liquids as an intermediary approach for virus treatment, are less prevalent, each constituting only 5.5 % of the total publications.

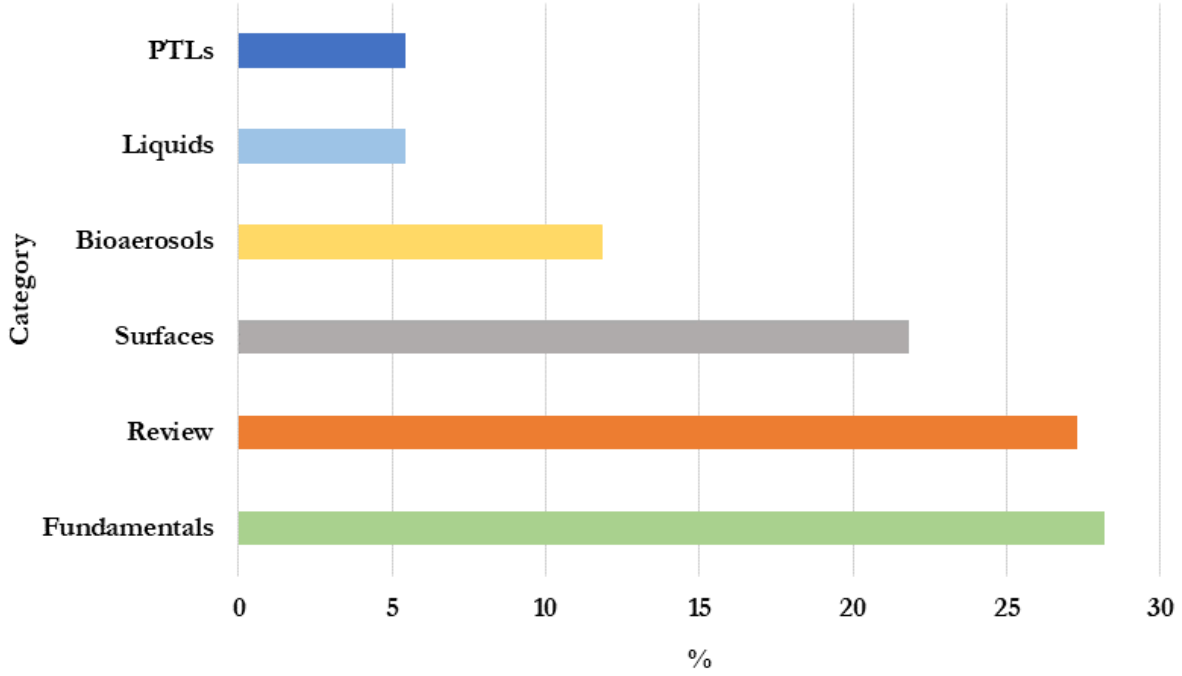

Figure 1.10 *- Distribution of the identified articles according to the six pre-defined categories.*

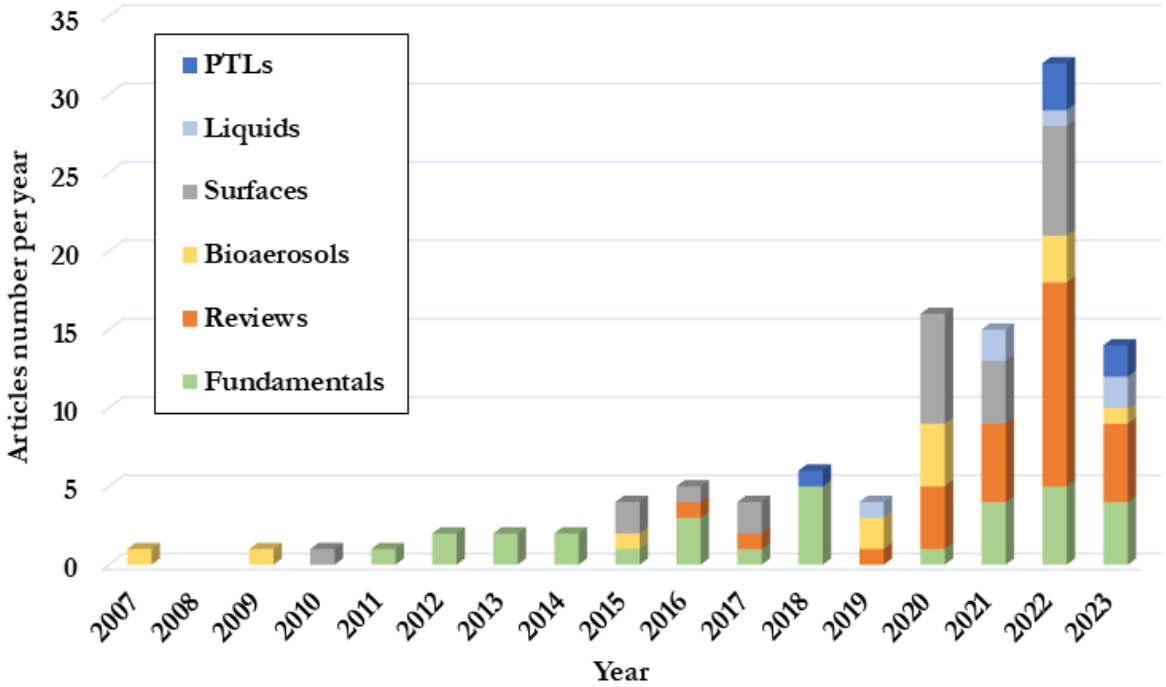

Figure 1.11 *- Yearly distribution of the identified articles considering the six pre-defined categories.*

1.3.3 Quantitative analysis of the plasma source identified within the articles

Among the CAP sources employed in the reviewed studies, DBDs emerged as the most prevalent architecture, accounting for 28.6 % of all cases (Figure 1.12). DBD jets followed closely behind at 25 %, while surface DBDs claimed a 13.1 % share. This prominence of DBDs and surface DBDs can likely be attributed to their design flexibility, making them well-suited for industrial applications. Conversely, DBD jets appear to be favored in fundamental research, where their role lies primarily in elucidating the mechanisms of CAP-virus interaction. The category labeled "others" includes a diverse range of CAP sources with characteristics distinct from the categories above. These sources often represent hybrid configurations that combine elements of the previously discussed technologies (e.g., the plasma source used by Sakudo *et al.* [16], which has two high-voltage electrodes and a ground electrode but without any dielectric material). Corona sources, including corona discharges (8.3 %) and corona jets (8.3 %), garnered comparatively lower usage.

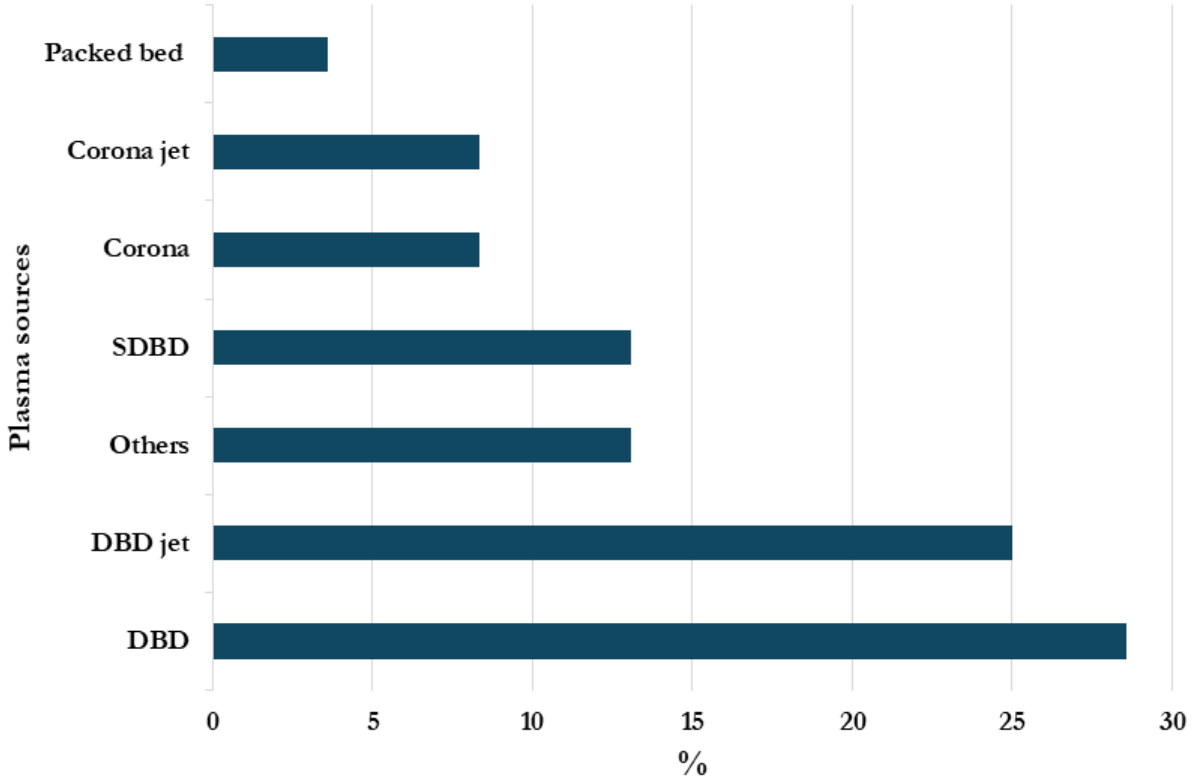

Figure 1.12 *- Distribution of plasma sources identified within the articles.*

1.3.4 Analysis of the different viruses within identified articles

Analysis of the experimental articles revealed a total of 41 distinct viral species investigated (a comprehensive listing of all identified viruses is included in the supplementary table of Appendix 2). The IV - Single-stranded positive RNA (ssRNA+) viruses emerged as the most extensively studied category, accounting for 51.2 %, as illustrated in Figure 1.13-a. Moreover, 51.2% of the studied viruses belong to the non-enveloped group (Figure 1.13-b). This emphasis on RNA viruses, as highlighted in Figure 1.13-c, can be attributed to their heightened public health risk due to their propensity for rapid genetic mutation. This observation can be readily understood, given the considerable focus on research on the SARS-CoV-2 virus, belonging to this particular viral class, since 2019. Consequently, SARS-CoV-2 has emerged as the foremost virus species under investigation in this field, together with the feline calicivirus, which is a highly contagious ssRNA+ virus that primarily affects cats, and is frequently used as a surrogate for Human Norovirus (HuNoV), the most common cause of gastroenteritis. Other viruses that are often studied are MS2 bacteriophages, Tulane virus, and Adenovirus. The effectiveness of plasma treatments against various viruses has been extensively investigated using various techniques. Among these techniques, plaque assays, infectivity assays (TCID50 assay), and PCR assays (RT-qPCR, RT-PCR, and qRT-PCR) have emerged as the most frequently employed methods for evaluating plasma-mediated viral inactivation. In addition to these prevalent methods, various other techniques have been employed to assess the efficacy of plasma treatments against viruses: Immunofluorescence (IF) Assay, End-point Titration Assay, DNA Damage Assay, Inhibition Analysis, Focus Forming Assay, Embryo Lethality Assay and Hemagglutination Test.

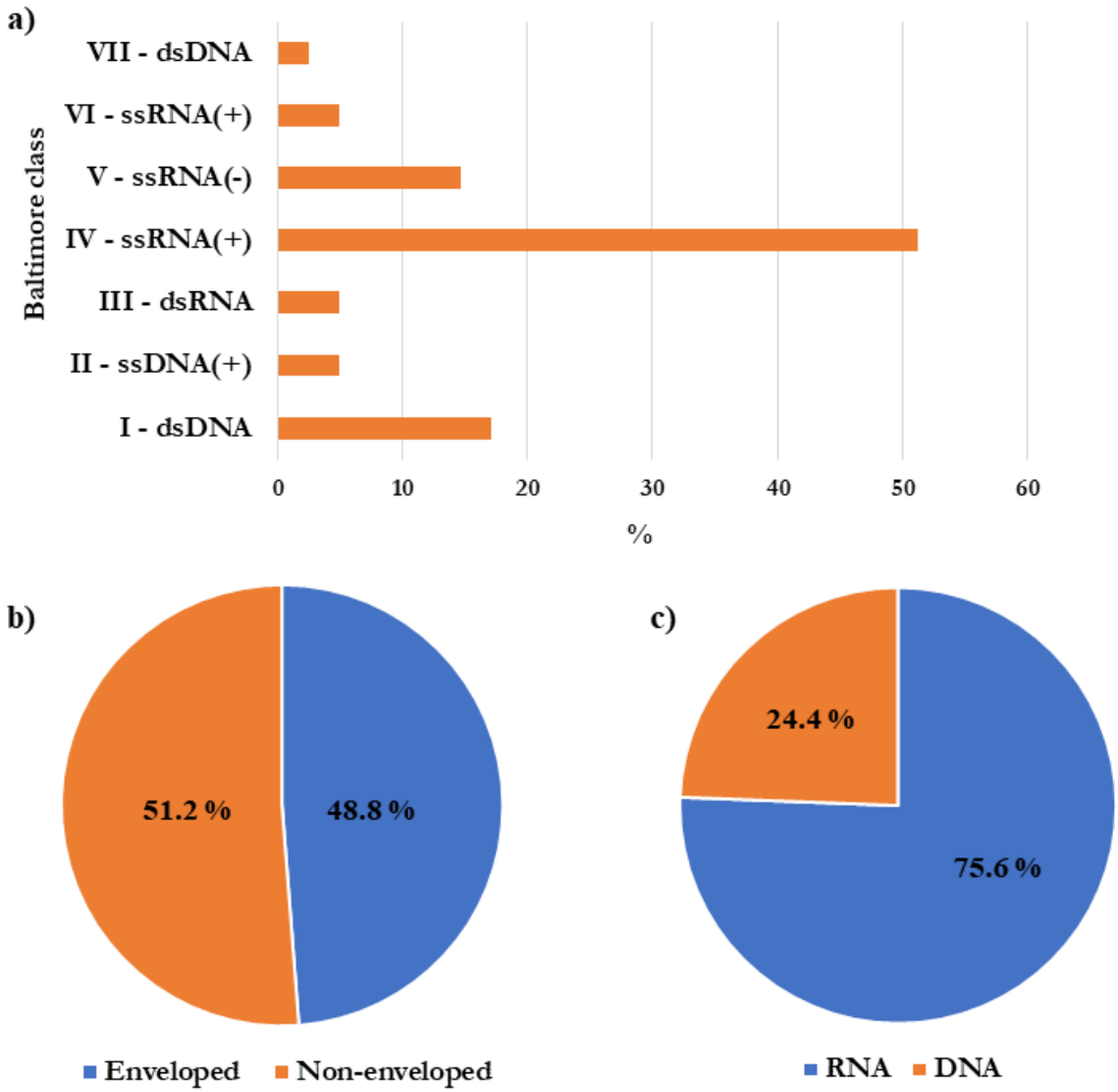

Figure 1.13 *– Distribution of identified viruses in the articles based on* ***a)*** *the Baltimore classification,* ***b)*** *the presence of envelope, and* ***c)*** *the type of nucleic acid.*

1.3.5 CAP and viruses interaction

The investigation of the interaction between CAP sources and viruses reveals a marked heterogeneity. The plasma sources are frequently custom-built within diverse research laboratories around the world, rendering direct comparisons challenging, but CAPs show great potential for viral inactivation.

1.3.5.1 Main CAP constituents interacting with viruses

This section summarizes the main CAP components and effects discussed in reviews and fundamental papers. Fundamental research articles and reviews demonstrate that researchers

constantly work to elucidate the intricate mechanisms governing the interaction of the various components involved in plasma generation and viruses. The aim of CAP treatments in virology is mainly to inactivate viruses, and often, this process involves the disruption of viral infectivity, resulting in the virus's inability to infect host cells successfully. Intervention within the viral replication cycle is essential to achieve virus inactivation effectively. This intervention disrupts or inhibits critical stages required for successful viral infection. Studies have demonstrated that exposure to CAPs or PTL treatments can lead to the alteration and/or destruction of these viral components, such as viral envelope proteins, nucleic acids, and lipids (Figure 1.14) [22]. Literature reveals an important role of RONS in the mechanisms underlying viral inactivation [22],[42],[43]. CAPs are able to produce a wide range of RONS, and their concentration depends on the plasma source, operating conditions, and gas composition. However, precisely attributing the contribution of each individual RONS species presents a significant challenge. This complexity arises from the simultaneous generation of numerous RONS, many of which possess short lifetimes, hindering their investigation. Despite these difficulties, it is well-established that RONS can exert antiviral effects by targeting viral proteins and genomes [42],[44]. Examples of these reactive species include hydroxyl radicals ($^{\cdot}OH$), superoxide radicals (O_2^{-*}), singlet oxygen ($^1O_2$), nitric oxide radicals ($^{\cdot}NO$), and excited nitrogen (N^*)[42]. Their formation occurs through the interaction of free electrons with gaseous molecules. Although significant concentrations of these short-lived and highly reactive species can be obtained using CAP sources, their precise quantification and assessment are hampered by their transient nature. The contribution of long-lived RONS further enhances the inactivation of viruses. These species are distinguished by their extended survival times before undergoing chemical interactions or transformations. Examples of long-lived RONS include ozone (O_3), nitrogen dioxide (NO_2), nitrous oxide (N_2O), nitrous acid (HNO_2), and nitric acid (HNO_3). Furthermore, PTLs (plasma-treated liquids) have also been demonstrated to have various RONS, including hydrogen peroxide (H_2O_2), nitrites (NO_2^-), and peroxynitrite ($ONOO^-$).

Investigating the mechanisms of CAP-mediated viral inactivation, Jin *et al.*[45] reported a significant interference of CAP treatments enriched in singlet oxygen and hydroxyl radicals on viral entry mechanisms of the SARS-CoV-2 virus. Their findings demonstrated that exposure to these RONS species resulted in alterations to the viral spike protein; indeed, authors saw an alteration of viral spike proteins, compromising the virus's ability to bind to host cell receptors. Additionally, Khanikar *et al.* demonstrated that the CAP plasma has the ability to degrade the RNA of the SARS-CoV-2 virus. These effects were associated with the high concentration of hydrogen peroxide [46].

Guo *et al.* investigated the efficacy of CAP and PTL treatments against various bacteriophages (T4, 174, and MS2) [47]. Bacteriophages, viruses that specifically infect bacteria, are valuable surrogates in scientific studies to analyze viral transmission dynamics within open-air environments [48]. Their analysis of DNA and protein structures revealed that the reactive species generated by CAP treatments inflicted damage on both the viral nucleic acids and proteins. This observation was further confirmed by morphological analysis, which revealed the clustering of bacteriophages following CAP treatment [47].

Aboubakr *et al.* [49] investigated the effect of CAP on Feline Calicivirus (FCV). Extended CAP exposure (2 minutes) disintegrated the viral capsid due to substantial oxidation of the capsid protein. Interestingly, a shorter exposure time of 15 seconds, while not affecting the overall capsid structure, demonstrably oxidized specific amino acids within critical regions of the capsid involved in viral attachment and host cell entry. This oxidation effectively blocks viral infection of host cells. The researchers further observed that CAP-induced oxidation could also impact viral RNA following capsid destruction. However, this effect was found to have a lesser influence on virus inactivation than capsid damage [49]. Another previous study investigating the mechanisms of FCV inactivation by CAP demonstrated that singlet oxygen plays a key role in inducing oxidative modifications to the viral capsid proteins [50]. Yamashiro *et al.* conducted a study that confirms the role of singlet oxygen in the inactivation of FCV and also underscores the contribution of peroxynitrite ($ONOO^-$) in disrupting viral RNA [51]. Similarly, Nayak *et al.* noted that FCV inactivation in the gas phase results from the combined effects of ozone and reactive nitrogen species (RNS), potentially including nitrogen oxides (NOx). In contrast, in the liquid phase, FCV inactivation is influenced by the pH and mainly driven by RNS, particularly acidified nitrite, while the ozone has a minimal effect [52].

Shi *et al.* explored the interaction between CAP and the Hepatitis B virus (HBV), a viral pathogen responsible for chronic liver disease transmitted through bodily fluids. Their study demonstrated that key HBV antigens were vulnerable to damage caused by RONS following CAP exposure [53].

Sakudo *et al.* propose hydrogen as the key agent responsible for the degradation and inactivation of influenza A and B viruses, which cause annual human infections during epidemic seasons. Their study shows that treatment with nitrogen gas plasma degrades several viral proteins, including nucleoprotein, hemagglutinin, and neuraminidase, while also damaging the viral RNA genome [54].

Additionally, Sutter *et al.* provided a comprehensive summary of CAP applications, highlighting its potential as a promising treatment for Herpes simplex virus type 1 (HSV-1)

infections. The antiviral efficacy of CAP is due to the production of RONS, which directly targets and inhibits HSV-1 [55].

In addition to viral decontamination, several studies have evaluated the effects of CAPs and PTLs on infected cells. For example, CAP has been shown to reduce HIV-1 infectivity in HIV-1-infected cells by interfering with virus-cell fusion and disrupting viral assembly. It has also been suggested that CAP exposure activates cellular factors in macrophages, creating conditions that inhibit further viral entry [56]. Similarly, PTL treatment led to a reduction in SARS-CoV-2 viral titers in infected cells [57]. In addition, CAPs were found to induce immunomodulatory changes in infected cells, stimulating anti-HSV-1 adaptive immune responses, highlighting CAPs as a potential therapeutic strategy for HSV-1 infection [55].

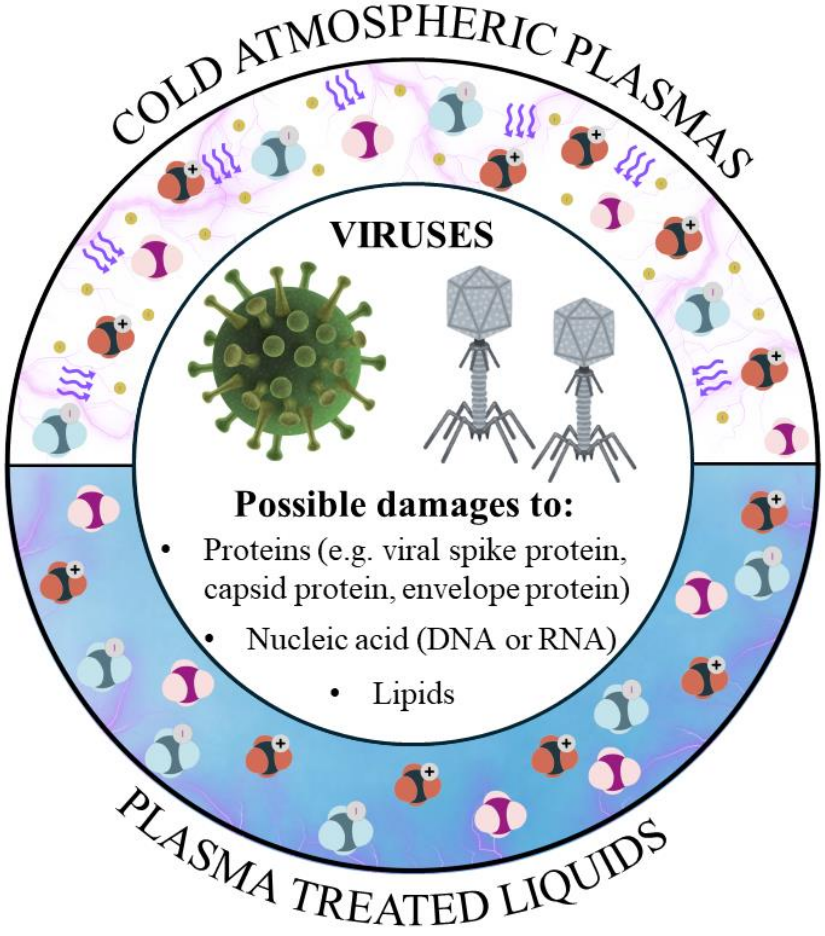

Figure 1.14 *- Potential damages to viruses induced by CAP and PTL.*

1.3.5.2 CAP interactions with viruses on surfaces

As illustrated in Figure 1.10, excluding reviews and fundamental studies, one of the primary applications of CAP is for surface decontamination. The analysis of 24 studies investigating CAP-based surface decontamination reveals promising efficacy. The average log reduction achieved in this application is approximately 3.2, suggesting significant potential for this decontamination method. A basic distinction between dry and wet CAP treatment can be established within this context. In dry CAP treatment, the plasma directly interacts with the dry surface; wet CAP treatment involves exposing the surface to plasma while it is partially submerged or covered by a liquid layer. The presence or absence of liquid during treatment affects the inactivation efficacy (Figure 1.15). An analysis of the log reduction values reported in the 24 experimental papers of this category reveals a clear distinction between dry and wet CAP treatment methods. Wet treatments demonstrate a higher average log reduction of 3.5 compared to dry treatments (Figure 1.15), which achieve an average log reduction of approximately 2.8. The presence of liquid can result in the formation of additional RONS that can potentially contribute to viral inactivation, such as hydrogen peroxide, which has a well-known disinfectant power, but also nitrites, that in an acid environment can exert an antimicrobial effect. Other studies have shown that the combination of ozone (O_3) and nitrogen dioxide (NO_2) in the gas phase allows the formation of dinitrogen pentoxide (N_2O_5), which mainly leads to the formation in liquid of peroxynitritous acid, precursor of antimicrobial agents, (·NO and ·OH) [44][58]. Peroxinitrous acid can also be formed in acid environments by the reaction between H_2O_2 and NO_2^-. According to this data, Moldgy *et al.* examined four different CAP sources used in air to decontaminate wet and dry surfaces (stainless steel discs) against feline calicivirus (FCV) [58]. FCV, a highly contagious single-stranded positive RNA virus, is a well-established model organism in the field of CAP-virus interactions. The study compared a direct-contact DBD source with three indirect plasma sources: a 2D DBD, a volumetric DBD, and a gliding arc discharge. These findings highlight the critical role of surface humidity in enhancing the efficacy of all four CAP-based decontamination methods [58]. However, only the direct plasma treatment approach yielded positive results for dry surface decontamination.

Furthermore, 24 studies investigate the impact of CAPs on various surface types. A primary distinction is drawn between non-biological (N95 respirators, FFP3 face masks, plastic, aluminum, paper, polyethylene terephthalate (PET), polypropylene (PP), stainless-steel, metal, cardboard, stainless steel discs, leather football, composite leather basketball, leather baseball)

and biological surfaces (raspberries, salmon, lettuce leaves, fresh oysters, raw chicken breasts, chicken breast, blueberries, romaine lettuce, fresh meats). Limited studies directly compare CAP's decontamination efficacy on biological and non-biological surfaces using the same experimental configurations and conditions. However, from the analysis of decontamination results, we observed that the use of CAPs for decontamination of biological surfaces results in an average log reduction of approximately 2.4, which is almost one unit lower than the overall average observed for the surfaces category (3.2). One possible explanation could be related to the presence of organic matter that may react with the reactive species produced by CAPs, reducing their effect on viruses. Moreover, the morphology of biological surfaces, particularly in the case of non-smooth surfaces, may also contribute to the reduced efficacy of CAPs [44][59].

To illustrate the application of CAPs in biological matrix decontamination, Velebit *et al.* [60] demonstrated the efficacy of CAP against murine norovirus (MNV) and hepatitis A virus (HAV) on aerosol-inoculated raspberries. MNV is a non-enveloped virus with a single-stranded positive RNA genome that belongs to the Caliciviridae family and is frequently used as a surrogate for the highly contagious Human Norovirus (HuNoV). Similarly, HAV is a non-enveloped virus with a single-stranded RNA genome that belongs to the Picornaviridae family. Both HuNoV and HAV have been linked to several foodborne illness outbreaks. In this case, a corona discharge plasma source was used with synthetic air, and CAP treatment resulted in a considerable 4 log reduction in infectivity in less than 5 minutes for MNV and around 10 minutes for HAV[60]. Notably, most (79.2%) of the documents analyzed in this application employed air as the process gas. In the rest of the studies, oxygen, argon, and nitrogen were also used as process gases, but air is the most interesting than other gases from a cost perspective for future applications.

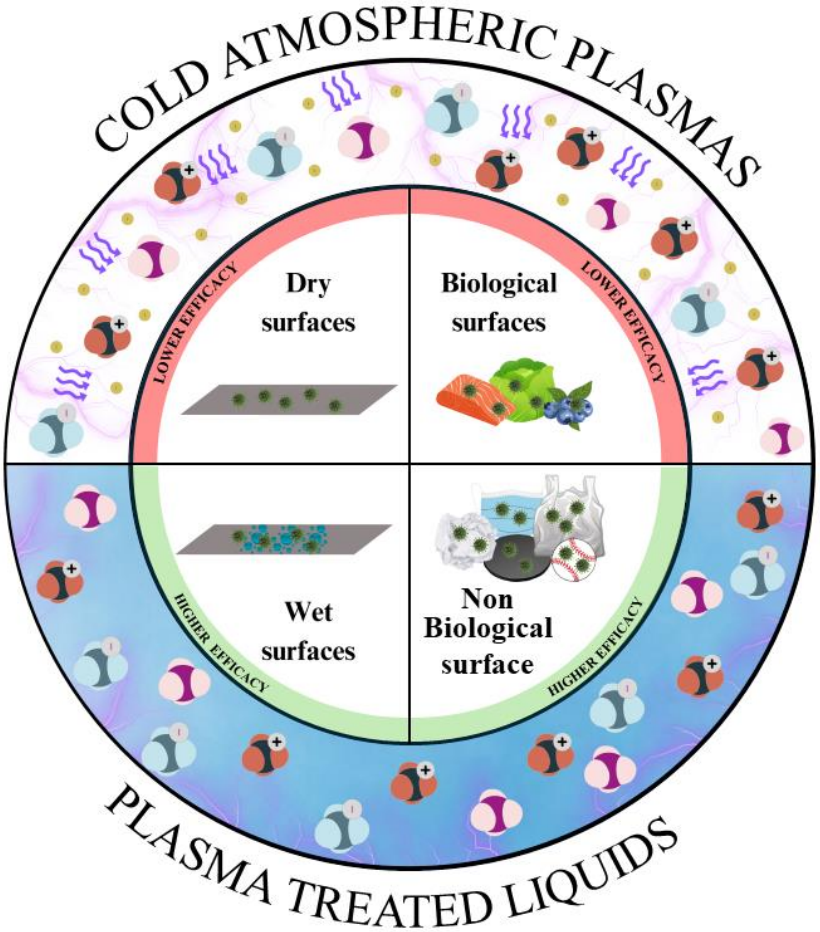

Figure 1.15 *– CAPs and PTLs efficacy on wet/dry biological/non biological surfaces.*

1.3.5.3 CAP interactions with bioaerosol-containing viruses

Interest in this application has increased since 2020, despite the existence of a relevant early study published in 2007. This growing interest likely coincides with the public health crisis caused by SARS-CoV-2 and the increased awareness of airborne viral transmission. The analysis of documents identified within this application reveals that CAP treatments applied to virus-containing bioaerosols achieve an average log reduction of approximately 3.9. DBD or its different architectures are popular for decontaminating virus-containing bioaerosols. This widespread adoption can likely be attributed to their ability to handle geometries suitable for treating large air volumes (> 20 m^3/h). Investigating the efficacy of CAP technology against airborne viruses, Nayak *et al.* [61] employed a packed-bed DBD plasma source within a wind tunnel. Their target pathogen was the single-stranded positive RNA porcine reproductive and respiratory virus (PRRV), a major swine disease. Their findings demonstrated a significant reduction in viral load, achieving a 3.5 $\log_{10}$ drop within a few milliseconds. A direct DBD

source with an average power of less than 5 W against the SARS-CoV-2 virus, another single-stranded positive RNA virus, was used by Bisag. *et al.* [62]. The authors reported the total inactivation of the SARS-CoV-2 contained in bioaerosols [62]. Finally, as expected, the documents reveal a correlation between the effectiveness of CAP treatments and the contact time between viral particles and the plasma or the zone rich in reactive species produced by the plasma (residence time). For the 42% of papers where residence time could be assessed, an average log reduction of 4.56 was achieved with an average residence time of less than 0.8 seconds, which is a compatible time to employ this technology in standard HVAC systems. The CAP's ability to achieve promising inactivation results in very short residence times (order of milliseconds) supports the hypothesis of an important contribution to virus inactivation by short-lived species such as O and OH radicals that can directly inactivate viruses or spread in micrometer droplets.

1.3.5.4 CAP interactions with liquids containing viruses and PTLs interactions with viruses

Although a significantly smaller fraction of research efforts focus on using CAPs to decontaminate viruses within liquid media or generate intermediary liquids for virus treatment, the observed results regarding viral inactivation are encouraging. Notably, the analysis of studies focused on the liquid application revealed an average 5.5 log reduction. Notably, all findings in this category pertain to the decontamination of virus-loaded water. This promising result is consistent with what has been shown regarding the use of CAP for decontaminating wet surfaces. A liquid environment seems to be a favorable factor for virus decontamination. Liquids in contact with plasma are rich in reactive species with strong antimicrobial power, such as OH radicals and H_2O_2, and in the presence of RNS in the gas phase and an acidic environment, nitric acid, nitrous acid, and peroxynitrous acid. In contrast, studies investigating the application of PTLs report an average log reduction of 3.6. An example of the liquid application is a corona plasma jet used by Filipić *et al.* for decontaminating water samples with pepper mild mottle virus (PMMoV). PMMoV is a highly resistant waterborne tobamovirus that can survive passage through the human digestive system. After 5 minutes, CAP totally inactivated PMMoV in water samples [63]. In previous work, the authors used the same plasma source to treat samples contaminated with Potato virus Y (PVY), a common contaminant in drinking water, along with organic plant material to simulate a more polluted environment [36]. The results showed complete inactivation of PVY after a 5-minute treatment. In contrast, in tap

water samples without organic residues, a shorter treatment time of just 1 minute was sufficient for full inactivation of PVY [64].

For the PTLs application, the idea is to produce intermediary liquids enriched with RONS for virus inactivation, such as the study proposed by Cortázar *et al.*[57] The authors used a DBD jet to create PTL to explore the sensitivity of the SARS-CoV-2 and PR8 H1N1 viruses (a specific strain of influenza A that has been widely used in scientific investigations for completely analyzing the influenza virus). The trials demonstrated lower viral infectivity based on in vitro analyses utilizing both isolated viruses and infected cells. The authors also noted that the antiviral effect was only minimally affected by pH changes resulting from the plasma treatment of the liquid [57].

Su *et al.* examined the efficacy of PTLs in inactivating the Newcastle disease virus (NDV). Their study found that short-lived reactive species, such as hydroxyl radicals (·OH) and nitric oxide (·NO), along with the long-lived hydrogen peroxide (H_2O_2), caused morphological changes in the virus, disrupted its RNA structure, and degraded its protein components [65].

1.4 Conclusions

The systematic review highlights the exponential interest in research concerning CAP-virus interaction and the potential of CAP technology for viral decontamination in various contexts. CAPs have the potential to decontaminate inanimate surfaces through direct exposure to the plasma discharge or RONS-rich atmosphere or PTLs, potentially fighting contact-based infections. Moreover, CAPs could be a useful tool to contrast the transmission of foodborne diseases by treating food product surfaces. CAPs have also demonstrated promising results in mitigating airborne transmission of viruses, as seen during the COVID-19 pandemic. Finally, the capability of CAPs to inactivate viruses presents a promising solution for enhancing water safety, benefiting both human consumption and agricultural irrigation.

Further efforts are needed to fully understand the potential risks of using CAPs in the previously discussed contexts. For example, in the context of surface decontamination, CAPs could be an innovative strategy to fight foodborne diseases by decontaminating material in contact with food (e.g., packaging) or the food itself. In this area, careful evaluation of the potential side effects induced by food, such as chemical modifications, nutritional alterations, and organoleptic changes, is needed.

In the frame of air decontamination, some devices on the market are based on the presence of DBD sources and ozone production to decontaminate microorganisms in the air. In this case,

careful evaluation of ozone production is necessary because it has important antimicrobial properties, but in high concentrations indoors and over long exposure times, it can be a problem for human health. So, efforts must ensure that ozone concentrations remain within safe limits. CAPs also have the potential for water decontamination, but there are still few studies on potential adverse effects, such as genotoxic and cytotoxic impacts on human or plant cells.

In-depth studies and risk assessments are critical to developing guidelines and protocols that optimize the advantages of CAPs while mitigating risks to human health and the environment. A thorough assessment will help determine the safety and feasibility of using CAP for water decontamination, ensuring that its benefits are maximized without compromising safety. Finally, the application of CAP in therapeutic interventions necessitates extensive investigation and development progression before reaching clinical implementation, despite promising initial results.

However, some aspects of the large-scale deployment of plasma technology for viral decontamination remain challenging. In particular, significant heterogeneity in the use of plasma devices, experimental conditions (working gas, voltage, frequency), environmental conditions, substrate type, and virus emerges from the experimental studies. Focusing only on the plasma devices and viruses used, it is evident how the reviewed studies explore a wide range of CAP sources that share underlying principles, such as DBDs, corona discharges, and plasma jets, implemented in varying structural configurations. Notably, DBDs, including DBD jets, direct DBDs, and surface DBDs, are frequently employed. From a biological point of view, 41 virus species have been studied, with an emphasis on RNA viruses, probably their heightened propensity for genetic mutations, rendering them a significant public health concern. Actually, there are no standard protocols for testing the antimicrobial efficacy of CAP devices, which are often designed and implemented by individual research groups, making a comparison of the various proposed solutions complicated. In fact, among the proposed articles, those that carry out a comparative study using the same experimental conditions are rare. In addition, there is also a lack of comparative studies on viral decontamination between CAP and traditional technologies.

CAPs and PTLs can induce damage to proteins (e.g., viral spike protein, capsid protein, or envelope protein), nucleic acid (DNA or RNA), and lipids, but the exact mechanisms driving viral inactivation by CAPs are currently unknown. As previously discussed, the intricate interplay between various plasma components and viral particles complicates the elucidation of precise inactivation processes. The role of RONS plays in viral inactivation mechanisms is significant, yet challenging to study. Short-lived species, such as singlet oxygen and radicals,

are particularly difficult to analyze due to their short reaction times (1 - 3 μs), and thus, a correlation between their concentrations and biological effects is not frequently reported. So, knowledge in this area is still limited and allows for extensive efforts for future research. Overall, applying CAP technology across various settings holds promise for preventing viral infections, controlling viral dissemination, and safeguarding public health.

1.5 Acknowledgments

The author thanks the support of COST Action CA20114 PlasTHER – Therapeutical applications of cold plasmas related to the COST (European Cooperation in Science and Technology) Association.

1.6 References

[1] A. Fridman, *Plasma chemistry*. Cambridge University Press, 2008.

[2] M. Laroussi, 'Cold Plasma in Medicine and Healthcare: The New Frontier in Low Temperature Plasma Applications', *Front. Phys.*, vol. 8, no. March, pp. 1–7, 2020, doi: 10.3389/fphy.2020.00074.

[3] S. Bekeschus and T. von Woedtke (Eds.), *Redox Biology in Plasma Medicine*. CRC Press, 2024

[4] M. Domonkos, P. Tichá, J. Trejbal, and P. Demo, 'Applications of cold atmospheric pressure plasma technology in medicine, agriculture and food industry', *Appl. Sci.*, vol. 11, no. 11, 2021, doi: 10.3390/app11114809.

[5] J. Flint, V. R. Racaniello, G. F. Rall, A. M. Skalka, and L. W. Enquist, *Principles of Virology, Volume 1*, 4th ed. ASM Press, 2015.

[6] E. V. Koonin and P. Starokadomskyy, 'Are viruses alive? The replicator paradigm sheds decisive light on an old but misguided question', *Stud. Hist. Philos. Sci. Part C Stud. Hist. Philos. Biol. Biomed. Sci.*, vol. 59, pp. 125–134, 2016, doi: 10.1016/j.shpsc.2016.02.016.

[7] W. Ryu, *Molecular Virology of Human Pathogenic Viruses Molecular Virology of Human Pathogenic Viruses*, 1st editio. Academic Press, 2016.

[8] A. Trilla, G. Trilla, and C. Daer, 'The 1918 "Spanish Flu" in Spain', *Clin. Infect. Dis.*, vol. 47, no. 5, pp. 668–673, 2008, doi: 10.1086/590567.

[9] C. Jackson, 'History lessons: The Asian Flu pandemic', *Br. J. Gen. Pract.*, vol. 59, no. 565, pp. 622–623, 2009, doi: 10.3399/bjgp09X453882.

[10] N. Vousden and M. Knight, 'Lessons learned from the A (H1N1) influenza pandemic', *Best Pract. Res. Clin. Obstet. Gynaecol.*, vol. 76, pp. 41–52, 2021, doi: 10.1016/j.bpobgyn.2020.08.006.

[11] L. Montagnier, 'A History of HIV Discovery', *Science*, vol. 298, no. 5599, pp. 1727–1728, 2002, doi: 10.1126/science.1079027.

[12] S. T. Jacob *et al.*, 'Ebola virus disease', *Nature reviewes Disease primers*, vol. 6, no. 1. Springer US, 2020, doi: 10.1038/s41572-020-0147-3.

[13] Jennifer Louten, 'Virus Transmission and Epidemiology', *Essential Human Virology*, vol. 21, 2016, doi: 10.1016/B978-0-12-800947-5.00005-3.

[14] N. Castano *et al.*, 'Fomite Transmission, Physicochemical Origin of Virus − Surface Interactions, and Disinfection Strategies for Enveloped Viruses with Applications to SARS-CoV - 2', *ACS omega*, vol. 6., no.10, 2021, doi: 10.1021/acsomega.0c06335.

[15] S. Kausar *et al.*, 'A review : Mechanism of action of antiviral drugs', *International journal of immunopathology and pharmacology,* vol. 35, 2021, doi:

10.1177/20587384211002621.

[16] F. Masotti, S. Cattaneo, M. Stuknytė, and I. De Noni, 'Airborne contamination in the food industry: An update on monitoring and disinfection techniques of air', *Trends in Food Science and Technology*, vol. 90. Elsevier Ltd, pp. 147–156, Aug. 01, 2019, doi: 10.1016/j.tifs.2019.06.006.

[17] M. K. Ijaz, B. Zargar, K. E. Wright, J. R. Rubino, and S. A. Sattar, 'Generic aspects of the airborne spread of human pathogens indoors and emerging air decontamination technologies', *Am. J. Infect. Control*, vol. 44, no. 9, pp. S109–S120, 2016, doi: 10.1016/j.ajic.2016.06.008.

[18] European Centre for Disease Prevention and Control, *Point prevalence survey of healthcare-associated infections and antimicrobial use in European acute care hospitals – 2022-2023*, 2024.

[19] S. Bekeschus, A. Kramer, E. Suffredini, T. von Woedtke, and V. Colombo, 'Gas Plasma Technology—An Asset to Healthcare During Viral Pandemics Such as the COVID-19 Crisis?', *IEEE Trans. Radiat. Plasma Med. Sci.*, vol. 4, no. 4, pp. 391–399, 2020, doi: 10.1109/trpms.2020.3002658

[20] I. Adamovich *et al.*, 'The 2022 Plasma Roadmap: low temperature plasma science and technology', *J. Phys. D. Appl. Phys.*, vol. 55, no. 37, 2022, doi: 10.1088/1361-6463/ac5e1c.

[21] Yuri P. Raizer, John E. Allen, V.I. Kisin, *Gas discharge physics*, Springer, 1991.

[22] A. Filipić, I. Gutierrez-Aguirre, G. Primc, M. Mozetič, and D. Dobnik, 'Cold Plasma, a New Hope in the Field of Virus Inactivation', *Trends Biotechnol.*, vol. 38, no. 11, pp. 1278–1291, 2020, doi: 10.1016/j.tibtech.2020.04.003.

[23] E. Feizollahi, N. N. Misra, and M. S. Roopesh, 'Factors influencing the antimicrobial efficacy of Dielectric Barrier Discharge (DBD) Atmospheric Cold Plasma (ACP) in food processing applications', *Crit. Rev. Food Sci. Nutr.*, vol. 61, no. 4, pp. 666–689, 2021, doi: 10.1080/10408398.2020.1743967.

[24] R. Brandenburg, 'Corrigendum:Dielectric barrier discharges: progress on plasma sources and on the understanding of regimes and single filaments, (2017 *Plasma Sources Science and Technology* 26 053001), *Plasma Sources Sci. Technol.*, vol. 27, no. 7, 2018, doi: 10.1088/1361-6595/aaced9.

[25] U. Kogelschatz, 'Fundamentals and applications of dielectric-barrier discharges', HAKONE VII Int. Symp. On High Pressure Low Temperature Plasma Chemistry, Greifswald. 2000

[26] U. Kogelschatz, 'Dielectric-barrier Discharges: Their History, Discharge Physics, and Industrial Applications', *Plasma Chem. Plasma Process.*, vol. 23, no. 1, pp. 1–46, 2003, doi: 10.1023/A:1022470901385.

[27] U. Kogelschatz, 'Filamentary, patterned, and diffuse barrier discharges', *IEEE Trans. Plasma Sci.*, vol. 30, no. 4 I, pp. 1400–1408, 2002, doi: 10.1109/TPS.2002.804201.

[28] J. Winter, R. Brandenburg, and K. D. Weltmann, 'Atmospheric pressure plasma jets: An overview of devices and new directions', *Plasma Sources Sci. Technol.*, vol. 24, no. 6, 2015, doi: 10.1088/0963-0252/24/6/064001.

[29] X. Lu, M. Laroussi, and V. Puech, 'On atmospheric-pressure non-equilibrium plasma jets and plasma bullets', *Plasma Sources Science and Technology*, vol. 21, no. 3, 2012, doi: 10.1088/0963-0252/21/3/034005.

[30] X. Lu, Z. Jiang, Q. Xiong, Z. Tang, X. Hu, and Y. Pan, 'An 11 cm long atmospheric pressure cold plasma plume for applications of plasma medicine', *Applied Physics Letters,* Vol. 92, no. 8, 2008, doi: 10.1063/1.2883945.

[31] Z. Falkenstein and J. J. Coogan, 'Microdischarge behaviour in the silent discharge of nitrogen-oxygen and water-air mixtures', *J. Phys. D. Appl. Phys.*, vol. 30, no. 5, pp. 817–825, 1997, doi: 10.1088/0022-3727/30/5/015.

[32] P. Bruggeman *et al.*, 'Electronic quenching of OH(A) by water in atmospheric pressure plasmas and its influence on the gas temperature determination by OH(A-X) emission', *Plasma Sources Sci. Technol.*, vol. 19, no. 1, 2010, doi: 10.1088/0963-0252/19/1/015016.

[33] F. J. Gordillo-Vzquez and Z. Donkó, 'Electron energy distribution functions and transport coefficients relevant for air plasmas in the troposphere: Impact of humidity and gas temperature', *Plasma Sources Sci. Technol.*, vol. 18, no. 3, 2009, doi: 10.1088/0963-0252/18/3/034021.

[34] E. Marode *et al.*, 'Physics and applications of atmospheric non-thermal air plasma with reference to environment', *Plasma Phys. Control. Fusion*, vol. 51, no. 12, 2009, doi: 10.1088/0741-3335/51/12/124002.

[35] D. Butscher, H. Van Loon, A. Waskow, P. Rudolf, V. Rohr, and M. Schuppler, 'Plasma inactivation of microorganisms on sprout seeds in a dielectric barrier discharge', *Int. J. Food Microbiol.*, vol. 238, pp. 222–232, 2016, doi: 10.1016/j.ijfoodmicro.2016.09.006.

[36] D. Butscher, D. Zimmermann, M. Schuppler, P. Rudolf, and V. Rohr, 'Plasma inactivation of bacterial endospores on wheat grains and polymeric model substrates in a dielectric barrier discharge', *Food Control*, vol. 60, pp. 636–645, 2016, doi: 10.1016/j.foodcont.2015.09.003.

[37] X. Lu, G. V Naidis, M. Laroussi, S. Reuter, D. B. Graves, and K. Ostrikov, 'Reactive species in non-equilibrium atmospheric-pressure plasmas : Generation , transport , and biological effects', *Physics Reports,* vol. 630, pp. 1–84, 2016, doi: 10.1016/j.physrep.2016.03.003.

[38] P. J. Bruggeman *et al.*, 'Plasma – liquid interactions : a review and roadmap', *Plasma sources science and technology,* vol. 25, no. 5 2016, doi: 10.1088/0963-0252/25/5/053002.

[39] A. Stancampiano *et al.*, 'Plasma and aerosols: Challenges, opportunities and perspectives', *Appl. Sci.*, vol. 9, no. 18, p. 3861, 2019, doi: 10.3390/app9183861.

[40] G. Oinuma, G. Nayak, and Y. Du, 'Controlled plasma – droplet interactions : a

quantitative study of OH transfer in plasma – liquid interaction', *Plasma Sources Science and Technology,* vol. 29, no. 9, 2020, doi: 10.1088/1361-6595/aba988.

[41] D. Moher, A. Liberati, J. Tetzlaff, and D. G. Altman, 'Preferred reporting items for systematic reviews and meta-analyses: The PRISMA statement', *BMJ*, vol. 339, no. 7716, pp. 332–336, 2009, doi: 10.1136/bmj.b2535.

[42] N. Kaushik *et al.*, 'The inactivation and destruction of viruses by reactive oxygen species generated through physical and cold atmospheric plasma techniques: Current status and perspectives', *J. Adv. Res.*, vol. 43, pp. 59–71, 2023, doi: 10.1016/j.jare.2022.03.002.

[43] J. Fu, Y. Xu, E. J. Arts, Z. Bai, Z. Chen, and Y. Zheng, 'Viral disinfection using nonthermal plasma: A critical review and perspectives on the plasma-catalysis system', *Chemosphere*, vol. 309, p. 136655, 2022, doi: 10.1016/j.chemosphere.2022.136655.

[44] H. Mohamed *et al.*, 'Non-Thermal Plasma as a Novel Strategy for Treating or Preventing Viral Infection and Associated Disease', *Front. Phys.*, vol. 9, pp. 1–25, 2021, doi: 10.3389/fphy.2021.683118.

[45] T. Jin, Y. Xu, C. Dai, X. Zhou, Q. Xu, and Z. Wu, 'Cold atmospheric plasma: A non-negligible strategy for viral RNA inactivation to prevent SARS-CoV-2 environmental transmission', *AIP Adv.*, vol. 11, no. 8, 2021, doi: 10.1063/5.0060530.

[46] R. R. Khanikar *et al.*, 'Cold atmospheric pressure plasma for attenuation of SARS-CoV-2 spike protein binding to ACE2 protein and the RNA deactivation', *RSC Adv.*, vol. 12, no. 15, p. 9466, 2022, doi: 10.1039/d2ra00009a.

[47] M. G. K. Li Guo, Ruobing Xu, Lu Gou, Zhichao Liu, Yiming Zhao, Dingxin Liu, Lei Zhang, Hailan Chen, 'Mechanism of Virus Inactivation by Cold Atmospheric-Pressure Plasma and Plasma-Activated Water', *Appl. Environ. Microbiol.*, vol. 84, no. 17, 2018, doi: doi.org/10.1128/AEM.00726-18.

[48] G. T. Machado, C. R. de C. Pinto, L. A. V. da Fonseca, T. C. dos S. Ramos, T. F. P. Paggi, and B. Spira, 'Bacteriophages as surrogates for the study of viral dispersion in open air', *Arch. Microbiol.*, vol. 203, no. 7, pp. 4041–4049, 2021, doi: 10.1007/s00203-021-02382-8.

[49] H. A. Aboubakr *et al.*, 'Cold argon-oxygen plasma species oxidize and disintegrate capsid protein of feline calicivirus', *PLoS One*, vol. 13, no. 3, pp. 1–24, 2018, doi: 10.1371/journal.pone.0194618.

[50] H. A. Aboubakr, U. Gangal, M. M. Youssef, S. M. Goyal, and P. J. Bruggeman, 'Inactivation of virus in solution by cold atmospheric pressure plasma: Identification of chemical inactivation pathways', *J. Phys. D. Appl. Phys.*, vol. 49, no. 20, 2016, doi: 10.1088/0022-3727/49/20/204001.

[51] R. Yamashiro, T. Misawa, and A. Sakudo, 'Key role of singlet oxygen and peroxynitrite in viral RNA damage during virucidal effect of plasma torch on feline calicivirus', *Sci. Rep.*, vol. 8, no. 1, pp. 1–13, 2018, doi: 10.1038/s41598-018-36779-1.

[52] G. Nayak, H. A. Aboubakr, S. M. Goyal, and P. J. Bruggeman, 'Reactive species responsible for the inactivation of feline calicivirus by a two-dimensional array of

integrated coaxial microhollow dielectric barrier discharges in air', *Plasma Process. Polym.*, vol. 15, no. 1, 2018, doi: 10.1002/ppap.201700119.

[53] X. M. Shi *et al.*, 'Effect of low-temperature plasma on deactivation of hepatitis B virus', *IEEE Trans. Plasma Sci.*, vol. 40, no. 10, pp. 2711–2716, 2012, doi: 10.1109/TPS.2012.2210567.

[54] Y. I. Akikazu Sakudo, Tatsuya Misawa, Naohiro Shimizu, 'N_2 gas plasma inactivates influenza virus mediated by oxidative stress', *Front. Biosci. 6,* vol. 6, pp. 69–79, 2014, doi: 10.2741/e692.

[55] J. Sutter, P. J. Bruggeman, B. Wigdahl, F. C. Krebs, and V. Miller, 'Manipulation of Oxidative Stress Responses by Non-Thermal Plasma to Treat Herpes Simplex Virus Type 1 Infection and Disease', *Int. J. Mol. Sci.*, vol. 24, no. 5, 2023, doi: 10.3390/ijms24054673.

[56] O. Volotskova, L. Dubrovsky, M. Keidar, and M. Bukrinsky, 'Cold atmospheric plasma inhibits HIV-1 replication in macrophages by targeting both the virus and the cells', *PLoS One*, vol. 11, no. 10, pp. 1–9, 2016, doi: 10.1371/journal.pone.0165322.

[57] O. D. Cortázar, A. Megía-Macías, S. Moreno, A. Brun, and E. Gómez-Casado, 'Vulnerability of SARS-CoV-2 and PR8 H1N1 virus to cold atmospheric plasma activated media', *Sci. Rep.*, vol. 12, no. 1, pp. 1–12, 2022, doi: 10.1038/s41598-021-04360-y.

[58] A. Moldgy, G. Nayak, H. A. Aboubakr, S. M. Goyal, and P. J. Bruggeman, 'Inactivation of virus and bacteria using cold atmospheric pressure air plasmas and the role of reactive nitrogen species', *J. Phys. D. Appl. Phys.*, vol. 53, no. 43, 2020, doi: 10.1088/1361-6463/aba066.

[59] N. N. Misra, B. K. Tiwari, K. S. M. S. Raghavarao, and P. J. Cullen, 'Nonthermal Plasma Inactivation of Food-Borne Pathogens', *Food Engineering Reviews*, vol. 3, pp. 159–170, 2011, doi: 10.1007/s12393-011-9041-9.

[60] B. Velebit *et al.*, 'Efficacy of cold atmospheric plasma for inactivation of viruses on raspberries', *Innov. Food Sci. Emerg. Technol.*, vol. 81, 2022, doi: 10.1016/j.ifset.2022.103121.

[61] G. Nayak *et al.*, 'Rapid inactivation of airborne porcine reproductive and respiratory syndrome virus using an atmospheric pressure air plasma', *Plasma Process. Polym.*, vol. 17, no. 10, 2020, doi: 10.1002/ppap.201900269.

[62] A. Bisag *et al.*, 'Cold atmospheric plasma decontamination of SARS-CoV-2 bioaerosols', *Plasma Process. Polym.*, vol. 19, no. 3, pp. 1–11, 2022, doi: 10.1002/ppap.202100133.

[63] A. Filipić *et al.*, 'Inactivation of Pepper Mild Mottle Virus in Water by Cold Atmospheric Plasma', *Front. Microbiol.*, vol. 12, pp. 1–12, 2021, doi: 10.3389/fmicb.2021.618209.

[64] A. Filipić *et al.*, 'Cold Atmospheric Plasma as a Novel Method for Inactivation of Potato Virus Y in Water Samples', *Food Environ. Virol.*, vol. 11, no. 3, pp. 220–228, 2019, doi: 10.1007/s12560-019-09388-y.

[65] X. Su *et al.*, ‘Inactivation efficacy of nonthermal plasmaactivated solutions against Newcastle disease virus’, *Appl. Environ. Microbiol.*, vol. 84, no. 9, pp. 1–12, 2018, doi: 10.1128/AEM.02836-17.

1.7 Appendix 1 – Supplementary table 1 with all documents included in the systematic review

	YEAR	DOI	AUTHORS	TITLE	COUNTRY	CATEGORY	PLASMA SOURCE	VIRUS	RESULT
1	2023	https://doi.org/10.3390/ijms241814106	*Ashokkumar et al.*	Persistence of Coronavirus on Surface Materials and Its Control Measures Using Nonthermal Plasma and Other Agents	South Korea	Reviews			
2	2023	https://doi.org/10.3389/finsc.2023.1216291	*Cook S. et al.*	Deformed wing virus of honey bees is inactivated by cold plasma ionized hydrogen peroxide	USA	PTLs	Corona	Deformed wing virus	~10^5 - fold reduction in viral infectivity
3	2023	https://doi.org/10.1016/j.envint.2023.108285	*Filipić A. et al.*	Cold plasma within a stable supercavitation bubble – A breakthrough technology for efficient inactivation of viruses in water	Slovenia	Liquids	Corona	MS2 bacteriophage	5 log reduction
4	2023	https://doi.org/10.1007/s11356-023-30298-x	*Hamza I. A. et al.*	Cold atmospheric plasma: a sustainable approach to inactivating viruses, bacteria, and protozoa with remediation of organic pollutants in river water and wastewater	Egypt	Liquids	Corona	PhiX174, Rotavirus	Full inactivation
5	2023	https://doi.org/10.1038/s41598-023-37014-2	*Jangra R. et al.*	Efficient deactivation of aerosolized pathogens using a dielectric barrier discharge based cold-plasma detergent in environment device for good indoor air qualitys	India	Bioaerosols	Surface DBD	MS2 bacteriophage	5 log reduction
6	2023	https://doi.org/10.1016/j.jare.2022.03.002	*Kaushik N. et al.*	The inactivation and destruction of viruses by reactive oxygen species generated through physical and cold atmospheric plasma techniques: Current status and perspectives	South Korea	Reviews			
7	2023	https://doi.org/10.1080/10408398.2022.2077298	*Kulawik et al.*	Recent developments in the use of cold plasma, high hydrostatic pressure, and pulsed electric fields on microorganisms and viruses in seafood	China	Reviews			
8	2023	https://doi.org/10.3390/biomedicines11010122	*Mohamed H. et al.*	Immunomodulatory Effects of Non-Thermal Plasma in a Model for Latent HIV-1 Infection: Implications for an HIV-1-Specific Immunotherapy	USA	Fundamentals	DBD	Human Immunodeficiency Virus type 1 (HIV-1)	
9	2023	https://doi.org/10.1021/acssuschemeng.2c07622	*Sahun M. et al.*	Inactivation of SARS-CoV-2 and Other Enveloped and Non-Enveloped Viruses with Non-Thermal Plasma for Hospital Disinfection	Belgium	Fundamentals	DBD	SARS-CoV-2, Porcine Respiratory Coronavirus, Coxsackievirus B3	
10	2023	https://doi.org/10.3390/ijms24054673	*Sutter at al.*	Manipulation of Oxidative Stress Responses by Non-Thermal Plasma to Treat Herpes Simplex Virus Type 1 Infection and Disease	USA	Reviews		Herpses simplex virus 1 - HSV-1	
11	2023	https://doi.org/10.3390/bioengineering10030280	*Thomas S. V. et al.*	Inactivation of SARS-CoV-2 on Surfaces by Cold-Plasma-Generated Reactive Species	USA	Fundamentals	DBD jet	SARS-CoV-2 Pseudotyped Lentivirus	
12	2023	https://doi.org/10.1093/jambio/lxad181	*Upadrasta A. et al.*	In situ g ener ation of cold atmospheric plasma-activated mist and its biocidal activity against surrogate viruses for COVID-19	Ireland	PTLs	Corona jet	Phi6, PhiX174, MS2 bacteriophage	7,4 log reduction, 3,1 log reduction, 1,26 log reduction

13	2023	https://doi.org/10.1615/PlasmaMed.2023051186	*Wang H. et al.*	Application of NaCl in Cold Atmospheric Plasma Jet and Plasma-Activated Solution to Enhance Virus Inactivation	China	Fundamentals	DBD jet	MS2 bacteriophage	
14	2023	https://doi.org/10.1016/j.jwpe.2023.103839	*Zver M. et al.*	Non-thermal plasma inactivation of viruses in water solutions	Slovenia	Reviews			
15	2022	https://doi.org/10.1038/s41598-022-13444-2	*Abdel-Wahed M.S. et al.*	Removal of chemical and microbial water pollutants by cold plasma combined with Ag/TiO2-rGO nanoparticles	Egypt	Liquids	Corona	PhiX174 bacteriophage, Adenovirus, Rotavirus	5.5 log reduction, 6 log reduction, 4.3 log reduction
16	2022	https://doi.org/10.1007/s11356-021-17486-3	*Assadi I. et al.*	Review on inactivation of airborne viruses using non-thermal plasma technologies: from MS2 to coronavirus	France	Reviews			
17	2022	https://doi.org/10.1016/j.envres.2021.111765	*Berry G. et al.*	A review of methods to reduce the probability of the airborne spread of COVID-19 in ventilation systems and enclosed spaces	USA	Reviews			
18	2022	https://doi.org/10.1002/ppap.202200054	*Bhartiya P. et al.*	Nonthermal plasma-generated ozone inhibits human coronavirus 229E infectivity on glass surface	South Korea	Surfaces	DBD	Human coronavirus 229E	2.1 log reduction (D, NB)
19	2022	https://doi.org/10.1002/ppap.202100133	*Bisag et al.*	Cold atmospheric plasma decontamination of SARS-CoV-2 bioaerosols	Italy	Bioaerosols	DBD	SARS-CoV-2	Full inactivation
20	2022	https://doi:10.1002/ppap.202200012	*Chen Z. et al.*	Cold atmospheric plasma for addressing the COVID-19 pandemic	USA	Reviews			
21	2022	https://doi.org/10.1038/s41598-021-04360-y	*Cortázar O.D. et al.*	Vulnerability of SARS-CoV-2 and PR8 H1N1 virus to cold atmospheric plasma activated media	Spain	PTLs	DBD jet	SARS-CoV-2, Influenzavirus A PR8 H1N1	ND
22	2022	https://doi.org 10.1111/1541-4337.12909	*Ezzatpanah H. et al.*	New food safety challenges of viral contamination from a global perspective: Conventional, emerging, and novel methods of viral control	Finland	Reviews			
23	2022	https://doi.org/10.1016/j.chemosphere.2022.136655	*Fu J. et al.*	Viral disinfection using nonthermal plasma: A critical review and perspectives on the plasma-catalysis system	Canada	Reviews			
24	2022	https://doi:10.1007/s11356-022-21160-7	*Guesmi A. et al.*	Disinfection of corona and myriad viruses in water by non-thermal plasma: a review	France	Reviews			
25	2022	https://doi.org/10.3390/v14122685	*Han I. et al.*	Nonthermal Biocompatible Plasma Inactivation of Coronavirus SARS-CoV-2: Prospects for Future Antiviral Applications	South Korea	Reviews			
26	2022	https://doi.org/10.7150/ijbs.71983	*Han P. et al.*	Cold Atmospheric Plasma Boosts Virus Multiplication via EGFR(Tyr1068) Phosphorylation-Mediated Control on Cell Mitophagy	China	Fundamentals	DBD jet	Infectious bovine rhinotracheitis virus (IBRV)	
27	2022	https://doi.org/10.1038/s41598-022-23660-5	*He J.J. et al.*	Plasma-generated reactive water mist for disinfection of N95 respirators laden with MS2 and T4 bacteriophage viruses	USA	Surfaces	DBD	MS2 Bacteriophage, T4 bacteriophage	2 log reduction (D, NB), 3 log reduction (D, NB)
28	2022	https://doi.org/10.1016/j.tifs.2022.04.006	*Jenns K. et al.*	Inactivation of foodborne viruses: Opportunities for cold atmospheric plasma	Australia	Reviews			
29	2022	https://doi.org/10.1039/D2RA00009A	*Khanikar R.R. et al.*	Cold atmospheric pressure plasma for attenuation of SARS-CoV-2 spike protein binding to ACE2 protein and the RNA deactivation	India	Fundamentals	DBD jet	SARS-CoV-2	

30	2022	https://doi:10.1111/jam.15599	*Kramer B. et al.*	Disinfection of an ambulance using a compact atmospheric plasma device	Germany	Surfaces	DBD	Φ6 bacteriophage	> 4.4 log reduction (D, NB)
31	2022	https://doi.org/10.1080/10408398.2022.2077298	*Kulawik P. et al.*	Recent developments in the use of cold plasma, high hydrostatic pressure, and pulsed electric fields on microorganisms and viruses in seafood	China	Reviews			
32	2022	https://doi.org/10.1016/j.freeradbiomed.2022.08.026	*Mrochen D.M. et al.*	Toxicity and virucidal activity of a neon-driven micro plasma jet on eukaryotic cells and a coronavirus	Germany	Fundamentals	DBD jet	Mouse Hepatitis virus	
33	2022	https://doi.org/10.1007/s11090-022-10269-9	*Nagar V. et al.*	Evaluation of Virucidal Efficacy of Cold Plasma on Bacteriophage Inside a Three-Layered Sterilization Chamber	India	Surfaces	Others	P2 bacteriophage	> 2 log reduction (ND)
34	2022	http://dx.doi.org/10.4274/mjima.galenos.2021.2021.12	*Nikmaram A. et al.*	The application of non-chloride-based disinfectants in inactivation of sars-cov-2 in personal protective equipment, air and surfaces of hospitals	Cyprus	Reviews			
35	2022	https://doi.org/10.33640/2405-609X.3234	*Nur M. et al.*	A Successful Elimination of Indonesian SARS-CoV-2 Variants and Airborne Transmission Prevention by Cold Plasma in Fighting COVID-19 Pandemic: A Preliminary Study	Indonesia	Bioaerosols	Others	SARS-CoV-2	23% of viral load reduction
36	2022	https://doi.org/10.3389/fbioe.2022.815393	*Obrová K. et al.*	Decontamination of High-Efficiency Mask Filters from Respiratory Pathogens Including SARS-CoV-2 by Non-thermal Plasma	Austria	Surfaces	Corona	SARS-CoV-2, Adenovirus, Rhinovirus, Influenza A virus H1N1	Full inactivation (D, NB)
37	2022	https://10.3390/buildings12101587	*Pourchez J. et al.*	Antimicrobial Performance of an Innovative Technology of Atmospheric Plasma Reactors against Bioaerosols: Effectiveness in Removing Airborne Viable Viruses	France	Bioaerosols	Others	Phage phi-11	6 log reduction
38	2022	https://doi.org/10.1016/j.jhazmat.2022.128414	*Qin H. et al.*	Efficient disinfection of SARS-CoV-2-like coronavirus, pseudotyped SARS-CoV-2 and other coronaviruses using cold plasma induces spike protein damage	China	PTLs	DBD jet	Pangolin coronavirus GX , Porcine epidemic diarrhea virus - PED	Inhibition rate > 99%
39	2022	https://doi:10.1088/1361-6463/ac6a8c	*Sasaki S. et al.*	Human coronavirus inactivation by atmospheric pressure helium plasma	Japan	Fundamentals	Corona jet	Human coronavirus 229E	
40	2022	https://doi.org/10.1111/jfs.12988	*Thirumdas R.*	Inactivation of viruses related to foodborne infections using cold plasma technology	India	Reviews			
41	2022	https://doi.org/10.3390/pr10030554	*Todorova Y. et al.*	Non-Thermal Atmospheric Plasma for Microbial Decontamination and Removal of Hazardous Chemicals: An Overview in the Circular Economy Context with Data for Test Applications of Microwave Plasma Torch	Bulgaria	Reviews			
42	2022	https://doi.org/10.1016/j.ifset.2022.103121	*Velebit B. et al.*	Efficacy of cold atmospheric plasma for inactivation of viruses on raspberries	Croatia	Surfaces	Corona	Murine norovirus, Hepatitis A virus (HAV)	4 log reduction (W, B)
43	2022	https://doi.org/10.1002/ppap.202200196	*Von Woedtke T. et al.*	Oral SARS-CoV-2 reduction by local treatment: A plasma technology application?	Germany	Reviews			

44	2022	https://doi.org/10.1088/1361-6463/ac360e	*Wang H. et al.*	Reactive force field-based molecular dynamics simulation of the interaction between plasma reactive oxygen species and the receptor-binding domain of the spike protein in the capsid protein of SARS-CoV-2	China	Fundamentals			
45	2022	https://doi.org/10.7150/thno.70098	*Wang P. et al.*	Cold atmospheric plasma for preventing infection of viruses that use ACE2 for entry	China	PTLs	DBD jet	SARS-CoV-2	/
46	2022	https://doi.org/10.1016/j.nbt.2021.10.001	*Wolfgruber S. et al.*	SARS-CoV-2 neutralizing activity of ozone on porous and non-porous materials	Austria	Surfaces	Others	SARS-CoV-2	6 log reduction (W, NB)
47	2021	https://doi.org/10.3390/app11094177	*Capelli et al.*	Decontamination of food packages from SARS-COV-2 RNA with a cold plasma-assisted system	Italy	Surfaces	Surface DBD	SARS-CoV-2	Full inactivation (D, NB)
48	2021	https://doi.org/10.3390/life11121333	*Csadek I. et al.*	Nitrogen Accumulation in Oyster (Crassostrea gigas) Slurry Exposed to Virucidal Cold Atmospheric Plasma Treatment	Austria	Fundamentals	Surface DBD	Bovine coronavirus BCoV, Equid alhaherpesvirus (EHV-1)	
49	2021	https://doi.org/10.1002/slct.202004716	*El-Kalliny A.S. et al.*	Efficacy of Cold Atmospheric Plasma Treatment on Chemical and Microbial Pollutants in Water	Egypt	Liquids	Corona	Rotavirus, phiX174	4.3 log reduction, 5 log reduction
50	2021	https://doi.org/10.3389/fmicb.2021.618209	*Filipić A. et al.*	Inactivation of Pepper Mild Mottle Virus in Water by Cold Atmospheric Plasma	Slovenia	Liquids	Corona jet	Pepper mild mottle virus	Full inactivation
51	2021	https://doi.org/10.1088/1361-6595/abf51b	*Gao H. et al.*	Atmospheric-pressure non-equilibrium plasmas for effective abatement of pathogenic biological aerosols	Australia	Reviews			
52	2021	https://doi.org/10.1007/s11356-021-16741-x	*Gururani P. et al.*	Cold plasma technology: advanced and sustainable approach for wastewater treatment	India	Reviews			
53	2021	https://doi.org/10.1016/j.foodres.2021.110108	*Huang Y.M. et al.*	Inactivation of norovirus by atmospheric pressure plasma jet on salmon sashimi	Taiwan	Surfaces	Corona jet	Human norovirus	Full inactivation (W, B)
54	2021	https:// doi: 10.1063/5.0060530	*Jin et al.*	Cold atmospheric plasma: A non-negligible strategy for viral RNA inactivation to prevent SARS-CoV-2 environmental transmission	China	Fundamentals	DBD	SARS-CoV-2	
55	2021	https://doi.org/10.3390/life11121292	*Le Bras F. et al.*	Inactivation of Enveloped Bovine Viral Diarrhea Virus and Non-Enveloped Porcine Parvovirus Using Low-Pressure Non-Thermal Plasma	France	Surfaces	Others	Bovine viral diarrhea virus (BVDV), porcine parvovirus	> 4 log reduction (D, NB)
56	2021	https://doi.org/10.3390/foods10061214	*Lee E.S. et al.*	Microbial inactivation and quality preservation of chicken breast salad using atmospheric dielectric barrier discharge cold plasma treatment	South Korea	Surfaces	DBD	Tulane virus	1 log reduction (D, NB)
57	2021	https://doi.org/10.1080/21505594.2021.1883933	*Miao Y. et al..*	Cold atmospheric plasma increases IBRV titer in MDBK cells by orchestrating the host cell network	China	Fundamentals	DBD jet	Bovine rhinotracheitis virus	
58	2021	https://doi.org/10.3389/fphy.2021.683118	*Mohamed H. et al.*	Non-Thermal Plasma as a Novel Strategy for Treating or Preventing Viral Infection and Associated Disease	USA	Reviews			
59	2021	https://doi.org/10.1111/jfs.12919	*Mohammadi et al.*	Inactivation of viruses using nonthermal plasma in viral suspensions and foodstuff: A short review of recent studies	Iran	Reviews			

60	2021	https://doi.org/10.1063/5.0062787	*Szili E.J. et al.*	On-demand cold plasma activation of acetyl donors for bacteria and virus decontamination	UK	Fundamentals	DBD jet	SARS-CoV-2	
61	2021	https://doi.org/10.3390/biomedicines9091259	*Yan D. et al.*	Multi-modal biological destruction by cold atmospheric plasma: Capability and mechanism	USA	Reviews			
62	2020	https://doi.org/10.1016/j.fm.2019.103307	*Aboubakr H. A. et al.*	In situ inactivation of human norovirus GII.4 by cold plasma: Ethidium monoazide (EMA)-coupled RT-qPCR underestimates virus reduction and fecal material suppresses inactivation	USA	Surfaces	Surface DBD	Human norovirus, Feline calicivirus	2.9 log reduction, >5 log reduction (W, NB,B)
63	2020	https://doi.org/10.1109/MERCon50084.2020.9185237	*Bekeschus et al.*	Gas Plasma Technology-An Asset to Healthcare during Viral Pandemics Such as the COVID-19 Crisis?	Italy	Reviews			
64	2020	https://doi.org/10.1002/ppap.202000154	*Bisag et al.*	Cold atmospheric plasma inactivation of aerosolized microdroplets containing bacteria and purified SARS-CoV-2 RNA to contrast airborne indoor transmission	Italy	Bioaerosols	DBD	SARS-CoV-2	Full inactivation
65	2020	https://doi.org/10.1099/jgv.0.001382	*Bunz O. et al.*	Cold atmospheric plasma as antiviral therapy – effect on human herpes simplex virus type 1	Germany	Fundamentals	DBD jet	Herpses simplex virus 1 - HSV-1	
66	2020	https://doi.org/10.1063/5.0031332	*Chen Z. et al.*	Cold atmospheric plasma for SARS-CoV-2 inactivation	USA	Surfaces	DBD jet	SARS-CoV-2	Full inactivation (D, NB)
67	2020	https://doi.org/10.3390/foods9121731	*Choi M. S. et al.*	Virucidal Effects of Dielectric Barrier Discharge Plasma on Human Norovirus Infectivity in Fresh Oysters (Crassostrea gigas)	South Korea	Surfaces	DBD	Norovirus	1.68 log reduction (W, B)
68	2020	https://doi.org/10.1016/j.tibtech.2020.04.003	*Filipić A. et al.*	Cold Plasma, a New Hope in the Field of Virus Inactivation	Slovenia	Review			
69	2020	https://doi.org/10.3390/app10186301	*Lee E.S. et al.*	Evaluation of in-package atmospheric dielectric barrier discharge cold plasma treatment as an intervention technology for decontaminating bulk ready-to-eat chicken breast cubes in plastic containers	South Korea	Surfaces	DBD	Tulane virus	1.08 log reduction (D, B)
70	2020	https://doi.org/10.1088/1361-6463/aba066	*Moldgy A. et al.*	Inactivation of virus and bacteria using cold atmospheric pressure air plasmas and the role of reactive nitrogen species	USA	Surfaces	DBD, 2D DBD, volumetric DBD, gliding arc	Felice calicivirus	> 4 log reduction (W, D, NB)
71	2020	https://doi.org/10.1002/ppap.201900234	*Moldgy A. et al.*	Comparative evaluation of the virucidal effect of remote and direct cold air plasmas with UV-C	USA	Surfaces	Surface DBD, DBD, 2D DBD	Feline calicivirus	Full inactivation (W, NB)
72	2020	https://doi.org/10.1002/ppap.201900269	*Nayak et al.*	Rapid inactivation of airborne porcine reproductive and respiratory syndrome virus using an atmospheric pressure air plasma	USA	Bioaerosols	Volumetric DBD	PRRS virus	3.5 log reduction
73	2020	https://doi.org/10.3390/foods9111520	*Pexara A. et al.*	Foodborne viruses and innovative non-Thermal food-Processing technologies	Greece	Review			

74	2020	https://doi.org/10.1016/j.lwt.2020.109429	*Roh S.H. et al.*	Inactivation of Escherichia coli O157:H7, Salmonella, Listeria monocytogenes, and Tulane virus in processed chicken breast via atmospheric in-package cold plasma treatment	South Korea	Surfaces	DBD	Tulane virus	2.2 log reduction (D, B)
75	2020	https://doi.org/10.13031/aea.13699	*Schiappacasse C. et al.*	Inactivation of Aerosolized Newcastle Disease Virus with Non-thermal Plasma	USA	Bioaerosols	DBD	Newcastle disease virus	Full inactivation
76	2020	https://doi.org/10.3390/foods9101435	*Varilla C. et al.*	Potential of cold plasma technology in ensuring the safety of foods and agricultural produce: A review	USA	Review			
77	2020	https://doi.org/10.1016/j.jhazmat.2020.122266	*Xia T. et al.*	Inactivation of airborne porcine reproductive and respiratory syndrome virus (PRRSv) by a packed bed dielectric barrier discharge non-thermal plasma	USA	Bioaerosols	Packed Bed NTP	Porcine reproductive and respiratory syndrome virus (PRRSv)	1.3 log reduction
78	2019	https://doi.org/10.1007/s12560-019-09388-y	*Filipić A. et al.*	Cold Atmospheric Plasma as a Novel Method for Inactivation of Potato Virus Y in Water Samples	Slovenia	Liquids	Corona jet	Potato virus Y	Full inactivation
79	2019	https://doi.org/10.33073/pjm-2019-028	*Niedzwiedz et al.*	The state of research on antimicrobial activity of cold plasma	Poland	Reviews			
80	2019	https://doi.org/10.1109/IAS.2019.8912457	*Xia T. et al.*	Field Operations of a Pilot Scale Packed-bed Non-thermal Plasma (NTP) Reactor Installed at a Pig Barn on a Michigan Farm to Inactivate Airborne Viruses	USA	Bioaerosols	Packed Bed NTP	Porcine reproductive and respiratory syndrome virus (PRRSv)	ND
81	2019	https://doi.org/10.1088/1361-6463/ab1466	*Xia T. et al.*	Inactivation of airborne viruses using a packed bed non-thermal plasma reactor	USA	Bioaerosols	Packed Bed NTP	MS2 phage	2.3 log reduction
82	2018	https://doi.org/10.1371/journal.pone.0194618	*Aboubakr H.A. et al.*	Cold argon-oxygen plasma species oxidize and disintegrate capsid protein of feline calicivirus	USA	Fundamentals	DBD jet	Feline Calicivirus	
83	2018	https://doi.org/10.1371/journal.pone.0202352	*Bunz et al.*	Effect of cold atmospheric plasma (CAP) on human adenoviruses is adenovirus type-dependent	Germany	Fundamentals	DBD jet	Human Adenoviruses (HAdVs)	
84	2018	https://doi.org/10.1128/AEM.00726-18	*Guo L. et al.*	Mechanism of virus inactivation by cold atmospheric-pressure plasma and plasma activated water	China	Fundamentals	Surface DBD	Bacteriophages T4, phi174, and MS2	
85	2018	https://doi.org/10.1007/s00705-018-3909-4	*Hanbal S. E. et al.*	Atmospheric-pressure plasma irradiation can disrupt tobacco mosaic virus particles and RNAs to inactivate their infectivity	Japan	Fundamentals	DBD	Tobacco mosaic virus (TMV)	
86	2018	https://doi.org/10.1128/AEM.02836-17	*Su et al.*	Inactivation Efficacy of Nonthermal Plasma-Activated Solutions against Newcastle Disease Virus	China	PTLs	DBD jet	Newcastle disease virus (NDV)	Full inactivation
87	2018	https://DOI:10.1038/s41598-018-36779-1	*Yamashiro R. et al.*	Key role of singlet oxygen and peroxynitrite in viral RNA damage during virucidal effect of plasma torch on feline calicivirus	Japan	Fundamentals	DBD	Feline calicivirus	
88	2017	https://doi.org/10.1615/PlasmaMed.2017019479	*Brun P. et al.*	Mechanisms of wound healing and disinfection in a plasma source for the treatment of corneal infections	Italy	Fundamentals	DBD jet	Herpses simplex virus 1 - HSV-1	
89	2017	https://doi.org/10.1016/j.fm.2016.10.030	*Lacombe A. et al.*	Nonthermal inactivation of norovirus surrogates on blueberries using atmospheric cold plasma	USA	Surfaces	Others	Tulane virus, murine norovirus (MNV)	3.5 log reduction, 5 log reduction (W, B)

90	2017	https://doi.org/10.1002/ppap.201700119	*Nayak et al.*	Reactive species responsible for the inactivation of feline calicivirus by a two-dimensional array of integrated coaxial microhollow dielectric barrier discharges in air	USA	Surfaces	Surface DBD	Feline Calicivirus	Full incativation (W, D, NB)
91	2017	https://doi.org/10.1002/jmv.24701	*Weiss M. et al.*	Virucide properties of cold atmospheric plasma for future clinical applications	Germany	Reviews			
92	2016	https://doi.org/10.1088/0022-3727/49/20/204001	*Aboubakr H. A. et al.*	Inactivation of virus in solution by cold atmospheric pressure plasma: Identification of chemical inactivation pathways	USA	Fundamentals	DBD jet	Feline calicivirus	
93	2016	https://doi.org/10.1016/j.ijfoodmicro.2016.08.025	*Min S. et al.*	Dielectric barrier discharge atmospheric cold plasma inhibits Escherichia coli O157:H7, Salmonella, Listeria monocytogenes, and Tulane virus in Romaine lettuce	USA	Surfaces	DBD	Tulane virus	1.3 log reduction (W, B)
94	2016	https://doi.org/10.1007/s11356-021-17486-3	*Puligundla et al.*	Non-thermal plasmas (NTPs) for inactivation of viruses in abiotic environment	South Korea	Reviews			
95	2016	https://doi.org/10.1371/journal.pone.0165322	*Volotskova et al.*	Cold atmospheric plasma inhibits HIV-1 replication in macrophages by targeting both the virus and the cells	USA	Fundamentals	DBD jet	Herpses simplex virus 1 - HSV-1	
96	2016	https://doi.org/10.1016/j.vaccine.2015.10.099	*Wang G. et al.*	Non-thermal plasma for inactivated-vaccine preparation	China	Fundamentals	Corona jet	Newcastle disease virus, H9N2 avian influenza virus	
97	2015	https://doi.org/10.1128/AEM.00054-15	*Aboubakr H. A. et al.*	Virucidal effect of cold atmospheric gaseous plasma on feline calicivirus, a surrogate for human norovirus	USA	Fundamentals	DBD jet	Feline calicivirus	
98	2015	https://doi.org/10.1128/mBio.02300-14	*Ahlfeld B. et al.*	Inactivation of a foodborne norovirus outbreak strain with nonthermal atmospheric pressure plasma	Germany	Surfaces	Surface DBD	Human norovirus (NoV)	1.69 log reduction (W, B)
99	2015	https://doi.org/10.1016/j.foodres.2015.06.039	*Bae S. C. et al.*	Inactivation of murine norovirus-1 and hepatitis A virus on fresh meats by atmospheric pressure plasma jets	South Korea	Surfaces	Corona jet	murine norovirus (MNV-1), hepatitis A virus (HAV)	2 log reduction (W, B)
100	2015	https://doi.org/10.1128/AEM.03322-14	*Wu Y. et al.*	MS2 virus inactivation by atmospheric-pressure cold plasma using different gas carriers and power levels	USA	Bioaerosols	DBD	MS2 bacteriophages	> 2 log reduction
101	2014	https://doi.org/10.2741/e692	*Sakudo A. et al.*	N_2 gas plasma inactivates influenza virus mediated by oxidative stress	Japan	Fundamentals	Others	Influenza A virus H1N1 and Influenza B	
102	2014	https://doi.org/10.1109/TIA.2013.2274260	*Tanaka et al.*	Analysis of the Inactivation Mechanism of Bacteriophage phi X174 by Atmospheric Pressure Discharge Plasma	Japan	Fundamentals	DBD	phiX174	
103	2013	https://doi.org/10.1111/jam.12331	*Alshraiedeh N. H. et al.*	Atmospheric pressure, nonthermal plasma inactivation of MS2 bacteriophage: Effect of oxygen concentration on virucidal activity	UK	Fundamentals	DBD jet	MS2 bacteriophages	
104	2013	http://dx.doi.org/10.1155/2013/694269	*Sakudo A. et al.*	N_2 Gas plasma inactivates influenza virus by inducing changes in viral surface morphology, protein, and genomic RNA	Japan	Fundamentals	Others	Influenza A virus H1N1 and Influenza B	
105	2012	https://doi.org/10.1371/journal.pone.0033245	*Braun P. et al.*	Disinfection of ocular cells and tissues by atmospheric-pressure cold plasma	Italy	Fundamentals	DBD jet	Herpes simplex virus-1	
106	2012	https://doi.org/10.1109/TPS.2012.2210567	*Shi X.M. et al.*	Effect of Low-Temperature Plasma on Deactivation of Hepatitis B Virus	China	Fundamentals	DBD	Hepatitis B virus (HBV)	

107	2011	https://doi.org/10.1088/0022-3727/44/50/505201	*Zimmermann et al.*	Effects of cold atmospheric plasmas on adenoviruses in solution	Germany	Fundamentals	Surface DBD	Adenovirus	
108	2010	https://doi.org/10.1002/ppap.200900088	*Yasuda et al.*	Biological evaluation of DNA damage in bacteriophages inactivated by atmospheric pressure cold plasma	Japan	Surfaces	DBD	Λ phage	ND
109	2009	https://doi.org/10.1016/j.jcv.2009.03.017	*Terrier O. et al.*	Cold oxygen plasma technology efficiency against different airborne respiratory viruses	France	Bioaerosols	Others	Influenza virus type A, human parainfluenza virus type 3, RSV	4 log reduction, 6.5 log reduction, 3.8 log reduction
110	2007	https://doi.org/10.1088/0022-3727/40/2/026	*Nojima H. et al.*	Novel atmospheric pressure plasma device releasing atomic hydrogen: Reduction of microbial-contaminants and OH radicals in the air	Japan	Bioaerosols	Others	Human influenza A virus	2.39 log reduction

ND = Not Defined
D = Dry treatment
W = Wet treatment
B = Biological substrate
NB= Non Biological substrate
* The best result was reported in the case of studies with different results.

1.8 Appendix 2 – Supplementary table 2 with all identified viruses in experimental articles

Included viruses in the articles	#	*Natural hosts*	*Transmission*	*Baltimore class*	*Order*	*Family*	*Genus*	*Enveloped/Non-enveloped*	*Virion size*
SARS-CoV-2	13	Vertebrates	Respiratory droplets, fecal-oral route	IV - ssRNA(+)	Nidovirales	Coroviridae	Betacoronavirus	Enveloped	120-160 nm
MS2 bacteriophage	9	Bacteria		IV - ssRNA(+)	Norzivirales	Fiersviridae	Emesvirus	Non-enveloped	26 nm
Feline Calicivirus	8	Feline	fecal-oral route	IV - ssRNA(+)	Picornavirales	Caliciviridae	Vesivirus	Non-enveloped	27-40 nm
Norovirus	4	Human/mammals	Fecal-ora route from contaminated water and food	IV - ssRNA(+)	Picornavirales	Caliciviridae	Norovirus	Non-enveloped	38-40 nm
Tulane virus	4	Vertebrates	Fecal-oral route	IV - ssRNA(+)	Picornavirales	Caliciviridae	Recovirus	Non-enveloped	27-40 nm
Adenovirus	4	Vertebrates	Respiratory droplets, fecal-oral route	I - dsDNA	Rowavirales	Adenoviridae		Non-enveloped	90 nm
Herpes simplex virus 1 - HSV-1	4	Vertebrates	Contact with lesions and body fluids	I - dsDNA	Herpesvirales	Herpesviridae	Simplexvirus	Enveloped	150-200 nm
PhiX174 bacteriophage	3	Bacteria	Passive diffusion	II - ssDNA(+)	Petitvirales	Microviridae	Sinsheimervirus	Non-enveloped	30 nm
Murine Norovirus (MNV)	3	Mice	Fecal-oral route from contaminated water and food	IV - ssRNA(+)	Picornavirales	Caliciviridae	Norovirus	Non-enveloped	23-40 nm
Newcastle disease virus (NDV)	3	Birds	Direct contact with droppings and secretions from the nose, mouth, and eyes	V - ssRNA(-)	Mononegavirales	Paramyxoviridae	Orthoavulavirus	Enveloped	150 nm
Porcine reproductive and respiratory syndrome virus (PRRS virus) or Betaarterivirus suid 1	3	Vertebrates	Transplacental, saliva, urine, semen and respiratory tract secretions.	IV - ssRNA(+)	Nidovirales	Arteriviridae	Betaarterivirus	Enveloped	45-60 nm
Rotavirus	3	Human, Vertebrates. Rotaviruses generally exhibit substantial host-range restriction.	Fecal-oral	III - dsRNA	Rotavirus	Reoviridae	Rotavirus	Non-enveloped	80 nm
Phi174	3	Bacteria		II - ssDNA(+)	Microviridae	Microvirus genus	phiX174-like viruses	Non-enveloped	30 nm
Hepatitis A virus (HAV)	2	Human, Vertebrates	Fecal-oral, blood	IV - ssRNA(+)	Picornavirales	Picornaviridae	Hepatovirus	Non-enveloped	30 nm
Human coronavirus 229E	2	Vertebrates	Respiratory droplets, fecal-oral route	IV - ssRNA(+)	Nidovirales	Coronaviridae	Alphacoronavirus	Enveloped	120-160 nm
Influenzavirus A PR8 H1N1	2	Aquatic birds, Human, Pig, Horse, Seals	Mammals: Respiratory_ Zoonosis, animal contact_Birds: Fecal-oral route from contaminated water	V - ssRNA(-)	Articulavirales	Orthomyxoviridae	Alphainfluenzavirus	Enveloped	80-120 nm
Influenza A virus H1N1	2	Aquatic birds, Human, Pig, Horse, Seals	Mammals: Respiratory_ Zoonosis, animal contact_Birds: Fecal-oral route from contaminated water	V - ssRNA(-)	Articulavirales	Orthomyxoviridae	Alphainfluenzavirus	Enveloped	80-120 nm
Influenza B	2	Human	Respiratory	V - ssRNA(-)	Articulavirales	Orthomyxoviridae	Betainfluenzavirus	Enveloped	80-120 nm
Infectious bovine rhinotracheitis virus (IBRV) or Bovine herpesvirus-1	2	Vertebrates	contact with lesions and body fluids	I - dsDNA	Herpesvirales	Herpesviridae	Varicellovirus	Enveloped	150-200 nm

Included viruses in the articles	#	Natural hosts	Transmission	Baltimore class	Order	Family	Genus	Enveloped/Non-enveloped	Virion size
Phi 6	2	Pseudomonas bacteria		III - dsRNA	Mindivirales	Cystoviridae	Cystovirus	Enveloped	85 nm
P2 bacteriophage	1	Bacteria	Passive diffusion through medium	I - dsDNA	Caudovirales	Myoviridae	Peduovirus	Non-enveloped	60 nm
Bovine coronavirus (BCoV)	1	Occasional hosts: Human, cattle, pig, mouse, rat, and bat.	Zoonosis, respiratory, fomites	IV - ssRNA(+)	Nidovirales	Coronaviridae	Betacoronavirus	Enveloped	120-160 nm
MHV virus (Mouse Hepatitis virus)	1	Occasional hosts: Human, cattle, pig, mouse, rat, and bat	Zoonosis, respiratory, fomites	IV - ssRNA(+)	Nidovirales	Coronaviridae	Betacoronavirus	Enveloped	120-160 nm
Pangolin coronavirus GX	1	Vertebrates	Respiratory droplets, fecal-oral route	IV - ssRNA(+)	Nidovirales	Coronaviridae	Betacoronavirus	Enveloped	120-160 nm
Swine acute diarrhea syndrome coronavirus (SADS-CoV) o Rhinolophus bat coronavirus HKU2	1	Human, pig, cat, dog and bat	Zoonosis, fomite. Respiratory or fecal-oral in humans.	IV - ssRNA(+)	Nidovirales	Coronaviridae	Alphacoronavirus	Non-enveloped	27-40 nm
Porcine epidemic diarrhea virus - PEDV	1	Human, pig, cat, dog and bat	Zoonosis, fomite. Respiratory or fecal-oral in humans.	IV - ssRNA(+)	Nidovirales	Coronaviridae	Alphacoronavirus	Non-enveloped	27-40 nm
Equid alhaherpesvirus (EHV-1)	1	Mammals	contact with lesions and body fluids	I - dsDNA	Herpesvirales	Herpesviridae	Varicellovirus	Enveloped	150-200 nm
Pepper mild mottle virus	1	Plants		IV - ssRNA(+)	Tymovirales	Virgaviridae	Tobamovirus	Non-enveloped	20-25 nm
Potato Virus Y	1	Plants	/	IV - ssRNA(+)	Potyvirales	Potyviridae	Potyvirus	Non-enveloped	One filamentous (650-900 nm) or two filamentous (500-600 and 200-300 nm lengths)
Tobacco mosaic virus	1	Plants	/	IV - ssRNA(+)	Virales	Virgaviridae	Tobamovirus	Non-enveloped	18 nm diameter - 300 nm length
Influenzavirus A H9N2	1	Aquatic birds, Human, Pig, Horse, Seals	Mammals: Respiratory_ Zoonosis, animal contact_Birds: Fecal-oral route from contaminated water	V - ssRNA(-)	Articulavirales	Orthomyxoviridae	Alphainfluenzavirus	Enveloped	80-120 nm
Phage λ	1	Bacteria	Passive diffusion through medium	I - dsDNA	Caudovirales	Siphoviridae	Lambdavirus	Non-enveloped	60 nm
Influenzavirus A H4N2	1	Aquatic birds, Human, Pig, Horse, Seals	Mammals: Respiratory_ Zoonosis, animal contact_Birds: Fecal-oral route from contaminated water	V - ssRNA(-)	Articulavirales	Orthomyxoviridae	Alphainfluenzavirus	Enveloped	80-120 nm
Hepatitis B virus (HBV)	1	Human, Apes, Birds	Parental, sexual, blood.	VII - dsDNA	Ortervirales	Hepadnaviridae	Orthohepadnavirus	Enveloped	42 nm
Human Immunodeficiency Virus type 1 (HIV-1)	1	Human	Sexual, blood	VI - ssRNA(+)		Retroviridae	Lentivirus	Enveloped	80-120 nm
SARS-CoV-2 Pseudotyped Lentivirus	1	Experimental, not natural	Experimental, not natural	VI - ssRNA(+)		Retroviridae	Lentivirus	Enveloped	80-120 nm
Coxsackievirus B3	1	Humans	Fecal-oral	IV - ssRNA(+)	Picornavirales	Picornaviridae	Enterovirus	Non-enveloped	30 nm
Porcine respiratory coronavirus	1	Pig	Respiratory	IV - ssRNA(+)	Nidovirales	Coronaviridae	Alphacoronavirus	Enveloped	80-160 nm
Human Rhinovirus A	1	Human, mammals	Fecal-oral or respiratory	IV - ssRNA(+)	Picornavirales	Picornaviridae	Enterovirus	Non-enveloped	30 nm
Phage phi-11	1	Bacteria	Passive diffusion	I - dsDNA	Caudoviricetes	Azeredovirinae	Dubowvirus	Non-enveloped	60 nm
Deformed wing virus	1	Insects	Varroa mite transmission	IV - ssRNA(+)	Picornavirales	Iflaviridae	Iflavirus	Non-enveloped	30-35 nm

Chapter 2

Cold plasma systems for bioaerosol decontamination: a proof of concept

2.1 Introduction

2.1.1 Focus on bioaerosols

The recent pandemic outbreak of COVID-19 has raised widespread concerns about the importance of bioaerosols. They are aerosol particles of biological origins, mainly including viruses, fungi, and pollen [1]. The size distribution of bioaerosols originating from humans, animals, and plants ranges from 0.001 μm to 100 μm [1].

Many studies demonstrated that pathogenic microorganisms could be transmitted, besides through direct or indirect physical contact (as also highlighted for viruses in 1.1.2), also through the air in droplets (respiratory transmission) and aerosols (airborne transmission) [2]–[4]. Bioaerosols have the ability to remain airborne for extended periods and travel long distances, which plays a critical role in disease transmission. The WHO and the Centers for Disease Control and Prevention (CDC) classify particles larger than 5 μm as droplets, while those smaller than 5 μm are referred to as aerosols, with particles under 1 μm specifically termed droplet nuclei [5].

In indoor environments, human activity is the main responsible for the formation of bioaerosols in different ways, as illustrated in Figure 2.1.

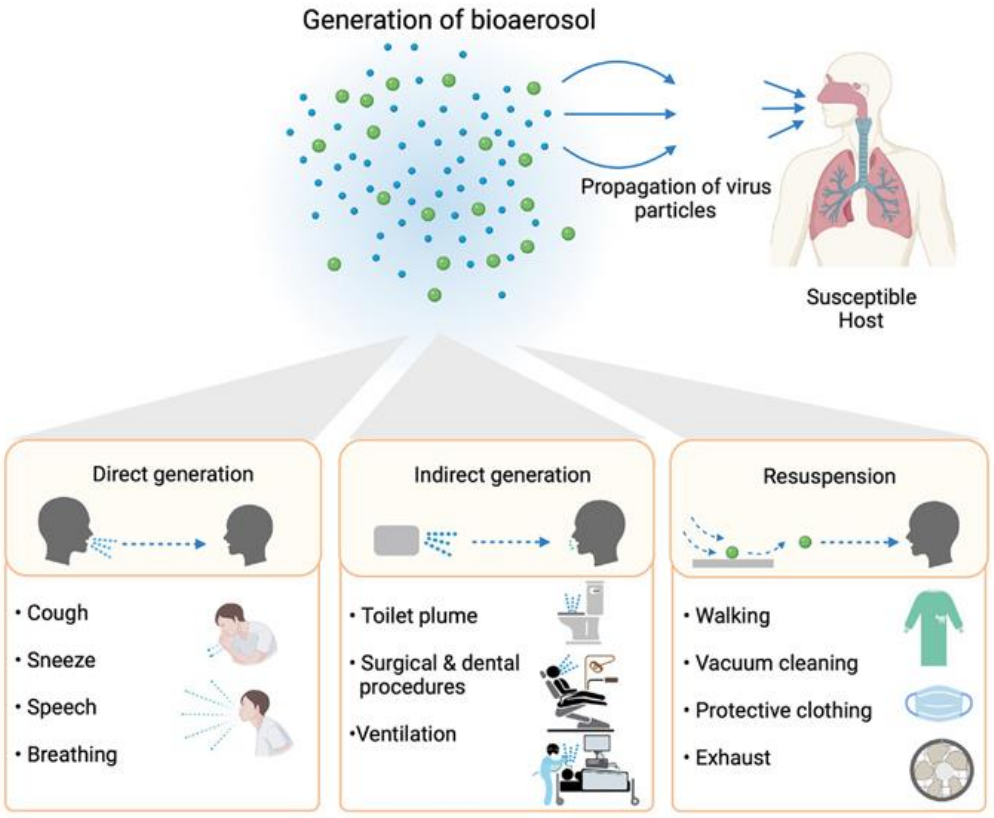

Figure 2.1 *– Different ways of bioaerosol generation. All rights to this image are owned by [6].*

Bioaerosols are generated directly when infected individuals cough, sneeze, speak, or even just breathe. Indirect generation occurs during activities such as toilet flushing, medical procedures, or mechanical ventilation. Additionally, bioaerosols can be produced by the resuspension of settled droplets, which is caused by mechanical forces from actions like walking, vacuuming, removing protective clothing, or the high-speed airflow of exhaust fans [6]. When droplets of various sizes are emitted from a source (e.g., a person), they are subject to two competing processes: sedimentation and evaporation [2]. As the droplet diameter decreases, evaporation becomes the dominant mechanism. Larger droplets are primarily influenced by gravity, and their sedimentation velocity can be estimated by approximating the droplet as a rigid sphere moving through still air. However, evaporation is more complex, as it involves a dynamic exchange of heat and mass at the droplet-air interface. Xie *et al.* [7] demonstrated that, in the absence of convection, a critical droplet size exists below which the particle evaporates entirely before it can fall (consistent with the earlier model proposed by Wells [8]). When convection is considered (focusing on mean airflow while neglecting turbulence), the behavior changes: larger droplets quickly settle due to gravity, intermediate-sized droplets exit the flow and evaporate completely before falling, and smaller droplets are carried by the airflow until they evaporate completely, forming aerosols. This aligns with the curves shown in Figure 2.2, based on an initial bioaerosol jet velocity of 10 m/s, which is comparable to the typical exhalation speed during a cough. Both the initial velocity and the surrounding relative humidity significantly affect how far a droplet travels before it either settles or evaporates [6]. Typically, larger droplets, influenced by gravity, settle to the ground from a height of 1 meter within approximately 5 seconds (Figure 2.3). However, during the sneeze, the largest particles can reach 50 m/s and travel up to 6 meters horizontally [9]. In contrast, smaller droplets can remain airborne for up to 30 minutes, traveling beyond 1 meter. These smaller droplets may also evaporate, reducing in size to form droplet nuclei or bioaerosols. These droplet nuclei can remain suspended in the air for extended periods, up to 12 hours, and travel distances of up to 45 meters, significantly increasing the risk of long-range infections [3][5][6][10][11][12].

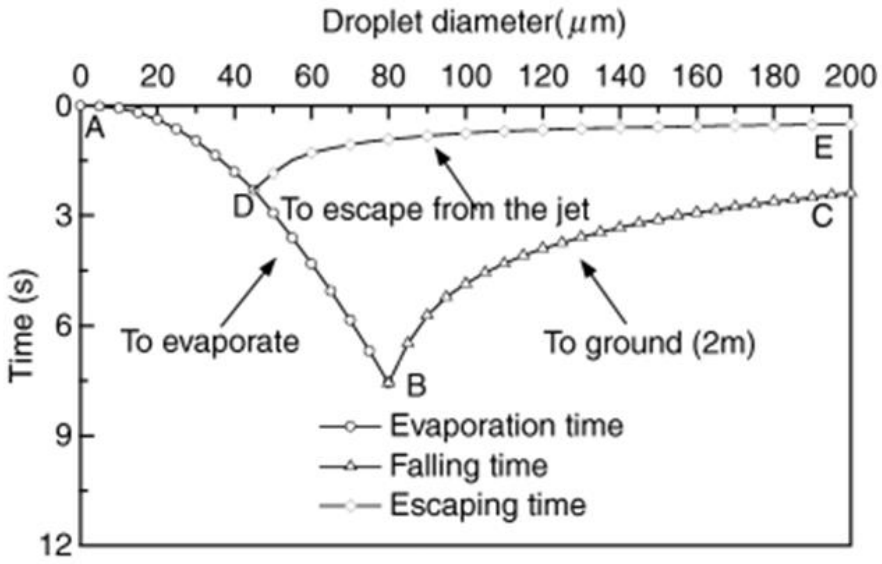

Figure 2.2 *- Evaporation time, falling time, and escape time of droplets of varying diameter. Curve AB represents the evaporation time, while Curve BC illustrates the fall time within a 2-meter distance. Curve DE corresponds to the jet escape time, with Point B marking the critical point in the process. All rights to this image are owned by* [7].

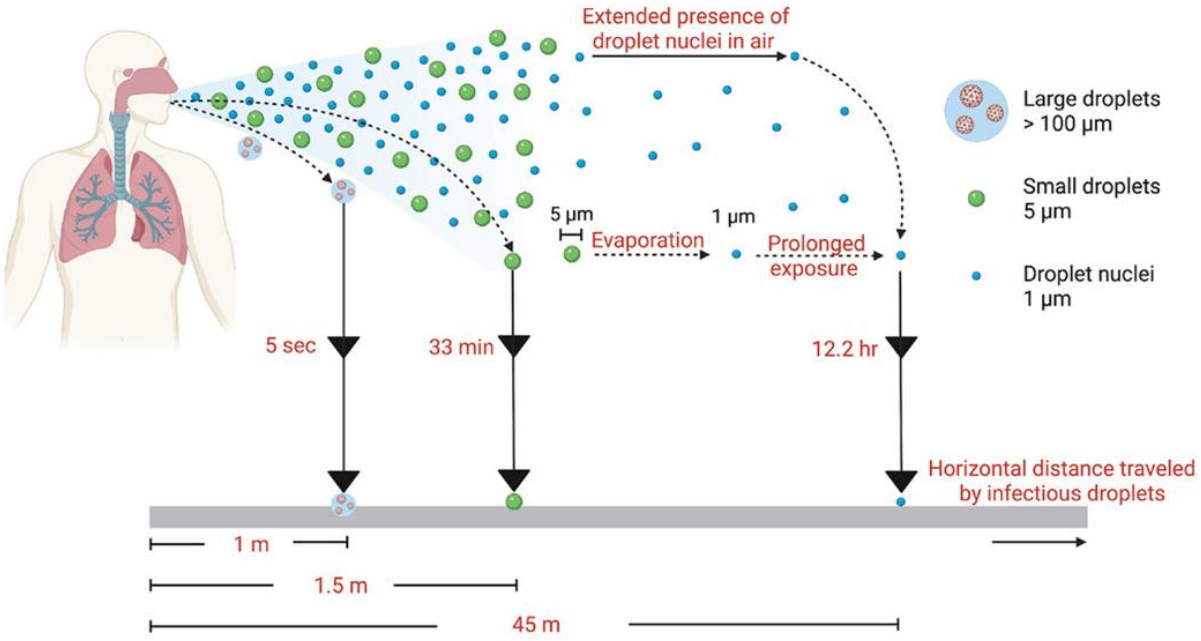

Figure 2.3 *- Trajectory, settling time, and conversion of droplets to droplet nuclei. All rights to this image are owned by [6].*

Finally, the trajectory and transmissibility of bioaerosols are complex and influenced by various factors, including environmental conditions like temperature and relative humidity.

These factors, along with the mechanisms of bioaerosol generation, significantly impact the viability and survival time of microorganisms within bioaerosols [13]-[15].

2.1.2 HAIs and COVID-19: the role of the airborne transmission

The airborne transmission of pathogens such as bacteria and viruses via aerosols is one of the most insidious ways of spreading diseases, such as COVID-19 and HAIs.

HAIs, also known as healthcare-associated infections, are infections that patients acquire while receiving care in healthcare settings such as hospitals, long-term care facilities, outpatient clinics, or even home care [16]. During medical care, patients can be exposed to various microorganisms from various sources, including other patients, healthcare personnel, or visitors [17]. The most common vectors for these infectious agents are patients themselves, medical devices or equipment, the hospital environment, healthcare workers, contaminated drugs, food, and patient care equipment [2],[17].

Pathogens responsible for HAIs include bacteria, viruses, and fungi. The prevalence of specific pathogens can vary depending on the healthcare setting, geographic location, and patient population. Bacterial infections are the most frequent, followed by viral and fungal infections. Among Gram-positive bacteria, common culprits include coagulase-negative *Staphylococci*, *Staphylococcus aureus*, *Streptococcus* species, and *Enterococcus* species, such as *Escherichia faecalis* and *Escherichia faecium* [18]. *Clostridium difficile* is the most commonly reported HAI pathogen in U.S. hospitals, responsible for approximately 15% of infections [19][20]. Gram-negative bacteria, particularly those from the Enterobacteriaceae family, have a significant role, such as *Klebsiella pneumoniae*, *Klebsiella oxytoca*, *Escherichia coli*, *Proteus mirabilis*, and *Enterobacter* species. Other notable Gram-negative pathogens include *Pseudomonas aeruginosa*, *Acinetobacter baumannii*, and *Burkholderia cepacia*. *Acinetobacter baumannii* is especially concerning in intensive care units (ICUs) due to its multidrug-resistant nature and the high mortality rates associated with its infections [21][22]

Multidrug-resistant bacteria significantly contribute to the morbidity and mortality of HAIs, with methicillin-resistant *Staphylococcus aureus* (MRSA) being one of the most prevalent and dangerous pathogens [22]-[24].

Estimating the percentage of HAIs caused by airborne transmission is challenging, particularly in hospital settings where patients are exposed to pathogens through multiple modes of transmission (see Section 1.1.2). However, some studies suggest that airborne transmission may account for approximately 10% to 16% of all HAIs [23]. Any respiratory pathogen has the potential to cause HAIs. The most frequently isolated pathogens include

Staphylococcus epidermidis, *Staphylococcus haemolyticus*, *Enterococcus* species, *Enterobacter*, *Pseudomonas* species, *Micrococcus*, *Corynebacterium*, and *Streptococcus faecalis* [18][23]. The concentration of airborne microorganisms in hospital environments exhibits significant variability due to a confluence of factors. These factors include the specific ward type, ongoing activities, the presence and number of patients potentially infectious carriers, air ventilation, and filtration systems, and the implemented cleaning and disinfection protocols. Stockwell *et al.* [25] conducted a systematic review investigating indoor air and the impact of ventilation on bioaerosols within hospital settings. Their findings revealed a higher concentration of bioaerosols in inpatient areas (77 CFU/m^3) compared to public areas (14 CFU/m^3). Notably, hospital areas with natural ventilation demonstrated the highest total bioaerosol concentrations (201 CFU/m^3) compared to those utilizing conventional mechanical ventilation systems (20 CFU/m^3). The review also identified *Staphylococcus* spp., *Streptococcus* spp., and *Escherichia* spp. as the predominant bacterial genera in these environments. HAIs pose significant social and economic challenges, though their full impact can be difficult to quantify. According to the European Centre for Disease Prevention and Control (ECDC), an estimated 4.8 million HAIs occur annually across EU/EEA countries [18]. In the United States, the direct medical costs of HAIs in hospitals are estimated to exceed $28.4 billion each year [26], highlighting the substantial financial burden on the healthcare system.

Moreover, the global healthcare system has recently been severely impacted by the outbreak of SARS-CoV-2, which has caused at least equally devasting social and economic repercussions. The pandemic's effect on the global economy is challenging to quantify but undoubtedly significant. The International Monetary Fund (IMF) estimates that the median global gross domestic product (GDP) fell by 3.9% from 2019 to 2020, making it the worst economic recession since the Great Depression [27]. The social impact is evident. According to the WHO, from the start of the pandemic until September 2024, there were over 776 million confirmed cases and over 7 million deaths [28]. Moreover, COVID-19 has significantly affected people's lives and habits. Personal protective equipment, disinfectants, social distancing, attention to air quality, and so on, have become a constant topic. COVID-19 forced the human population to adapt rapidly to the new, highly contagious virus. At the same time, the COVID-19 crisis highlighted the vulnerability of human societies and healthcare systems in a pandemic. Airborne transmission, as in the spread of HAIs, played a key role in the spread of SARS-CoV-2. However, in the early stages of the COVID-19 pandemic, declared by the WHO on 11 March 2020 [29], the role of airborne transmission in the spread of SARS-CoV-2 was a topic of intense

debate [2]. Initially, the WHO downplayed the significance of this transmission route, emphasizing droplet and contact-based spread. However, as the pandemic progressed, mounting scientific evidence[3],[10],[30],[31] and an open letter signed by 239 experts [2] underscored the importance of airborne transmission, particularly through aerosolized nuclei droplets in poorly ventilated indoor environments. The CDC also confirmed that SARS-CoV-2 can be transmitted via respiratory droplets produced when an infected person coughs, sneezes, talks, or breathes.

Multiple studies have highlighted the role of airborne transmission of SARS-CoV-2. Factors such as ventilation systems, air temperature, relative humidity, and social distancing all significantly influence the risk of airborne transmission, particularly in enclosed indoor spaces [30]-[34]. For instance, Li *et al.* [34] examined an outbreak involving three unrelated families at a restaurant in Guangzhou, China. Individuals seated at two neighboring tables became infected, while the other 68 customers in the restaurant remained unaffected. Simulation models (Figure 2.4) demonstrated how fine droplets exhaled by the infected individual dispersed within the dining area, with families B and C seated in the direct path of these aerosols. The specific configuration of the air-conditioning units and the lack of open windows contributed to the formation of a concentrated droplet cloud, leading to localized transmission. Nissen *et al.* [35] detected viral RNA in ventilation exhaust filters located at least 50 m from the vent openings of a patient room. These findings prove that SARS-CoV-2 may be dispersed and potentially transmitted by aerosols directly or through ventilation systems.

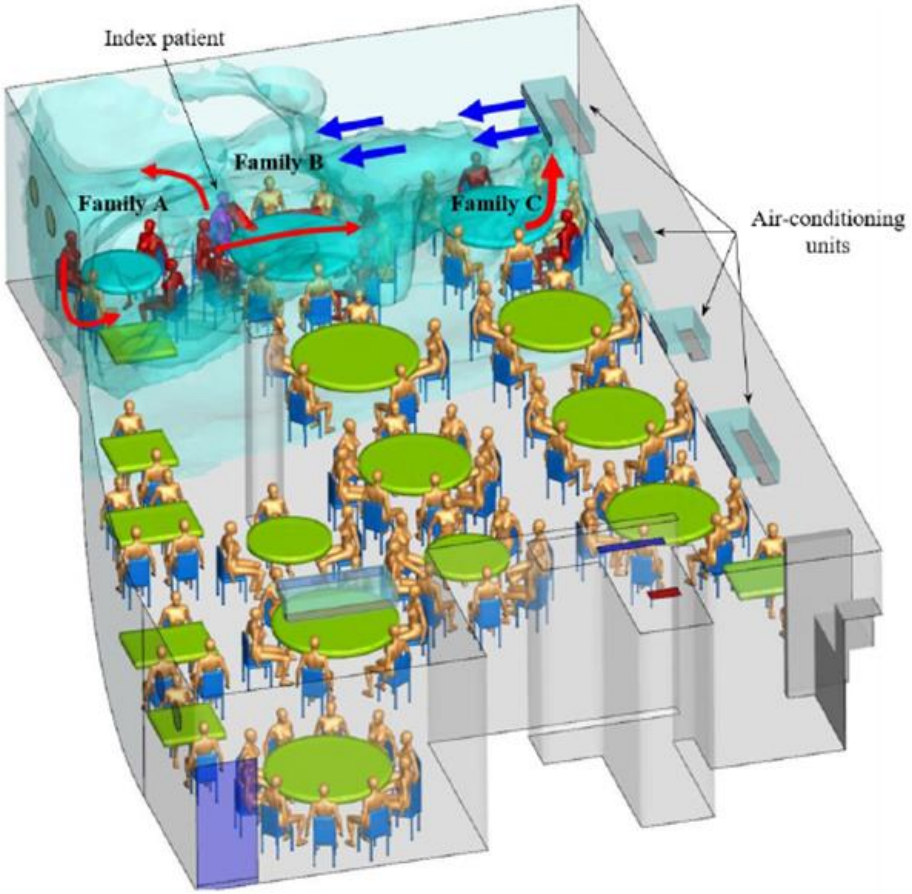

Figure 2.4 *– A fluid dynamic analysis of air-containing droplet nuclei involved in the transmission of SARS-CoV-2 among the affected families in a restaurant. The figure highlights infected individuals in red and non-infected individuals in gold. All rights to this image are owned by* [34].

2.1.3 Airborne transmission containment strategies

Air decontamination is thus an important topic in the perspective of mitigating the airborne transmission of pathogens. Different measures can be adopted to contain the spread of pathogens, such as controlling air pollution and maintaining Indoor Air Quality (IAQ) through ventilation improvement, air filtration, and purification. To limit the release of droplets and aerosols from an infected individual and reduce the risk of inhalation by others, one widely adopted strategy is the use of personal protective equipment, such as face masks. Masks serve as a source-control measure by filtering exhaled air and were one of the primary interventions during the COVID-19 pandemic. However, face masks are not foolproof. Jayaweera *et al.* [9] examined the effectiveness of various mask types in preventing the leakage of large droplets and aerosols from infected individuals. Even when wearing surgical masks, approximately 20-

30% of droplets and aerosols can still escape. This percentage decreases to 5 % with N95 or elastomeric respirators.

A key approach to minimizing exposure to airborne pathogens in enclosed spaces is improving the air dilution rate. Ventilation is a highly effective engineering strategy that promotes the dilution and dispersion of aerosolized particles. By replacing contaminated indoor air with fresh outdoor air, ventilation plays a crucial role in maintaining indoor IAQ [31],[36]. In mechanically ventilated buildings, ventilation is typically supplied by HVAC systems. While air recirculation helps conserve energy, it poses a risk of spreading airborne pathogens by transporting them between interconnected spaces, potentially increasing the transmission risk in otherwise uncontaminated areas [31],[36]. Indeed, in recent years, many scientific works emphasized the importance of HVACs in the transmission/spreading of infectious diseases, especially in healthcare facilities [37]–[39]. Moreover, during the COVID-19 pandemic, the Federation of European HVAC Association published updated guidance, recommending the cessation of air recirculation and the increase in the inflow of outdoor air [40].

Other strategies to mitigate airborne transmission include the use of air cleaning or disinfection devices, such as filters and air purifiers. However, no single method can entirely eliminate the risk of infection, and a combination of strategies is often necessary. Systems such as HEPA (High-Efficiency Particulate Air) filters can reduce bioaerosols by up to 99.95% [41]. While they are cost-effective in terms of initial capital, they have higher maintenance and energy costs, and they do not inactivate pathogens but merely trap them. Additionally, their efficiency can decline for particle sizes in the 200-250 nm range [42].

In conclusion, while multiple measures, including masks, ventilation, and air filtration, can help reduce the risk of airborne transmission, each comes with its limitations, necessitating an integrated approach to infection control. Finding innovative solutions to reduce the chance of exposure to airborne pathogens has a significant impact in several contexts, particularly in healthcare environments where the risk of contamination is high. CAPs technology represents a promising technology in the ecosystem of valuable methods to prevent airborne transmission of pathogens and thus decontaminate the indoor air, reducing the risk of spreading HAIs or viruses such as SARS-CoV-2.

2.1.4 CAP devices for bioaerosols treatment

In Chapter 1, the antimicrobial properties of CAPs were thoroughly explored, emphasizing their efficacy due to a combination of bioactive components, such as RONS,

electric fields, and UV radiation. Notably, section 1.3.5.3 focused on the potential of CAPs for decontaminating virus-laden bioaerosols. CAPs can inactivate aerosolized viruses through a variety of oxidative mechanisms, leading to damage to nucleic acids, proteins, and lipids. Studies identified through the systematic review revealed an average CAP efficacy in virus-laden bioaerosol decontamination, achieving a 3.9 Log reduction in viral load.

Beyond virus-laden bioaerosols, CAPs also have a significant potential for the decontamination of bacterial bioaerosols. Gallagher *et al.* employed a dielectric barrier grating discharge (DBGD) plasma device to inactivate high concentrations of airborne bacteria in ventilation systems, achieving Log reductions of 1.5 and 5.5 for *Escherichia coli* after single plasma exposures of 10 seconds and 2 minutes, respectively [43]. Similarly, a study using a wire-to-plate type DBD reactor showed effective inactivation of *Bacillus subtilis* and *Pseudomonas fluorescens* in bioaerosols [44]. Park *et al.* further demonstrated the effectiveness of CAPs in deactivating *Staphylococcus epidermidis* bioaerosols, achieving significant results with a residence time of just 0.24 seconds using a different DBD configuration [1]. Romero-Mangado *et al.* also examined the effect of DBD on aerosolized *E. coli*, observing varying degrees of cell damage and severe oxidation of the cell membrane, confirming bacterial inactivation [45]. Additionally, their research demonstrated the successful inactivation of both *Staphylococcus epidermidis* and *Aspergillus niger* (fungal spores) with CAP treatment. Scanning Electron Microscope (SEM) images revealed deformations in the cell structure of these microorganisms, suggesting leakage of essential cellular components, which is a key mechanism for microbial inactivation [46].

This chapter presents the design and characterization of a direct DBD plasma source developed for the decontamination of bacterial and viral bioaerosols. Serving as a proof of concept for the project, this device was one of the first prototypes based on CAP technology to undergo biological testing against the SARS-CoV-2 virus in scientific literature. Biological tests were carried out in collaboration with Prof. Vittorio Sambri from the Unit of Microbiology, The Great Romagna Hub Laboratory, Pievesestina (FC), Italy.

Part of the results presented within this chapter was published as part of the article Bisag A., Isabelli P. *et al.* 'Cold atmospheric plasma decontamination of SARS-CoV-2 bioaerosols.' *Plasma Processes and Polymers* 19.3 (2022): e2100133 [47].

2.2 Materials and Methods

2.2.1 Plasma source design

The plasma device designed as a proof of concept for bioaerosol decontamination is a direct parallel-plate DBD configuration (Volume DBD - see Section 1.1.4.1). Figure 2.5-a shows the CAP device used for bioaerosol inactivation, composed of two aluminum electrodes (5 × 150 × 2 mm) encased within two PMMA (Polymethylmethacrylate) supports and fixed by epoxy resin. Both the electrodes were covered by 2 mm thick ceramic layers (ε_r = 6 - 8), and, thanks to the presence of two T-section PMMA walls, an interelectrode gap of 2 mm was maintained between them (Figure 2.5-b). The plasma source is equipped with a bioaerosol inlet at the top, allowing the bioaerosol to flow directly into the interelectrode gap for the treatment and exit through the bottom of the device.

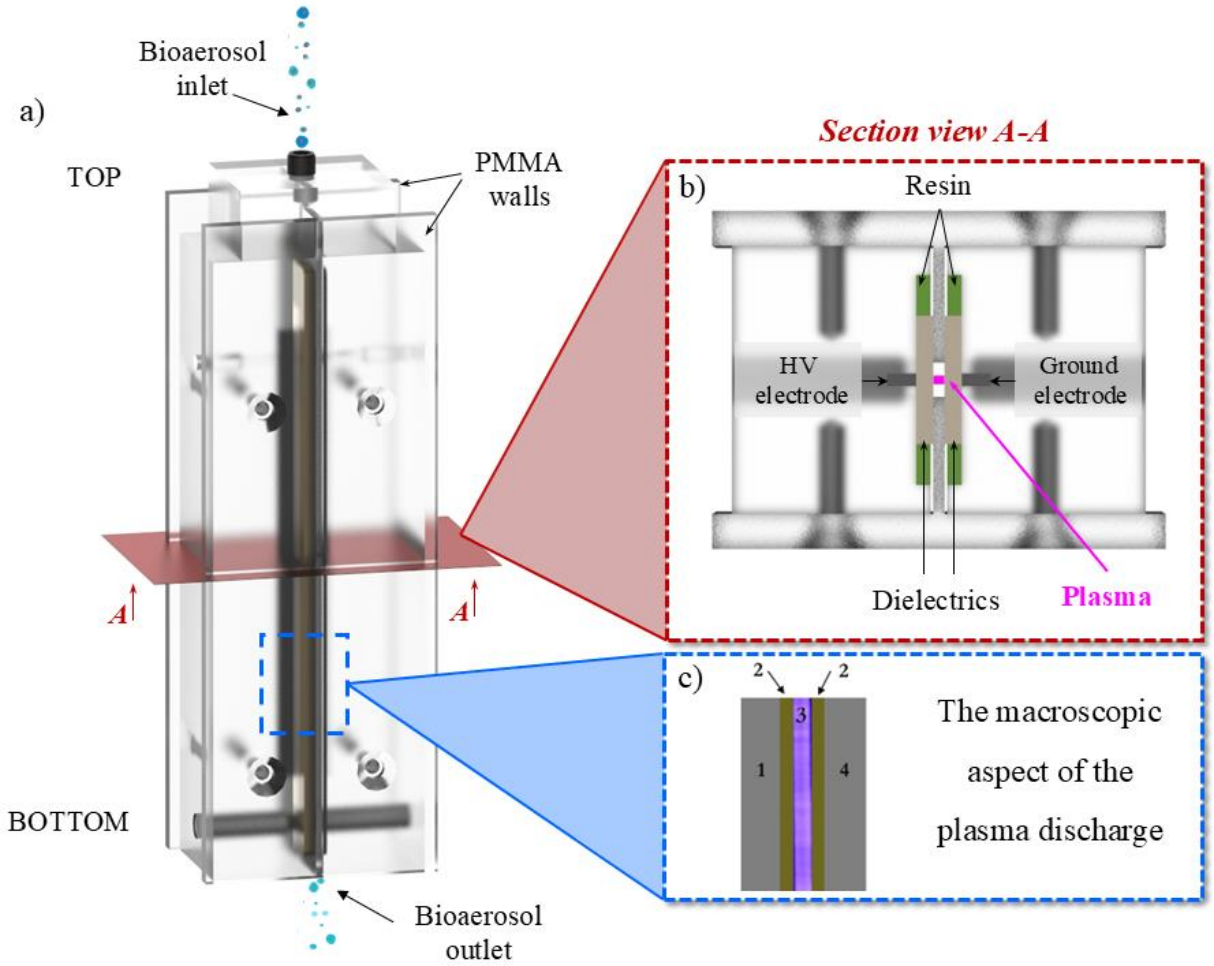

Figure 2.5 *– **a)** Direct DBD plasma source used for bioaerosol decontamination; **b)** Section view, highlighting the high-voltage (HV) and ground electrodes covered by the dielectric material; **c)** the macroscopic aspect of the plasma discharge ((1) HV electrode, (2) dielectrics, (3) plasma discharge, (4) ground electrode)).*

The main challenge in developing this plasma source regarded the selection of a suitable dielectric material and ensuring its reliable bonding to the PMMA substrates, crucial for maintaining the prototype's performance over multiple work cycles. Two dielectric materials were tested: mica and ceramic. Mica exhibited some issues due to interactions with the bioaerosol; after several cycles, contact with liquid promoted detachment from the support and subsequent deterioration. Similarly, ceramic dielectric suffered from detachment, leading to unwanted plasma discharges between the dielectric and the support, resulting in power loss and prototype degradation (Figure 2.6).

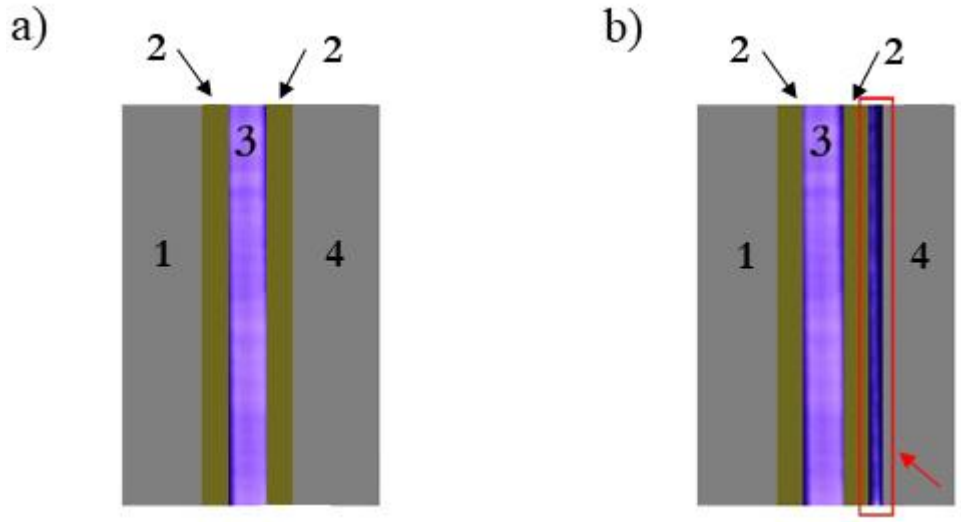

***Figure 2.6** – **a)** The macroscopic aspect of the plasma discharge during the normal operation; **b)** unwanted plasma discharge between the HV electrode or the ground electrode and the dielectrics ((1) HV electrode, (2) dielectrics, (3) plasma discharge, (4) ground electrode)).*

In the final electrode version (Figure 2.7), this issue was resolved by increasing the support area for dielectric layer bonding and securing it with epoxy resin, ensuring better adhesion and stability. To further enhance adhesion, both the dielectric and the PMMA support were pre-treated using a CAP jet device.

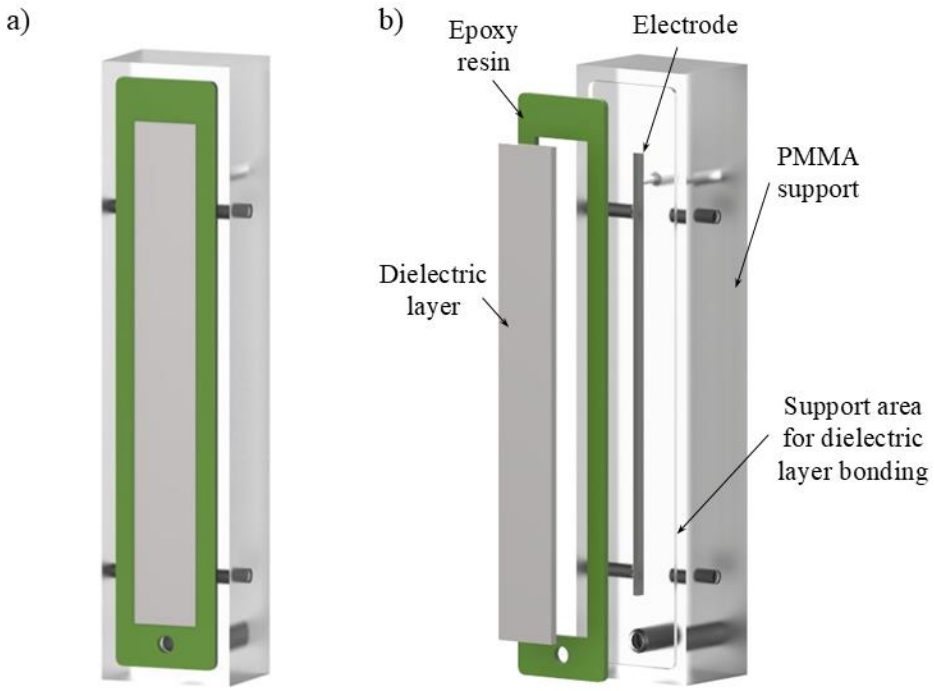

Figure 2.7 – **a)** Final electrode version; **b)** explode view of the final electrode version.

2.2.2 Statistical analysis

All experiments were performed in three independent replications. The results are presented as the mean ± standard deviation (SD). Significant differences in the results were assessed using the Student's test and were specified with asterisks (* $p \leq 0.05$, ** $p \leq 0.001$).

2.2.3 Direct parallel-plate DBD electrical characterization

Figure 2.8 illustrates the experimental setup used for electrical characterization tests to evaluate the electrical performance of the prototype. The plasma device was driven by a micro pulsed HV generator (AlmaPULSE, AlmaPlasma srl, Italy), applying two different operating conditions (Table 2.1). A single jet Blaustein Atomizer (BLAM, CH Technologies – USA), fed with an airflow of 1.2 slpm by a digital mass flow controller (Bronkhorst, EL-FLOW), was used to aerosolize a bacterial o viral suspension contained in a syringe fixed on a syringe pump (Legato®100, kdScientific – USA); bioaerosol was flown through the interelectrode gap and exposed to the plasma discharge.

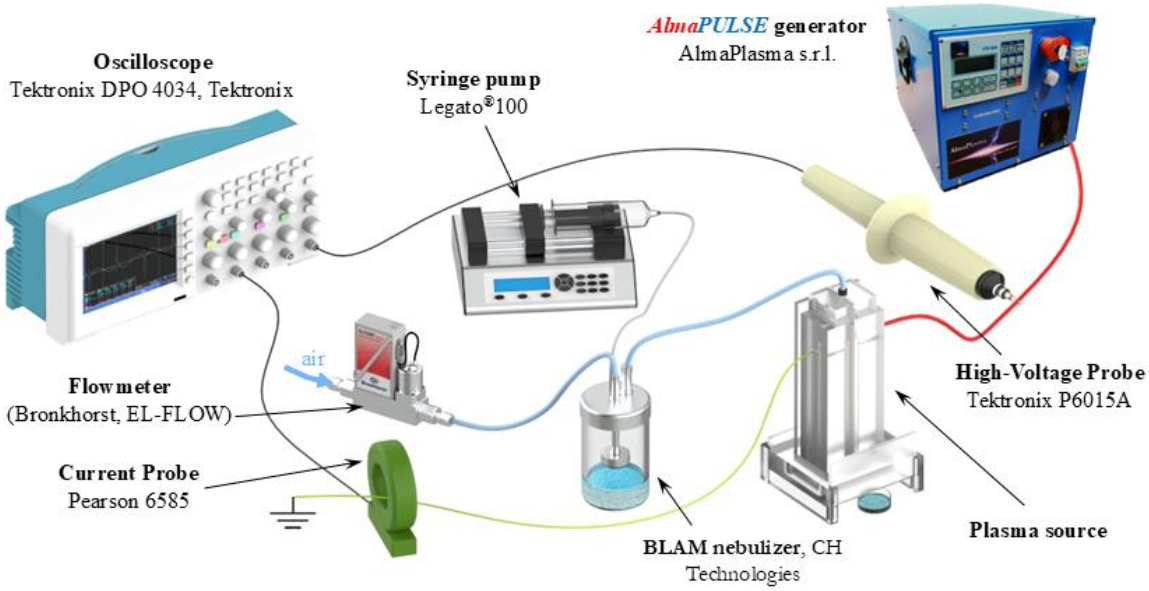

Figure 2.8 – Experimental setup for the electrical characterization and biological tests.

Operating conditions (O.C.)	***Voltage [kV_{p-p}]***	***Frequency [kHz]***
A	56	4
B	61	4

Table 2.1 – Direct parallel-plate DBD operating conditions.

The applied voltage (V) and the current (I) were measured by means of a high-voltage probe (Tektronix P6015A) positioned on the HV cable and a current probe (Pearson 6585) positioned on the ground cable. The corresponding waveforms were recorded using a digital oscilloscope (Tektronix DPO4034, 350 MHz, 2.5 GSa/s). The average discharge power (P) dissipated over the applied voltage period (T) was determined by applying the following formula (1):

$$P = \frac{1}{T}\int_0^T V(t)I(t)dt \qquad (1)$$

2.2.4 Gas phase characterization

Optical absorption spectroscopy (OAS) is a non-intrusive technique used to analyze plasma characteristics by observing its light absorption [48]. This technique measures how much light at specific wavelengths is absorbed by atoms, ions, or molecules produced by CAP [48].

In this study, OAS was used to evaluate the concentration of ozone, one of the long-lived species produced by CAP, in the downstream to have information about part of the chemistry induced by CAP treatment, focusing on a long-lived species.

The setup for OAS is illustrated in Figure 2.9. A deep UV LED, characterized by a narrow band spectrum radiation, was used as a light source. Aiming to investigate the plasma afterglow, the UV light beam was focused inside a measurement cell connected to the plasma source by a 20 cm long tube (4 mm internal diameter). The measurement cell had two quartz optical windows, which enabled the measurements to avoid interference with the plasma discharge emission in the optical analysis. The light beam passing through the measurement cell was collected into a 500 mm spectrometer (Acton SP2500i, Princeton Instruments) to spectrally resolve the light beam in the UV, VIS, and near-infrared (NIR) regions. The width of the inlet slit of the spectrometer was fixed at 25 μm for OAS acquisitions, and a grating with a resolution of 150 mm^{-1} was used. A photomultiplier tube (PMT-Princeton Instruments PD439) connected to a fast oscilloscope (Tektronix DPO40034) was used as a detector, allowing fast acquisitions with a time resolution of 40 ms. The PMT amplification factor was kept constant for all acquisitions. To ensure identical initial conditions, fresh air was flushed for 30 seconds inside the plasma source before every measurement. In order to quantitatively evaluate the species concentrations from absorption measurements, the Lambert-Beer law has to be taken into account:

$$\frac{I}{I_0} = e^{(-L\sigma n)} \qquad (2)$$

I/I_0 is the ratio between the initial light intensity I_0 and the light intensity I after an optical path length L, *and n is the* concentration of absorbers. The absorption cross-section σ is a function of the wavelength ($\sigma = \sigma(\lambda)$).

In general, when N species absorb at the same λ_j wavelength, the Lambert-Beer equation can be re-written as:

$$\left.\frac{I}{I_0}\right|_j = e^{\left(-L\sum_{i=1}^{N}\sigma_{i,j}n_i\right)} \qquad (3)$$

$\sigma_{i,j}$ represents the absorption cross section of the i-species at λ_j and the ratio between the light intensities I and I_0 is referred to the j-wavelength. The concentration n of each absorbing species can thus be obtained from the following expression, where the suffix k indicated a generic absorber:

$$n_k = -\frac{1}{L\sigma_{k,j}}\ln\left(\left.\frac{I}{I_0}\right|_j\right) - \sum_{i\neq k}^{N}\frac{\sigma_{i,j}}{\sigma_{k,j}}n_i \qquad (4)$$

A wavelength value of 253 nm was selected to perform the study; the corresponding absorption cross-sections for O_3 is $(1{,}12\pm0{,}02)*10^{-17}$. This wavelength was defined, in accordance with T. Moiseev *et al.* [49], to maximize the absorption of the molecules relevant to this study while minimizing the contribution, and thus the disturbance, of other absorbing molecules. For all experiments, the optical path length L is 8 cm, and the contributions of background radiation and spontaneous plasma emission were duly considered in the data processing, subtracting them from the acquired values of I and I_0. All measurements were performed three times.

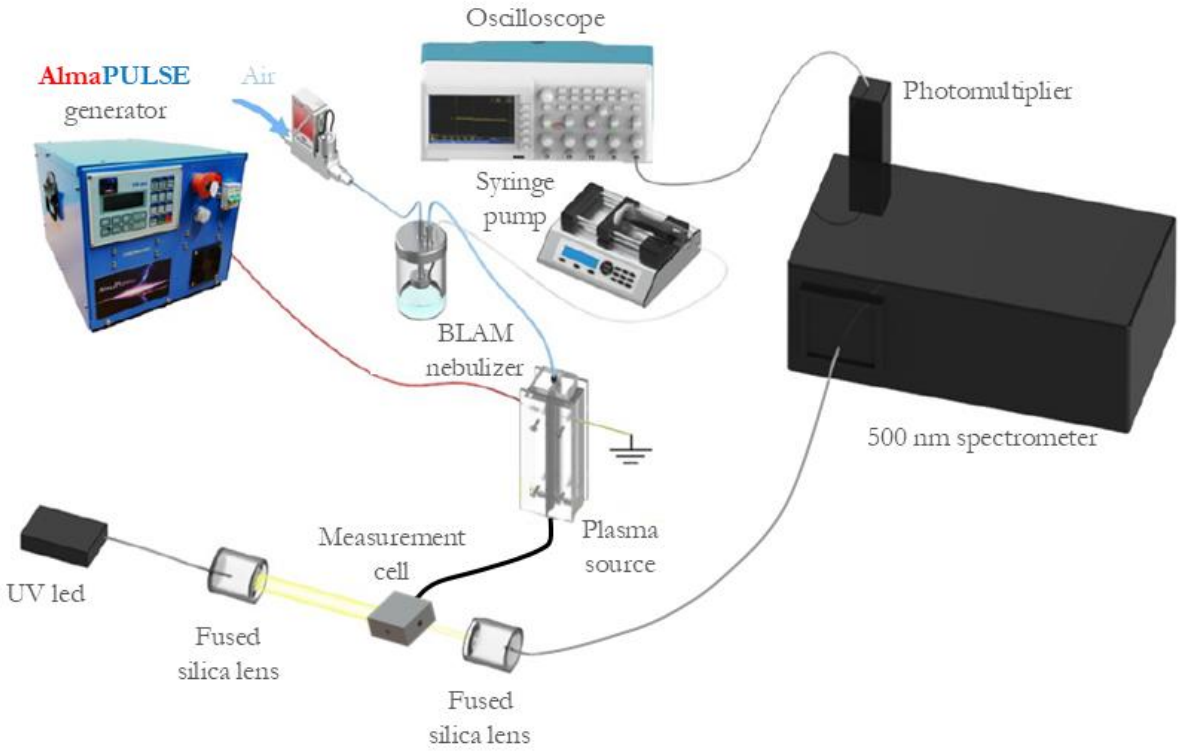

Figure 2.9 *– Experimental setup for OAS analysis.*

2.2.5 Droplets size distribution evaluation

Real-time measurement of particle distribution at the outlet of the single-jet Blaustein Atomizer was conducted using a laser diffraction system, SPRAYTECH (Malvern Panalytical, UK) [50], [51]. For this measurement, the atomizer was positioned between the transmitter and receiver modules, which were fixed on an optical bench with a spacing of approximately 100 mm. Data acquisition was carried out over 120 seconds, and the results were analyzed using SPRAYTECH software. The Sauter diameter (d_{32}) and the De Brouckere diameter (d_{43}) were evaluated using the formula (5) and (6).

$$d_{32} = \frac{\sum_{i=1}^{N} x_i d_i^3}{\sum_{i=1}^{N} x_i d_i^2} \quad (5)$$

$$d_{43} = \frac{\sum_{i=1}^{N} x_i d_i^4}{\sum_{i=1}^{N} x_i d_i^3} \quad (6)$$

where x_i is the numerical fraction of the total particle number associated with a diameter d_i and N is the number of discrete size classes used.

2.2.6 CAP treatment of bioaerosol containing bacteria and virus

The antimicrobial efficacy of the direct parallel-plate DBD plasma source was assessed using bioaerosol containing *Staphylococcus epidermidis*, a Gram-positive bacterium commonly found on human skin and associated with HAIs [47], as well as bioaerosol containing the SARS-CoV-2 virus.

2.2.6.1 *S. epidermidis* culture conditions

S. epidermidis (ATCC 12228) was cultivated on Tryptic Soy Agar (TSA) plates and incubated at 37°C for 24 hours; colonies were used to prepare a standardized suspension in Phosphate Buffered Saline (PBS), a buffered solution commonly used in biological research, at OD_{600nm} = 0.2 (i.e. 10^7–10^8 CFU/mL).

2.2.6.2 Evaluation of CAP efficacy on bioaerosol containing *S. epidermidis*

To evaluate the CAP antibacterial activity on *S. epidermidis* bioaerosol, a syringe was loaded with 20 ml of the standardized suspension and fixed to the syringe pump. This setup delivered a liquid flow rate of 0.852 mL/min into the nebulizer, which generated bioaerosol. The bioaerosol flowed through the plasma discharge region for 150 seconds before being collected in 1 mL of a liquid substrate. The collected samples were subsequently plated for analysis. Control samples were collected using the same procedure, but the plasma discharge was not generated. The liquid substrates for collecting samples were DPBS (Dulbecco's Phosphate Buffered Saline) or DPBS containing sodium thiosulphate, $Na_2S_2O_3$ (100 mM), which acted as a quenching solution for reactive species that dissolve into liquid after plasma exposure, e.g., O_3 [52], [53]. The plates were incubated at 37°C for 24 h for viable colonies counting according to the Formula (7).

$$Log\ R = Log\ N_0 - Log\ N_t \quad (7)$$

N_0 represents the viable colonies count in control samples, and N_t represents the viable colonies count in treated samples. The results are presented as the mean Log R ± standard deviation, based on data from at least three independent experiments.

Finally, as shown in Figure 2.10, a control test was conducted to evaluate the potential presence of residual bacterial load on the electrode surfaces following CAP treatment. A sterile cotton swab was gently rubbed across the electrode surfaces, using a systematic approach with horizontal and vertical strokes to ensure full coverage of the interelectrode gap surfaces through which the bioaerosol flows. After sampling, the swab was immediately streaked across the quadrants of a TSA (tryptone soy agar) plate to isolate bacterial colonies. The plates were incubated at 37°C for 24 hours, after which colony formation was assessed for bacterial growth.

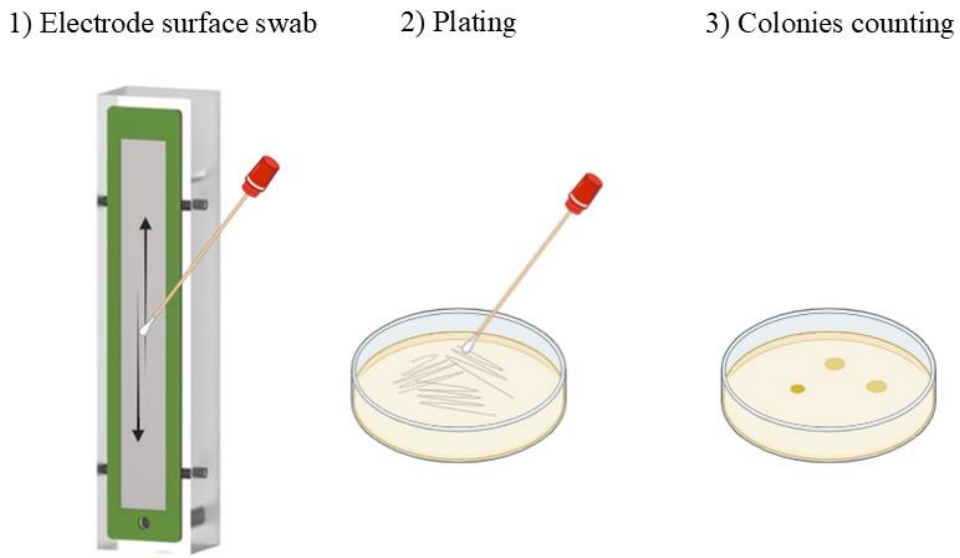

***Figure 2.10** – Procedure for bacterial swab tests on electrode surfaces.*

2.2.6.3 Preparation of viral stocks

A clinical isolate of SARS-CoV-2, obtained from an reverse transcription polymerase chain reaction (RT-PCR positive nasopharyngeal) swab of a COVID-19 patient in March 2020, was initially cultured in a monolayer of Vero E6 cells, following the protocol described by B. La Scola *et al.* [54]. Before starting the culture to increase viral titer, an aliquot of the original cell supernatant was tested using multiplex RT-PCR (FilmArray Respiratory Panel, bioMérieux, Marcy l'Etoile, France) to rule out co-infection with other respiratory viruses. VERO E6 cells were propagated following the protocol of N. C. Ammerman *et al.* [55]. The day before infection, approximately 1×10^6 cells were seeded in a T25 flask containing 5% FBS DMEM and incubated overnight at 37°C in a humidified chamber with 5% CO_2. Before infection, the

culture medium was aspirated, the cells were gently washed with DPBS, and 5 mL of fresh 2% FBS DMEM was added to each T25 flask. The cells were grown to 80% confluence, avoiding full confluence to prevent contact inhibition [56], [57]. A 0.5 mL aliquot of the clinical sample was then added to a 25 cm² VERO E6 cell flask, and after 72 hours of incubation, the cell culture supernatant was harvested and titrated following the protocol of M. A. Ramakrishnan [58], with minor modifications. This process was repeated four times to increase the viral concentration. After each cycle, three aliquots of the supernatant were tested by RT-PCR to determine the viral titer. The titration was performed by using a PCR method. The supernatant from the flask was processed for the RNA extraction using Nextractor (Genolution Inc., Seoul, Korea), and amplified with the CFX96 real-time PCR detection system (CFX96; Bio-Rad, USA) using SeeGene Allplex SARS-CoV-2 RT-PCR (AllPlex SARS-CoV-2, SeeGene, Seoul, Republic of Korea). This method targets four different SARS-CoV-2 genes (N, E, S, and RdRp), and the positive results were determined using the dedicated SeeGene Viewer software. This assay calculated the mean Cycle threshold (C_t) value from three replicates, which was then applied to a conversion file [56] to get the number of RNA/µL copies based on the Ct (Table 2.2). In particular, the correlation was acquired by the following equation: $y = -0.3062x + 10.50$, SE (slope) = 0.01427, SE (Y-intercept) = 0.3596, $r^2 = 0.9127$, p value < 0.0001.[56] (Table 2.2).

Titration	***Ct value (N gene) of the stock supernatant***	***Average RNA copies/µL (N gene)***	***Average Ct value (N gene) of the stock supernatant***	***Average RNA copies/µL (N gene)***
Virus stock (1st replicate)	4.84	1 042 298 229	4.91	992 236 405 = ~10^9
Virus stock (2nd replicate)	4.93	978 214 283		
Virus stock (3rd replicate)	4.95	964 517 251		

Table 2.2 - *PCR titration of the viral stock with Ct, the relatives with Ct, and respective RNA copies/µL.*

2.2.6.4 Evaluation of CAP efficacy on bioaerosol containing SARS-CoV-2

A stock of viral suspension containing approximately $1x10^9$ RNA copies/µL was diluted 1:1000 to prepare the working viral suspension with an approximate concentration of $1x10^6$ RNA copies/µL. This suspension was prepared in Minimum Essential Medium (MEM, EuroClone, Milan, Italy) without Fetal Bovine Serum (FBS, EuroClone, Milan, Italy).

To evaluate the CAP activity on bioaerosol containing SARS-CoV-2, a syringe was loaded with 20 mL of viral suspension and mounted onto a syringe pump. The pump delivered

viral suspension into the nebulizer at a flow rate of 0.852 mL/min to generate bioaerosol. It was flowed through the plasma discharge zone for 150 seconds and collected in a 35 mm well containing 1 mL of distilled water, positioned 5 mm from the plasma source bioaerosol outlet. Control samples were prepared following the same procedure but without generating the plasma discharge (Untreated), meaning they were not exposed to CAP treatment. Additionally, RT-PCR and a cell culture assay were performed on aliquots taken directly from the working viral suspension to serve as control samples (CNT).

Two methods were used to evaluate the efficacy of the CAP treatment in inactivating SARS-CoV-2: a direct genome amplification by using a commercial RT-PCR technique (AllPlex SARS-CoV-2, SeeGene, Seoul, Republic of Korea) and Vero E6 cells culture.

2.2.6.4.1 Multiplex PCR

Direct genome identification was performed using the standard RT-PCR previously described, following the manufacturer's instructions. The CAP-treated viral suspension was extracted from the collection vial and amplified. The reported Ct values correspond to the amplification of the N gene, which is also the target gene used in digital PCR [56].

2.2.6.4.2 CAP-treated viruses with Vero cells

A total of 0.5 mL of viral suspension collected at the end of the CAP treatment was inoculated into a confluent monolayer of Vero E6 cells in a 25 cm^2 flask, using the same conditions as those employed for preparing the viral stock. After incubation at 37°C in a 5% CO_2 atmosphere for 24, 48, and 72 hours, 0.5 mL aliquots of the cell culture supernatant were collected and processed via RT-PCR as described earlier. Each experiment was conducted in duplicate. The C_t values presented in Table 2.3 correspond to the amplification of the N gene. These values enabled titration by correlating them with the line obtained in digital PCR [56].

2.3 Results

2.3.1 Direct parallel-plate DBD electrical characterization results

The average discharge power, calculated directly from the measured current and voltage using Formula (1), is 4.86 ± 0.12 W for O.C. B. In contrast, O.C. A exhibits the highest average discharge power at 7.28 ± 0.15 W, with the two values being statistically different ($p \leq 0.001$) (Figure 2.11).

Figure 2.12 presents the current and voltage waveforms for the DBD plasma source operating at 56 kVp-p and 61 kVp-p, both with a fixed frequency of 4 kHz. The waveforms for both operational conditions show similar behavior, with the main difference being the higher voltage measured for O.C. A. During each voltage cycle, two distinct active discharge phases are observed, characterized by multiple current spikes corresponding to filamentary discharges typical of DBDs operating in air at atmospheric pressure. These discharges, lasting approximately 10 ns, occur within the active discharge phases [59].

Accurately determining the average discharge power is crucial, as this parameter directly influences the production of RONS, which are key to the antimicrobial effects of CAPs [60].

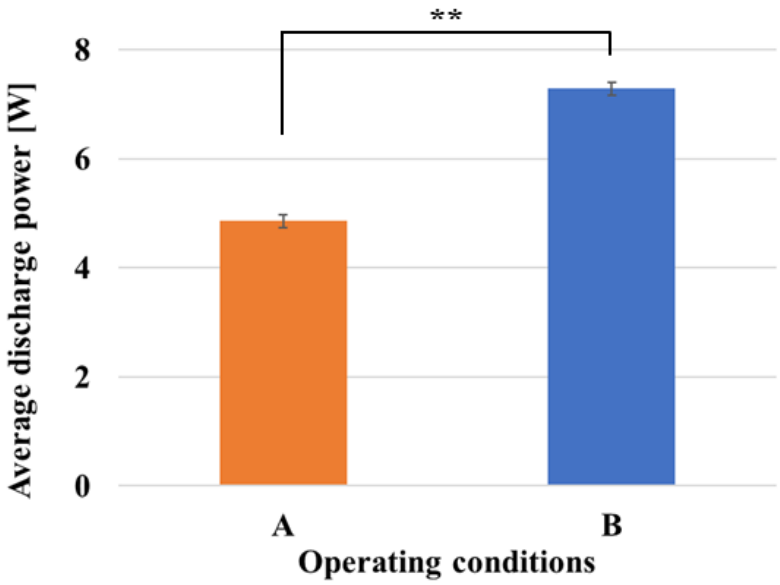

Figure 2.11 *– Average discharge powers for direct parallel-plate DBD operating conditions.*

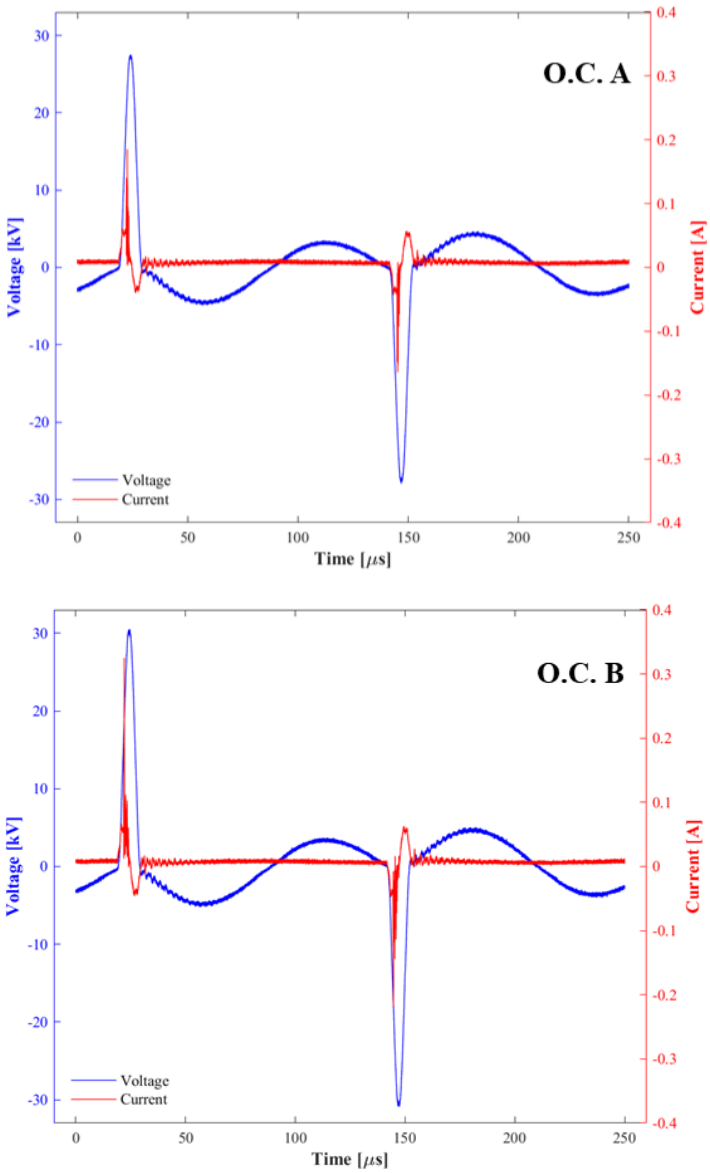

Figure 2.12 *– Current and applied voltage waveforms at O.C. A, and O.C. B.*

2.3.2 Ozone concentration

The ozone concentration was analyzed in the measurement cell 20 cm downstream. The ozone concentration reached a steady state regime 10 seconds after the plasma ignition, achieving an average ozone concentration of 870±40 ppm for O.C. A and 1330±80 ppm for O.C. B, as reported in Figure 2.13. Moreover, these two average concentrations are statistically different. These concentrations are representative of the ozone production in the plasma discharge and represent only part of the plasma bioactive components (i.e., UV rays, RONS, electric field) able to inactivate viruses and bacteria.

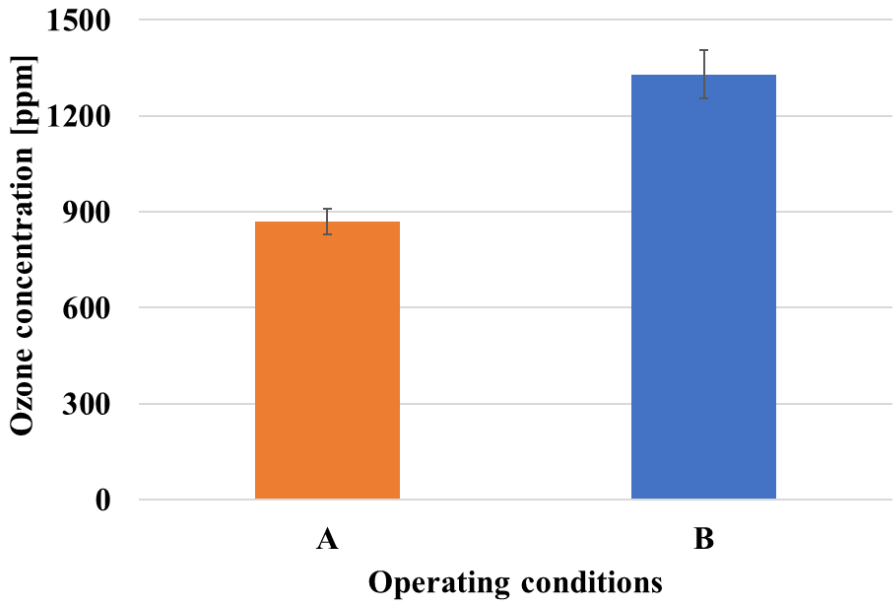

Figure 2.13 *– Average ozone concentrations produced by the DBD plasma at O.C. A, and O.C. B.*

2.3.3 Droplets size distribution

The Sauter diameter (surface-volume mean diameter) is defined as the diameter with the same ratio of volume to the surface area of the entire ensemble. Therefore, it provides information on processes in which the active area is important. The De Brouckere diameter (volume-weighted mean diameter) is defined as the mean of a particle size distribution weighted by the volume. Compared to the Sauter diameter, it is more sensitive to the larger particles; they contain most of the sample volume.

The Sauter diameter (d_{32}) and The De Brouckere diameter (d_{43}) were calculated using the Formula (5) and (6), obtaining values of d_{32} = 3.58 µm and d_{43} = 5.57 µm, respectively.

Figure 2.14-A illustrates the frequency distribution of droplet sizes, revealing that the most frequent class, representing approximately 15.2%, consists of droplets with a diameter of 1.47 µm. In contrast, Figure 2.14-B shows the distribution of the liquid phase volume across the droplet size classes, where the peak shifts toward larger droplets compared to the frequency distribution in Figure 2.14-A. Specifically, Figure 2.14-B highlights that 8.7% of the liquid phase is contributed by droplets with a diameter of 4.31 µm. Assuming that the volumetric concentration of the pathogen is independent of droplet size, the distribution of the liquid volume fraction can be considered as the distribution of the pathogen within the emitted aerosol.

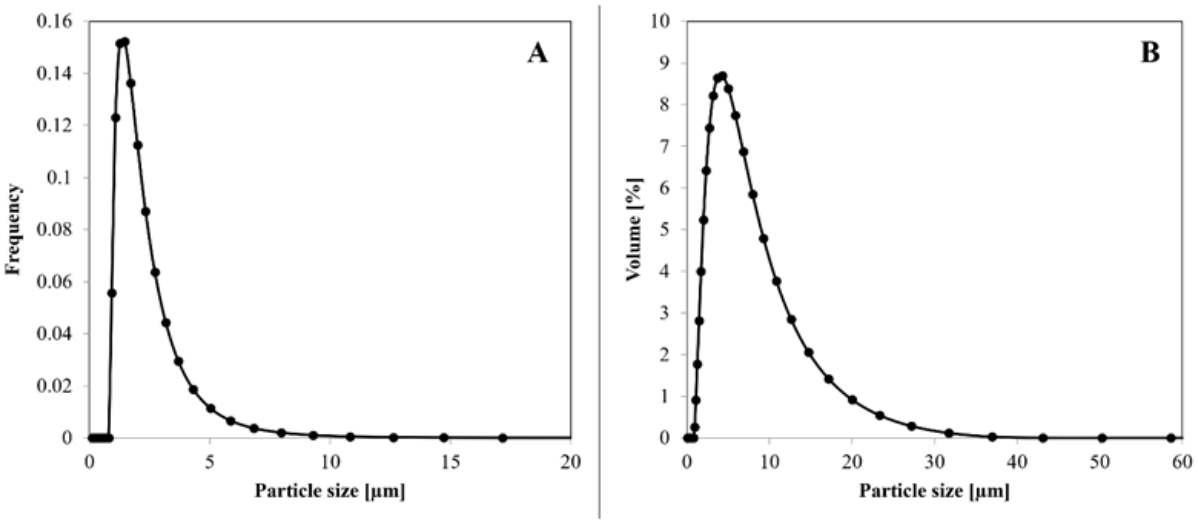

Figure 2.14 - *Size distribution of aerosol droplets at the outlet of the single jet Blaustein Atomizer:* ***A)*** *distribution of the number fraction and* ***B)*** *distribution of the volumetric fraction.*

2.3.4 CAP efficacy on bioaerosol

2.3.4.1 CAP efficacy on *S. epidermidis* bioaerosol

The antibacterial activity of CAP on *S. epidermidis* bioaerosol was assessed using two different liquid substrates for sample collection: PBS and $Na_2S_2O_3$ in PBS. Figure 2.15 shows that CAP demonstrated significant antibacterial effects on bioaerosol within a short residence time (<0.1 s). For O.C. A, the Log R was 1.5 ± 0.34, indicating a 90–99% reduction, while for O.C. B, a Log R of 3.71 ± 0.16 corresponded to an inactivation higher than 99.9%. Furthermore, biological tests revealed no statistically significant differences ($p > 0.001$) between the results obtained with samples collected in PBS and those collected in PBS containing $Na_2S_2O_3$. This means that the result is not affected by the possible presence of ozone potentially diffusing from the gas phase into the liquid phase of the sample.

Regarding the control test for evaluating the potential residual bacterial load on the electrode surfaces after plasma treatment, no bacterial growth was observed on the TSA plates under both operating conditions.

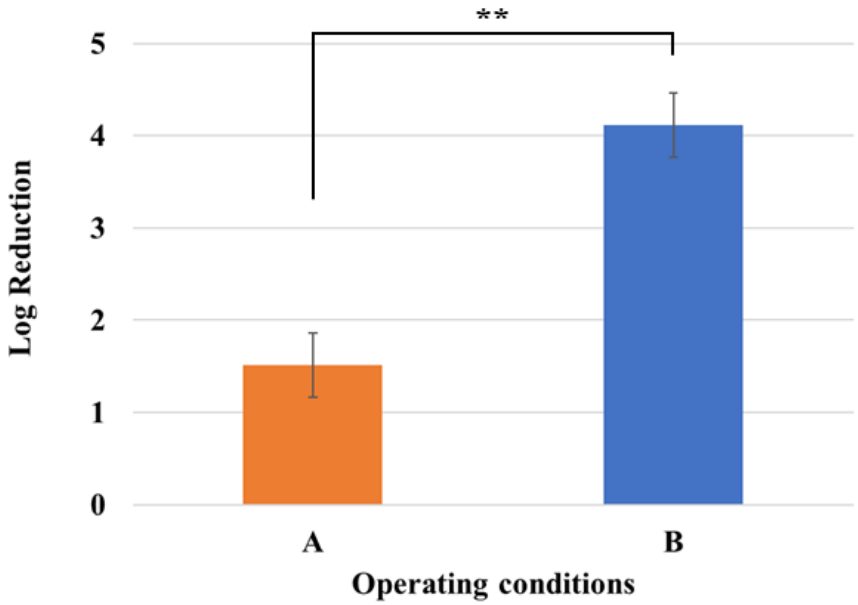

Figure 2.15 *– Log Reduction of S. epidermidis bioaerosol.*

2.3.4.2 Direct genome identification

Before CAP treatment, an RT-PCR assay was conducted using a viral suspension passed through the CAP device without generating the plasma discharge. The mean C_t value for the N gene was 25, likely due to the dilution effect caused by the flow inside the CAP device. However, following CAP treatment with both operating conditions, the RT-PCR results were entirely negative, indicating effective viral inactivation.

2.3.4.3 Vero E6 cell cultures

Table 2.3 reports the RT-PCR data, including RNA copies/µL, measured at 24, 48, and 72 hours after the start of incubation. As shown in the table, no positive results (ND[1]) were observed when RT-PCR was performed on cell cultures inoculated with virus suspensions treated with CAP under conditions A and B. Figure 2.16 displays pictures of the Vero E6 cell culture flasks. In the flasks inoculated with the control virus (CTN), a decrease in Ct value was observed, corresponding to an increase in virions, which was further evidenced by the rise in RNA copies/µL and the resulting cytopathic effect. By 72 hours, this led to the complete destruction of the cell monolayer. In contrast, flasks inoculated with the CAP-treated virus showed no detectable amplification in the RT-PCR assay, and no cytopathic effects were observed in the cells.

Treatment condition	*Average CT value (N gene) after 24 hours of culture*	*Average RNA copies/µL (N gene) after 24 hours of culture*	*Average CT value (N gene) after 48 hours of culture*	*Average RNA copies/µL (N gene) after 48 hours of culture*	*Average CT value (N gene) after 72 hours of culture*	*Average RNA copies/µL (N gene) after 72 hours of culture*
CNT	26	345	24	1 416	13	3 306 739
CAP-treated	ND	ND	ND	ND	ND	ND
Untreated	30	20	27	170	16	398 841

Table 2.3 *– Average Ct of the N gene in CNT, untreated, and CAP-treated samples.* [1] *ND: not determined (negative).*

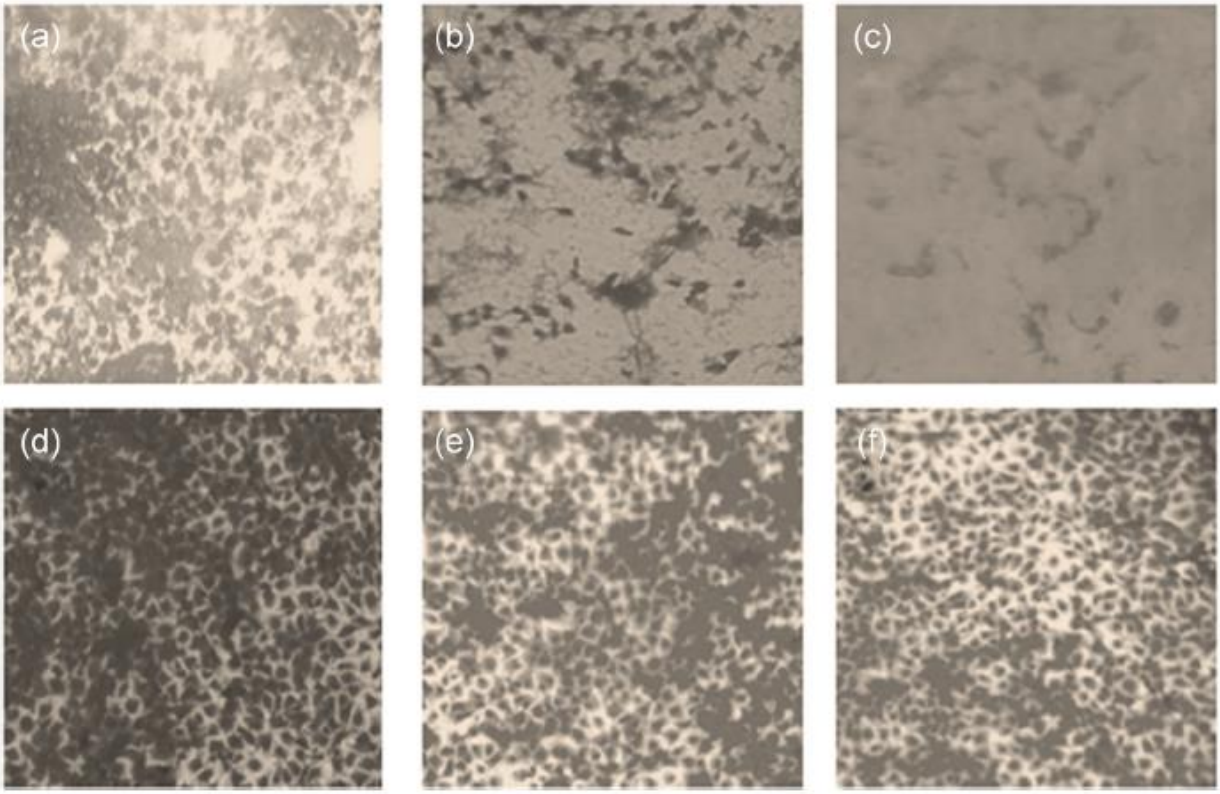

Figure 2.16 *– The upper panel shows Vero E6 cell cultures for the untreated viral suspension at 24 h postinfection (a), 48h postinfection (b), and 72 h postinfection (c). The pictures at the bottom show the Vero E6 cell culture for the CAP-treated suspension at 24 h postinfection (d), 48 h postinfection (e), and 72 h postinfection (f). No cytopathic effect is visible on the CAP-treated suspension. X100 magnification*

2.4 Discussion and conclusions

The presence of bioaerosol is generally correlated with human activity, particularly in indoor and poorly ventilated spaces, and it has been suspected as one of the causes of spreading diseases, such as HAIs and COVID-19. For example, the possibility that SARS-CoV-2 contained in aerial materials emitted by infected patients could contribute to the contamination

of the environment has been raised since the very beginning of the current pandemic, as it has been a major concern during the first SARS outbreak in 2003 [61]. Hence, increasing indoor air quality can play a pivotal role in human health. In this field, there is a need for innovative technology that could inactivate microbes and viruses in a short time.

One of the major issues in defining the optimal strategy for reducing the infectivity of environmentally dispersed SARS-CoV-2 virions is the balance between the effective reduction of the infectivity with respect to the potential damages that chemical or physical treatment could generate to the structure of the materials. CAP is among the possible treatments to reduce the presence of infecting SARS-CoV-2 virions in the air and surface of environmental materials. CAP has proven to be safe and effective in damaging capsid and nucleic acids thanks to its content of RONS generated during treatment [62] and inactivating SARS-CoV-2 on surfaces.[63]

In this chapter, CAP technology is explored as a novel approach to inactivate bioaerosol containing *S. epidermidis* and SARS-CoV-2 using a lab-scale volumetric DBD plasma source. Results show that CAP can induce a Log Reduction up to 3.71 on bacterial bioaerosol. Furthermore, the results indicate a decrease in the antimicrobial efficacy of the CAP treatment when utilizing O.C. A with a lower average discharge power, which corresponds to a reduced average ozone concentration compared to O.C. B. This finding highlights the impact of both average discharge power and ozone concentration on the treatment of bioaerosols containing bacteria. The results of the swab test, conducted to assess the potential presence of bacteria on the electrode surfaces after CAP treatment, suggest that the prototype does not function as an electrostatic filter. These filters are a specific category of devices used for air purification. They operate by employing a strong electric field to remove suspended particles from the air. In this process, particles become electrically charged and are subsequently attracted to the oppositely charged surfaces of the filter [64]. For instance, if the filter is positively charged, negatively charged particles are drawn towards it. As a result, these particles settle on the filter surfaces, effectively trapping them. However, this technology necessitates periodic cleaning of the filter to remove the accumulated particles. Instead, CAP effectively decontaminates bacteria as they pass through the plasma discharge, primarily due to the mixture of biocidal components generated by CAPs.

Moreover, the CAP treatment was highly effective in deactivating aerosolized SARS-CoV-2 viral particles, even when using low-power settings (less than 5 W) to generate plasma. After CAP treatment, no residual viral RNA was detectable by RT-PCR, even with short exposure times, indicating the high efficiency of the process. This suggests that the CAP

treatment destroyed the structural integrity of the viral RNA sequences targeted by RT-PCR. Since the viral RNA is encapsulated within a complex protein structure essential for infecting eukaryotic cells, it is highly likely that the CAP treatment compromised the structural integrity of the SARS-CoV-2 virions. To verify this hypothesis, the efficacy of CAP treatment was further evaluated by inoculating a portion of the CAP-treated viral suspension into a highly permissive cell line. After three days of incubation, no viral replication was observed, providing conclusive evidence that the infectivity of SARS-CoV-2 was entirely neutralized by CAP.

Furthermore, a comparison of the inactivation efficacy results reveals that SARS-CoV-2 bioaerosols are more susceptible to plasma treatment than those containing *S. epidermidis*. Even under operating condition A, which utilized lower power and a relatively reduced ozone concentration, complete virus decontamination was achieved. In contrast, the same conditions were less effective in decontaminating *S. epidermidis* bioaerosols. This difference in sensitivity to plasma treatment can be attributed to the structural differences between *S. epidermidis* and SARS-CoV-2. It is well established that the efficacy of CAP depends on both process parameters and the type of microorganism being treated. SARS-CoV-2, an enveloped virus with a lipid membrane, is highly vulnerable to RONS generated by plasma discharge. Once the lipid envelope is compromised, the virus loses its ability to infect host cells [65][66]. Moreover, plasma treatment may also damage the spike proteins of SARS-CoV-2, further preventing it from binding to and entering host cells [67]. In contrast, *S. epidermidis*, a Gram-positive bacterium, has a thick peptidoglycan cell wall that provides greater resistance to oxidative treatments like CAP [68][69]. While CAP can still decontaminate *S. epidermidis*, it may require longer exposure times or higher power settings and concentrations of RONS to achieve the same level of effectiveness as with SARS-CoV-2.

The direct parallel-plate DBD plasma source serves as a proof of concept, and the results from this study offer promising insights into the potential application of CAP technology for reducing bacterial and SARS-CoV-2 particles in ambient air.

Finally, the SARS-CoV-2 inactivation results using the proof of concept represented one of the first demonstrations of CAP efficacy against this recent virus in the scientific literature. These findings laid the groundwork for designing and developing novel CAP-based systems for bioaerosol decontamination in indoor environments, which will be detailed in the next chapter.

2.5 References

[1] C. W. Park and J. Hwang, 'Susceptibility constants of airborne bacteria to dielectric barrier discharge for antibacterial performance evaluation', *J. Hazard. Mater.*, vol. 244, pp. 421–428, 2013, doi: 10.1016/j.jhazmat.2012.12.006.

[2] J. D. Siegel, E. Rhinehart, M. Jackson, and L. Chiarello, '2007 Guideline for Isolation Precautions : Preventing Transmission of Infectious Agents in Healthcare Settings', *Am J Infect Control*, vol. 35, pp. 65–164, 2007.

[3] L. Morawska and D. K. Milton, 'It is Time to Address Airborne Transmission of COVID-19', *Clin. Infect. Dis.*, pp. 1–9, 2020.

[4] A. G. Somsen, C. van Rijn, S. Kooij, R. A. Bern, and D. Bonn, 'Small droplet aerosols in poorly ventilated spaces and SARS-CoV-2 transmission', *Lancet. Respir. Med.*, vol. 8, no. 7, p. 1, 2020, doi: 10.1007/s00134-020-05991-x.Bizzarro.

[5] C. C. Wang *et al.*, 'Airborne transmission of respiratory viruses', *Science*, vol. 373, no. 6558, p. 1, 2021, doi: 10.1126/science.abd9149.

[6] J. Joseph *et al.*, 'Role of bioaerosol in virus transmission and material-based countermeasures', *Exploration*, vol. 2, no. 6, 2022, doi: 10.1002/EXP.20210038.

[7] X. Xie *et al.*, 'How far droplets can move in indoor environments – revisiting the Wells evaporation – falling curve', vol.17, no.3, pp. 211–225, 2007, doi: 10.1111/j.1600-0668.2006.00469.x.

[8] W. F. Wells, 'On air-borne infection: Study II. Droplets and droplet nuclei.', *Am. J. Epidemiol.*, vol. 20, no. 3, pp. 611–618, 1934, doi: 10.1093/oxfordjournals.aje.a118097.

[9] M. Jayaweera, H. Perera, B. Gunawardana, and J. Manatunge, 'Transmission of COVID-19 virus by droplets and aerosols: A critical review on the unresolved dichotomy', *Environ. Res.*, vol. 188, p. 109819, 2020, doi: 10.1016/j.envres.2020.109819.

[10] S. H. Smith *et al.*, 'Aerosol persistence in relation to possible transmission of SARS-CoV-2', *Phys. Fluids*, vol. 32, no. 10, p. 107108, 2020, doi:10.1063/5.0027844.

[11] J. Yan *et al.*, 'Infectious virus in exhaled breath of symptomatic seasonal influenza cases from a college community', *Proc. Natl. Acad. Sci. U. S. A.*, vol. 115, no. 5, pp. 1081–1086, 2018, doi: 10.1073/pnas.171656111.

[12] W. G. Lindsley *et al.*, 'Viable influenza a virus in airborne particles from human coughs', *J. Occup. Environ. Hyg.*, vol. 12, no. 2, pp. 107–113, 2015, doi: 10.1080/15459624.2014.973113

[13] L. Chen, 'International Journal of Hygiene and Effects of ambient temperature and humidity on droplet lifetime – A perspective of exhalation sneeze droplets with COVID-19 virus transmission', *Int. J. Hyg. Environ. Health*, vol. 229,p. 113568, 2020, doi: 10.1016/j.ijheh.2020.113568.

[14] S. Yuan, 'Corrigendum : Do Humidity and Temperature Impact the Spread of the Novel Coronavirus ?', vol. 8, p. 3389, 2020, doi: 10.3389/fpubh.2020.00317.

[15] N. Pica and N. M. Bouvier, 'Environmental factors affecting the transmission of respiratory viruses', *Curr. Opin. Virol.*, vol. 2, no. 1, pp. 90–95, doi: 10.1016/j.coviro.2011.12.003.

[16] H. J. Kolmos, ‘Health Care Associated Infections : Sources and Routes of Transmission’, *Infection Control–Updates* 22, pp. 21-38, 2012, doi: 10.5772/36470.

[17] S. D. Judson and V. J. Munster, ‘Nosocomial transmission of emerging viruses via aerosol-generating medical procedures’, *Viruses*, vol. 11, no. 10, p. 940, 2019, doi: 10.3390/v11100940.

[18] European Centre for Disease Prevention and Control, *Point prevalence survey of healthcare-associated infections and antimicrobial use in European acute care hospitals – 2022-2023*, 2024.

[19] S.S. Magill *et al.*, ‘Changes in prevalence of health care–associated infections in US hospitals’, *New England Journal of Medicine,* vol. 379, no. 18, pp. 1732–1744, 2018, doi: 10.1056/NEJMoa1801550.Changes.

[20] S.S. Magill *et al.*, ‘Multistate point-prevalence survey of health care–associated infections.’, vol. 370, no. 13, pp. 1198–1208, 2014, doi: 10.1056/NEJMoa1306801.Multistate.

[21] J. Vincent, J. Marshall, A. Anzueto, C. D. Martin, and C. Gomersall, ‘International study of the prevalence and outcomes of infection in intensive care units’, *Jama,* vol. 302, no. 21, pp. 2323–2329, 2009, doi: 10.1001/jama.2009.1754

[22] R. E. Nelson *et al.*, ‘Multidrug-Resistant Bacterial Infections in U.S. Hospitalized Patients, 2012–2017’, *New England Journal of Medicine,* vol. 382, no.14, 2020, doi: 10.1056/NEJMoa1914433.

[23] W. J. Kowalski, ‘Hospital-Acquired Infections’, *HPAC engineering*, 2007.

[24] A. S. Collins, ‘Chapter 41 . Preventing Health Care – Associated Infections’, In: Patient Safety and Quality: An Evidence-Based Handbook for Nurses. Agency for Healthcare Research and Quality (US), Rockville (MD); 2008. PMID: 21328782.

[25] R. E. Stockwell, E. L. Ballard, P. O’Rourke, L. D. Knibbs, L. Morawska, and S. C. Bell, ‘Indoor hospital air and the impact of ventilation on bioaerosols: a systematic review’, *J. Hosp. Infect.*, vol. 103, no. 2, pp. 175–184, 2019, doi: 10.1016/j.jhin.2019.06.016.

[26] R. D. Scott, ‘The direct medical costs of healthcare-associated infections in U.S. hospitals and the benefits of prevention’, *Natl. Cent. Prep. Detect. Control od Infect. Dis.*, 2009, doi: 10.1093/acprof:oso/9780199234295.003.0002.

[27] R.H. Wade, "The world development report 2022: finance for an equitable recovery in the context of the international debt crisis." *Development and Change* (2023.

[28] World Health Organization, ‘Number of COVID-19 cases reported to WHO (cumulative total)’, https://data.who.int/dashboards/covid19/cases?n=o.

[29] R. Zhang, Y. Li, A. L. Zhang, Y. Wang, and M. J. Molina, ‘Identifying airborne transmission as the dominant route for the spread of COVID-19’, *Proceedings of the National Academy of Sciences* vol. 117, no. 26, 2020, doi: 10.1073/pnas.2009637117.

[30] N. van Doremalen *et al.*, ‘Aerosol and Surface Stability of SARS-CoV-2 as Compared with SARS-CoV-1’, *N. Engl. J. Med.*, vol. 382, no. 16, pp. 1564–1567, 2020, doi: DOI: 10.1056/NEJMc2004973.

[31] L. Morawska *et al.*, ‘How can airborne transmission of COVID-19 indoors be

minimised?', *Environ. Int.*, vol. 142, p. 105832, 2020, doi: 10.1016/j.envint.2020.105832.

[32] G. A. Somsen, C. Van Rijn, S. Kooij, R. A. Bem, and D. Bonn, 'Small droplet aerosols in poorly ventilated spaces and SARS-CoV-2 transmission COVID-19 and the impact of social determinants of health', *Lancet Respir.*, vol. 8, no. 7, pp. 658–659, 2020, doi: 10.1016/S2213-2600(20)30245-9.

[33] X. Zhao, S. Liu, Y. Yin, T. T. Zhang, and Q. Chen, 'Airborne transmission of COVID- - 19 virus in enclosed spaces : An overview of research methods', *Indoor air,* vol.32, no. 6, pp. 1–14, 2022, doi: 10.1111/ina.13056.

[34] Y. Li *et al.*, 'Probable airborne transmission of SARS-CoV-2 in a poorly ventilated restaurant', *Building and environment,* vol. 196, doi: 10.1016/j.buildenv.2021.107788.

[35] K. Nissen *et al.*, 'Long-distance airborne dispersal of SARS-CoV-2 in COVID-19 wards', *Sci. Rep.*, vol. 10, no. 1, pp. 1–9, 2020, doi: 10.1038/s41598-020-76442-2.

[36] A. N. Nair, P. Anand, A. George, and N. Mondal, 'A review of strategies and their effectiveness in reducing indoor airborne transmission and improving indoor air quality', *Environ. Res.*, vol. 213, no. May, p. 113579, 2022, doi: 10.1016/j.envres.2022.113579.

[37] G. Correia, L. Rodrigues, M. Gameiro da Silva, and T. Gonçalves, 'Airborne route and bad use of ventilation systems as non-negligible factors in SARS-CoV-2 transmission', *Med. Hypotheses*, vol. 141, 2020, doi: 10.1016/j.mehy.2020.109781.

[38] Y. Li *et al.*, 'Evidence for probable aerosol transmission of SARS-CoV-2 in a poorly ventilated restaurant', *Build. Environ.*, vol. 196, 2020, doi: 10.1016/j.buildenv.2021.107788.

[39] Y. Liu *et al.*, 'Aerodynamic analysis of SARS-CoV-2 in two Wuhan hospitals', *Nature*, vol. 582, no. 7813, pp. 557–560, 2020, doi: 10.1038/s41586-020-2271-3.

[40] Federation of European Heating, Ventilation and Air Conditioning Associations 'REHVA COVID-19 guidance document, How to operate and use building services in order to prevent the spread of the coronavirus disease (COVID-19) virus (SARS-CoV-2) in workplaces', 2020.

[41] P. Kumar and L. Morawska, 'Could fighting airborne transmission be the next line of defence against COVID-19 spread?', *City Environ. Interact.*, vol. 4, no. 2019, p. 100033, 2019, doi: 10.1016/j.cacint.2020.100033.

[42] S. D. Lowther *et al.*, 'How efficiently can HEPA purifiers remove priority fine and ultrafine particles from indoor air?', *Environ. Int.*, vol. 144, no. July, 2020, doi: 10.1016/j.envint.2020.106001.

[43] M. Gallagher *et al.*, 'Rapid Inactivation of Airborne Bacteria Using Atmospheric Pressure Dielectric Barrier Grating Discharge', *IEEE Trans. Plasma Sci.*, vol. 35, no. 5, pp. 1501–1509, 2007, doi: 10.1109/TPS.2007.905209.

[44] Y. Liang *et al.*, 'Rapid Inactivation of Biological Species in the Air using Atmospheric Pressure Nonthermal Plasma', *Environ. Sci. Technol.*, vol. 46, no. 6, pp. 3360–3368, 2012, doi: 10.1021/es203770q.

[45] J. Romero-Mangado *et al.*, 'Morphological and chemical changes of aerosolized E . coli treated with a dielectric barrier discharge', *Biointerphases*, vol. 11, no. 1, p. 011009,

2016, doi: 10.1116/1.4941367.

[46] J. Romero-Mangado *et al.*, 'Efficacy of atmospheric pressure dielectric barrier discharge for inactivating airborne pathogens', *J. Vac. Sci. Technol. A*, vol. 35, no. 4, p. 041101, 2017, doi: 10.1116/1.4990654.

[47] A. Bisag *et al.*, 'Cold atmospheric plasma decontamination of SARS-CoV-2 bioaerosols', *Plasma Process. Polym.*, vol. 19, no. 3, pp. 1–11, 2022, doi: 10.1002/ppap.202100133.

[48] M. I. Boulos, P. L. Fauchais, and E. Pfender, *Handbook of Thermal Plasmas*, 2023.

[49] T. Moiseev *et al.*, 'Post-discharge gas composition of a large-gap DBD in humid air by UV–vis absorption spectroscopy', *Plasma Sources Sci. Technol.*, vol. 23, no. 6, p. 065033, doi: 10.1088/0963-0252/23/6/065033.

[50] M. Legrand, J. Nogueira, P. A. Rodriguez, A. Lecuona, and R. Jimenez, 'Generation and droplet size distribution of tracer particles for PIV measurements in air, using propylene glycol/water solution', *Exp. Therm. Fluid Sci.*, vol. 81, pp. 1–8, 2017, doi: https://doi.org/10.1016/j.expthermflusci.2016.09.015.

[51] E. Brunazzi and A. Paglianti, 'Design of Wire Mesh Mist Eliminators', *AlChE J.*, vol. 44, no. 3, pp. 505–512, 1998, doi: 10.1002/aic.690440302.

[52] C. Schiappacasse *et al.*, 'Inactivation of aerosolized Newcastle disease virus with non-thermal plasma', *Appl. Eng. Agric.*, vol. 36, no. 1, pp. 55–60, 2020, doi: 10.13031/aea.13699.

[53] G. Nayak *et al.*, 'Rapid inactivation of airborne porcine reproductive and respiratory syndrome virus using an atmospheric pressure air plasma', *Plasma Process. Polym.*, vol. 17, no.10, , 2020, doi: 10.1002/ppap.201900269.

[54] B. La Scola *et al.*, 'Viral RNA load as determined by cell culture as a management tool for discharge of SARS-CoV-2 patients from infectious disease wards', *Eur. J. Clin. Microbiol. Infect. Dis.*, vol. 39, no. 6, pp. 1059–1061, 2020, doi: 10.1007/s10096-020-03913-9

[55] N. Ammerman, M. Beier-Sexton, and A. Azad, 'Vero cell line maintenance', *Curr Protoc Microbiol*, vol. Appendix 4, pp. 1–10, 2008, doi: 10.1002/9780471729259.mca04es11.Growth.

[56] M. Brandolini *et al.*, 'Correlating qrt-pcr, dpcr and viral titration for the identification and quantification of sars-cov-2: A new approach for infection management', *Viruses*, vol. 13, no. 6, 2021, doi: https://doi.org/10.3390/v13061022.

[57] F. Hasler, A. Duda, T. M. Kündig, and P. Johansen, 'A tissue culture infectious dose-derived protocol for testing of SARS-CoV-2 neutralization of serum antibodies on adherent cells', *STAR Protoc.*, vol. 2, no. 4, p. 100824, 2021, doi: 10.1016/j.xpro.2021.100824.

[58] M. A. Ramakrishnan, 'Determination of 50% endpoint titer using a simple formula', *World J. Virol.*, vol. 5, no. 2, pp. 85–86, 2016, doi: 10.5501/wjv.v5.i2.85.

[59] X. Zhang and M. S. Cha, 'Electron-induced dry reforming of methane in a temperature-controlled dielectric barrier discharge reactor', *J. Phys. D. Appl. Phys.*, vol. 46, no. 41, p. 415205, doi: 10.1088/0022-3727/46/41/415205.

[60] U. Kogelschatz, B. Eliasson, and M. Hirth, ‘Ozone Generation From Oxygen And Air: Discharge Physics And Reaction Mechanisms’, *Ozone Sci. Eng.*, vol. 10, no. 4, pp. 367–377, 1988, doi: 10.1080/01919518808552391.

[61] J. C. Luongo, K. P. Fennelly, J. A. Keen, Z. J. Zhai, B. W. Jones, and S. L. Miller, ‘Role of mechanical ventilation in the airborne transmission of infectious agents in buildings’, *Indoor Air*, vol. 26, no. 5, pp. 666–678, 2016, doi: 10.1111/ina.12267.

[62] E. H. Choi, H. S. Uhm, and N. K. Kaushik, ‘Plasma bioscience and its application to medicine’, *AAPPS Bull.*, vol. 31, no. 1, pp. 1–38, 2021, doi: 10.1007/s43673-021-00012-5.

[63] Z. Chen, G. Garcia Jr., V. Arumugaswami, and R. E. Wirz, ‘Cold atmospheric plasma for SARS-CoV-2 inactivation’, *Phys. Fluids*, vol. 32, no. 11, p. 111702, Nov. 2020, doi: 10.1063/5.0031332.

[64] M. S. Sodha, *Kinetics of complex plasmas*. Vol. 81., Springer, 2014.doi: 10.1007/978-81-322-1820-3_16.

[65] A. Filipić, I. Gutierrez-Aguirre, G. Primc, M. Mozetič, and D. Dobnik, ‘Cold Plasma, a New Hope in the Field of Virus Inactivation’, *Trends Biotechnol.*, vol.30, no. 11, pp.1278-1294, 2020, doi: 10.1016/j.tibtech.2020.04.003.

[66] N. Kaushik *et al.*, ‘The inactivation and destruction of viruses by reactive oxygen species generated through physical and cold atmospheric plasma techniques: Current status and perspectives’, *J. Adv. Res.*, vol. 43, pp. 59–71, 2023, doi: 10.1016/j.jare.2022.03.002.

[67] R. R. Khanikar *et al.*, ‘Cold atmospheric pressure plasma for attenuation of SARS-CoV-2 spike protein binding to ACE2 protein and the RNA deactivation’, *RSC Adv.*, vol. 12, no. 15, p. 9466, 2022, doi: 10.1039/d2ra00009a.

[68] I. Niedzwiedz, A. Wasko, J. Pawlat, and M. Polak-Berecka, ‘The state of research on antimicrobial activity of cold plasma’, *Polish J. Microbiol.*, vol. 68, no. 2, pp. 153–164, 2019, doi: 10.33073/PJM-2019-028.

[69] N. M. Coutinho, M. R. Silveira, and R. S. Rocha, Chapter 4 - Cold Plasma, in: Sustainable food processing and engineering challenges. Academic Press, 2021. 109-135.

Chapter 3

Scale-up of a cold plasma system for bioaerosol decontamination

3.1 Introduction

The onset of the COVID-19 pandemic has marked an increase in research focused on CAP as a tool for mitigating the airborne transmission of pathogens.

Chapter 1 demonstrated the potential of CAP as a promising technology for viral disinfection across various applications, including surface decontamination, bioaerosols, and liquids. As discussed in section 1.3.5.1, the scientific community increasingly focuses on elucidating the mechanisms underlying plasma-mediated viral inactivation.

As highlighted in section 2.1.4, CAP exhibits substantial potential for decontaminating bacterial bioaerosols. Moreover, Chapter 2 of this thesis presents a proof of concept, demonstrating the efficacy of CAP in decontaminating bioaerosols containing *Staphylococcus epidermidis* and SARS-CoV-2, yielding promising results.

This Ph.D. project arose in response to the urgent need for innovative solutions to reduce the spread of SARS-CoV-2 and other healthcare-associated pathogens and, in general, to investigate an innovative solution to enhance indoor air quality. However, while the proof of concept and other CAP prototypes in the scientific literature have proven effective in laboratory-scale systems, scaling up these systems to industrial levels without compromising performance remains challenging.

3.2 Scaling up of CAP systems

Scaling up technology can take several forms, but in all cases, it means to "adapt the newly developed technology to the needs, and under the conditions, of the industrial environment it will eventually be used in."[1]

Among the different possibilities, scale-up can refer to increasing the size, capacity, or scope of a system or technology to meet the demands of large-scale applications. In CAP systems, scaling up involves transitioning from laboratory-scale devices to industrial-scale systems that can handle more significant volumes or areas while maintaining or enhancing efficacy. Scaling up CAP systems involves more than simply increasing their size. Several critical factors must be addressed, including ensuring uniform plasma discharge, effective power distribution, managing potentially hazardous reactive species, and efficient heat dissipation [2]. For example, achieving uniform plasma discharge in laboratory-scale devices is relatively manageable. However, in larger systems, where the plasma generation zone encompasses more significant areas or volumes, achieving uniform discharge without the presence of 'dead zones' (regions of reduced plasma activity) becomes increasingly complex

and may reduce the overall efficacy of the system. Small devices typically need a few watts of power, but scaling up to an industrial scale could mean increasing the power requirements and identifying power supplies capable of sustaining significant plasma discharge volumes. Efficient power scaling is necessary to avoid excessive energy consumption. At the same time, increasing power can introduce heat management challenges. Overheating can affect both the stability of the plasma discharge and the durability of the system.

Several strategies are available for scaling CAP devices. One approach involves employing multiple plasma sources or modular arrays of identical sources to enhance coverage and increase capacity without compromising plasma uniformity. Each module operates independently but can be arranged in the most appropriate configuration depending on the application. Figure 3.1 illustrates an example of this scaling-up approach. In this case, a large multi-jet array, designed for the continuous treatment of food, was created by arranging multiple jet source modules in a well-defined distribution.

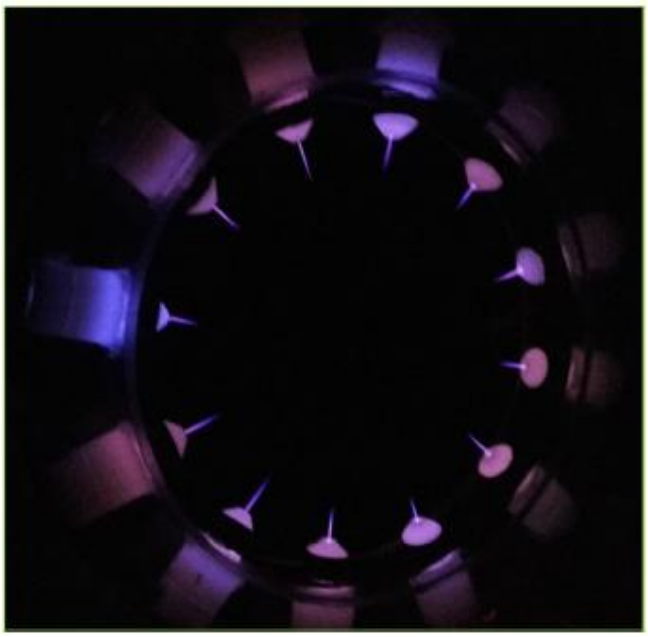

Figure 3.1 *– Multi-jet array designed for continuous treatment of food. All rights to this image are owned by [2].*

An alternative strategy focuses on utilizing configurations with adaptable geometries capable of operating at moderate voltages under atmospheric pressure conditions. A particularly promising configuration for scaling is the SDBD system, in which both electrodes are in direct contact with a dielectric barrier, and the plasma is generated along the surface of the electrodes (see Section 1.1.4.1). This configuration imposes few limitations on the voltage required to initiate plasma discharge, allowing for effective operation at relatively low voltages, typically

in a few kilovolts range [3]. They are scalable by extending the surface area of the plasma discharge while maintaining efficient operation. Due to these advantages, SDBD configurations are among the most widely adopted solutions in commercially available air decontamination systems.

Plasma-based technologies for air decontamination are commercially available, with manufacturers employing various approaches to develop systems capable of treating substantial volumes of air, typically ranging from 10 to 1000 m^3/h. One common scaling method involves increasing the number of plasma modules within the device, particularly in systems utilizing SDBD architectures.

A widely adopted solution in the commercial sector, depicted in Figure 3.2-a, is a cylindrical SDBD configuration. In this design, the high-voltage and ground electrodes are structured as grids, while the dielectric material consists of a glass tube (Figure 3.2-b). Plasma discharge is generated within the mesh of the high-voltage grid.

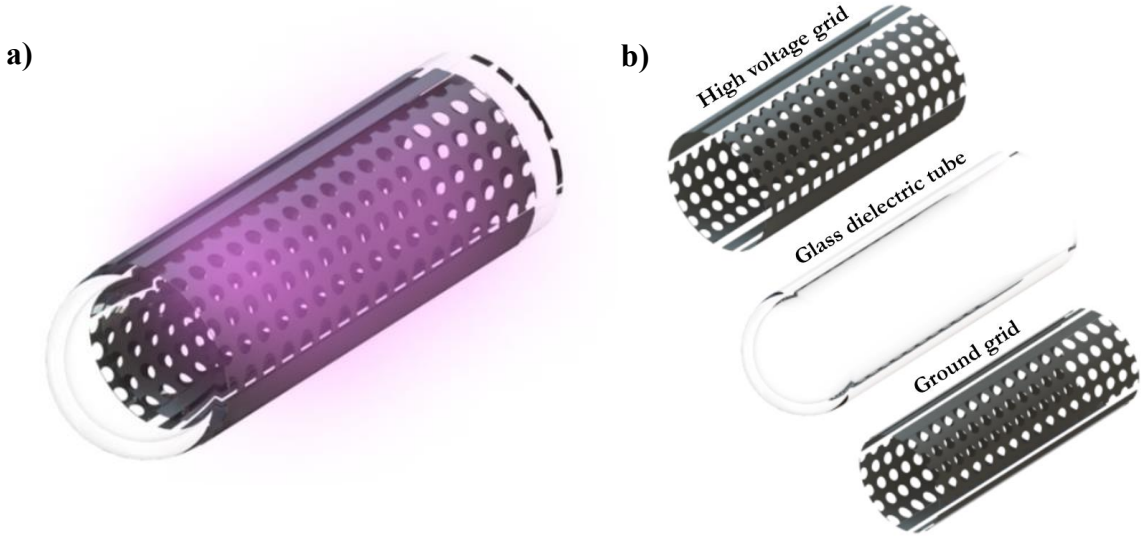

Figure 3.2 a) *– Typical cylindrical SDBD plasma source configuration used for commercial air decontamination devices and* ***b)*** *main components.*

Indeed, several companies (Novaerus - https://www.novaerus.com, Jonix - https://jonixair.com/, AtmosAir - https://atmosair.com/, Bioxigen - https://www.bioxigen.com/, Bioclimatic - https://bioclimatic.de/en/, Varionix - https://www.varionix.ch/index.php/en/) have adopted this configuration in their air decontamination devices, incorporating various customizations in arranging plasma sources and employing different strategies for integrating the system's three primary components (Figure 3.3).

For example, Novaerus offers a series of products based on this type of plasma source (https://www.novaerus.com/products). The devices vary in their capacity to treat different air

volumes and in their ability to integrate traditional systems, such as filters, in synergy with CAP modules. The scale-up strategy of Novaerus is exemplified by the DEFEND 1050 [4], a device capable of treating air volumes exceeding 900 m^3/h, which utilizes six plasma sources and a three-stage filtration system.

A similar approach has been adopted by other companies, such as Jonix (https://jonixair.com/), which adjusts both the number of plasma sources and the size of the electrode grids to modulate the plasma generation surface in different products. In some of these devices, filters are also incorporated to work synergistically with the plasma technology, enhancing the overall efficacy of air decontamination.

In the SDBD configuration, the air to be treated does not come into direct contact with the plasma discharge. Consequently, a portion of the biocidal components produced by the CAP are not utilized in the decontamination process within these devices. Instead, decontamination primarily depends on the long-lived reactive species generated by plasma, such as ozone, which are responsible for the antimicrobial efficacy of these systems. However, in larger systems, the production of reactive species such as ozone must be carefully managed. Effective scaling requires mechanisms to control the generation of toxic by-products and prevent their accumulation in indoor environments.

3.3 Standards for indoor ozone concentrations

Ozone (O_3) is a triatomic allotrope of oxygen characterized by a distinct pungent odor [5]. It is significantly less stable than atmospheric oxygen (O_2) [6], which necessitates its generation on demand using specialized ozone-generating systems, as it does not persist in the environment [7]. Ozone rapidly decomposes into oxygen in gaseous and aqueous environments, with a notably high oxidation potential of 2.07 V [5]. This powerful oxidative property, coupled with its fast decomposition, makes ozone highly effective against a wide range of microorganisms [8].

Ozone has been widely used for decontamination purposes across multiple industries, and its application gained prominence during the COVID-19 pandemic [9] as many companies developed ozone-based technologies to disinfect organic and inorganic surfaces and indoor environments. Despite claims by certain manufacturers promoting ozone as a “healthier” form of oxygen, it is, in fact, a toxic gas with properties markedly distinct from oxygen. Therefore, governmental health agencies worldwide have established stringent limits on ozone concentrations in the air to protect public health.

The regulation of ozone emissions varies across agencies, but the limits are generally stringent to protect human health. The U.S. Food and Drug Administration (FDA) mandates that the ozone output of indoor medical devices must not exceed 0.05 ppm [10]. Similarly, Underwriters Laboratories (UL), in its Standard UL 867 [11], limits ozone emissions from indoor air cleaning devices to a maximum of 0.05 ppm. The Environmental Protection Agency (EPA) enforces the National Ambient Air Quality Standard, which sets a maximum allowable 8-hour average outdoor ozone concentration of 0.08 ppm [12].

In occupational settings, the National Institute for Occupational Safety and Health (NIOSH) recommends an upper exposure limit of 0.10 ppm, which must not be exceeded at any time [13]. The Occupational Safety and Health Administration (OSHA) also regulates workplace exposure, stipulating that workers should not be exposed to an average concentration greater than 0.10 ppm over 8 hours [14].

While the European Union (EU) does not have a unified standard for ozone emissions from devices, member states commonly refer to the WHO guidelines [15]. In line with international recommendations, devices are generally required to meet the 0.05 ppm threshold for indoor environments across many EU nations. Grignani *et al*. [9] summarized in Table 3.1 the occupational exposure limit values in different European and extra-European countries.

Several strategies exist to mitigate ozone concentrations in indoor environments and ozone-generating devices. One of the most effective methods involves the use of activated carbon filters. These filters are highly efficient in neutralizing ozone present in air streams. Typically composed of a bed of granular activated carbon derived from carbon-rich materials like coconut shells, these filters undergo a high-temperature activation process, resulting in a highly porous structure. The activation process significantly increases the carbon's surface area, enhancing its ability to adsorb and capture ozone molecules [14][16] . Furthermore, ozone can react chemically with carbon, breaking into oxygen through direct oxidation.

An alternative approach to ozone removal is the use of catalytic air treatment. In this method, a solid catalyst facilitates ozone decomposition by accelerating the chemical reactions that convert it into molecular oxygen [17]. This catalytic process provides a sustainable solution, as the catalyst itself is not consumed in the reaction, enabling continuous ozone reduction [18].

Photocatalytic oxidation (PCO) is a technology that employs a photocatalyst in conjunction with UV light to enhance oxidation reactions, facilitating the degradation of both organic and inorganic pollutants, including ozone [19]. Among the most widely utilized photocatalysts in PCO systems is titanium dioxide (TiO_2), which becomes activated upon

exposure to UV light. Typically, the TiO_2 is applied as a coating on a substrate, such as a mesh or filter, which is positioned to receive UV irradiation. This arrangement promotes the generation of reactive species that catalyze the breakdown of pollutants into less harmful by-products.

Country or Agency	Limit Value—Eight Hours		Limit Value—Short Term	
	ppm	mg/m^3	ppm	mg/m^3
Austria	0.1	0.2	0.2	0.4
Belgium			0.1	0.2
Denmark	0.1	0.2	0.1	0.2
Finland	0.05	0.1	0.2	0.4
France	0.1	0.2	0.2	0.4
Hungary	0.1	0.2	0.1	0.2
Ireland	heavy work 0.05	heavy work 0.1	heavy, moderate and light works < 2 h 0.2	heavy, moderate and light works < 2 h 0.4
	moderate work 0.08	moderate work 0.16		
	light work 0.1	light work 0.2		
Latvia	0.05	0.1		
Poland	0.075	0.15		
Romania	0.05	0.1	0.1	0.2
Spain	heavy work 0.05	heavy work 0.1	heavy, moderate and light works < 2 h 0.2	heavy, moderate and light works < 2 h 0.4
	moderate work 0.08	moderate work 0.16		
	light work 0.1	light work 0.2		
Sweden	0.1	0.2	0.3	0.6
Switzerland	0.1	0.2	0.1	0.2
The Netherlands	0.06	0.12		
ACGIH (American Conference of Governmental Industrial Hygienists)	heavy work 0.05	heavy work 0.1	heavy, moderate and light works < 2 h 0.2	heavy, moderate and light works < 2 h 0.4
	moderate work 0.08	moderate work 0.16		
	light work 0.1	light work 0.2		
USA—NIOSH (National Institute for Occupational Safety and Health)			0.1	0.2
USA—OSHA (Occupational Safety and Health Administration)	0.1	0.2		
United Kingdom			0.2	0.4
Canada—Ontario	0.1	0.2	0.3	0.6
Canada—Québec			0.1	0.2
Japan JSOH (Japan Society for Occupational Health)	0.1	0.2		
New Zealand			0.1	0.2
Republic of China			0.15	0.3
Singapore			0.1	0.2
South Korea	0.08	0.16	0.2	0.4

Table 3.1 *- The occupational exposure limit values in different European and extra-European countries [9].*

3.4 Process design and optimization

The final goal of the project was to develop a novel CAP solution distinct from existing state-of-the-art and commercially available systems, with the capacity to employ all reactive plasma components (both long-lived and short-lived species) for the decontamination of airborne bacteria and viruses. A further aim was to design devices that could be applied in real-world settings, capable of processing significant air flow rates (≥ 30 m³/h), and to verify their antimicrobial efficacy.

An iterative approach was employed to achieve these goals. The process began with an extensive literature review and the insights gained during the initial design and characterization of a proof of concept device (Chapter 2). A plasma source was designed and realized. Subsequent steps involved detailed characterization of the plasma using various diagnostic techniques. Biological assays were then conducted to assess the antimicrobial efficacy of the prototype and to find a correlation between plasma parameters and microbial inactivation.

Insights obtained from the first prototype informed the development of a second, optimized version, improving its mechanical durability, electrical stability, and antimicrobial efficacy. This optimization process was paralleled by improvements in the experimental setup used for biological testing, ensuring accurate verification of prototype antimicrobial performance.

3.5 CAP devices proposed in this thesis

The proof of concept described in Chapter 2 evaluated the efficacy of a CAP solution against bioaerosols containing bacteria and viruses, including SARS-CoV-2. In scaling up this proof of concept, the decision was made to utilize the same type of plasma source (Volume DBD) but to explore different architectures that would enable the processing of significant airflow rates.

The iterative design and characterization process of CAP devices, outlined in the previous section, resulted in the development of two distinct CAP solutions for decontaminating airborne pathogens.

The first device, called the Rotating Dielectric Barrier Discharge (RDBD), will be detailed in Chapter 4. This tabletop device is specifically designed to treat the air in various environments, including hospital rooms, residential spaces, offices, and classrooms.

The second device, the InDuct plasma source, will be described in Chapter 5. This system is engineered for direct installation within ventilation or air distribution ducts, enhancing its capability to purify air in larger settings.

3.6 References

[1] Vekinis, George, *Mastering Technology Transfer: From Invention to Innovation*. Springer, 2023.

[2] P. J. Cullen *et al.*, 'Translation of plasma technology from the lab to the food industry', *Plasma Processes and Polymers*, vol. 15, no. 2,2018, pp. 1–11, 2018, doi: 10.1002/ppap.201700085.

[3] A. Fridman, *Plasma chemistry*. Cambridge University Press, 2008.

[4] Novaerus, 'Specifications DEFEND 1050', https://www.novaerus.com/products.

[5] E. I. Epelle *et al.*, 'Ozone application in different industries : A review of recent developments', *Chem. Eng. J.*, vol. 454, no. P2, p. 140188, 2023, doi: 10.1016/j.cej.2022.140188.

[6] A. Powell and J. W. S. Scolding, 'Direct application of ozone in aquaculture systems', *Reviews in Aquaculture,* vol. 10, no. 2, pp. 424–438, 2018, doi: 10.1111/raq.12169.

[7] C. G. Joseph *et al.*, 'Journal of Environmental Chemical Engineering Ozonation treatment processes for the remediation of detergent wastewater : A comprehensive review', *J. Environ. Chem. Eng.*, vol. 9, no. 5, p. 106099, 2021, doi: 10.1016/j.jece.2021.106099.

[8] G. Giuliani, G. Ricevuti, A. Galoforo, and M. Franzini, 'Microbiological aspects of ozone: bactericidal activity and antibiotic/antimicrobial resistance in bacterial strains treated with ozone', *Ozone therapy*, vol. 3, no.3, pp. 1–4, 2018, doi: 10.4081/ozone.2018.7971.

[9] E. Grignani *et al.*, 'Safe and E ff ective Use of Ozone as Air and Surface Disinfectant in the Conjuncture of Covid-19', *Gases*, vol.1, no. 1, pp. 19–32, 2020, doi: 10.3390/gases1010002.

[10] Food and Drug Administration, 'Code of Federal Regulations Title 21: Medical Device Ozone Limits'.

[11] Underwriters Laboratories, 'UL Ozone Standard 867', vol. 867, no. 867. pp. 5–6.

[12] Environmental Protection Agency, 'National Ambient Air Quality Standards (NAAQS) for Ozone', vol. 85, no. 251, 2020.

[13] National Institute for Occupational Safety and Health, 'Ozone Recommended Exposure Limits'.

[14] Occupational Safety and Health Administration, 'Ozone Limits in the Workplace: OSHA Standards', vol. 1200. pp. 23–25, 1994.

[15] World Health Organization, *Air Quality Guidelines for Europe*, 2nd edition, 2020.

[16] W. W. Nazaroff and C. J. Weschler, 'Indoor ozone : Concentrations and influencing factors', *Indoor air,* vol. 32, no.1, pp. 1–21, 2022, doi: 10.1111/ina.12942.

[17] T. Batakliev, V. Georgiev, M. Anachkov, S. Rakovsky, and G. E. Zaikov, ‘Ozone decomposition’, *Interdisciplinary toxicology,* vol. 7, no. 2, pp. 47–59, 2014, doi: 10.2478/intox-2014-0008.

[18] X. Li, J. Ma, and H. He, ‘Recent advances in catalytic decomposition of ozone’, *J. Environ. Sci.*, vol. 94, pp. 14–31, 2020, doi: 10.1016/j.jes.2020.03.058.

[19] L. Lin *et al.*, ‘Photocatalytic oxidation for degradation of VOCs’, *Journal of Inorganic Chemistry,* vol. 2013, no. 1, pp. 14–25, 2013, doi: 10.4236/ojic.2013.31003.

Chapter 4

Rotating Dielectric Barrier Discharge plasma source

4.1 Introduction

This chapter will present the design, development, and characterization of a novel tabletop system based on CAP technology to decontaminate indoor environments, targeting airborne pathogens in hospital rooms, residential spaces, offices, and classrooms. To achieve this, a distinctive architecture for a DBD plasma source, referred to as the Rotating DBD (RDBD) plasma source, has been designed and implemented. The efficacy of this RDBD plasma source in decontaminating *S. epidermidis* bioaerosol in an enclosed airtight test chamber was assessed through rigorous experimentation, considering different operating conditions. Moreover, the ozone concentration generated by the RDBD plasma source within the chamber was quantitatively monitored employing OAS. The antimicrobial efficacy and ozone production of the RDBD plasma source were compared against those of a commercially available CAP-based air purifier, specifically the Jonix Cube device (https://jonixair.com/en/products/cubeline). Biological tests were carried out in collaboration with Dr. Klaas De Baerdemaker from the Research Unit Food Microbiology and Food Preservation, Department of Food Technology, Safety and Health, Ghent University, Ghent, Belgium, in the frame of a short-term scientific mission (STSM) founded by the COST Action CA19110 PlAgri – Plasma application for smart and sustainable agriculture.

Part of the results presented within this chapter were published as part of the article Isabelli *et al.* 'Rotating Dielectric Barrier Discharge Plasma Source for Effective Bacterial Decontamination of Bioaerosols.' Plasma Medicine 14.1 (2024) [1].

4.2 Materials and Methods

4.2.1 Design of a stand-alone CAP system: the RDBD plasma source

The RDBD plasma source (Figure 4.1-a) is confined in a case and is equipped with a large upper circular section (A=211.25 cm^2) for the air inlet and three bottom sections (A=78.2 cm^2) for plasma-treated air output. The plasma source consists of six AISI 328L steel high voltage electrode rods fixed by epoxy resin inside glass dielectric tubes (with ε_r between 5 and 10) (Figure 4.1-a); the electrodes are opposed to a grounded aluminum fan which has a dual function: it is an essential component for plasma generation being the grounded electrode, and it is the element able to drive the airflow inside the prototype (airflow rate around 130 m^3/h). Therefore, six plasma discharge zones are formed between the HV rods and the fan blades (Figure 4.1-b). This study also compared the RDBD plasma source with the Jonix cube device

(Figure 4.2), which is a device based on CAP technology for indoor air decontamination and consisting of two SDBD (see section 3.2) plasma sources with a tubular shape. The HV and ground electrodes are concentrical metal grids spaced by a glass tube that serves as a dielectric. The plasma discharge is localized between the meshes of the external grid. The datasheet of the device mentions a power consumption of 10 W and an airflow rate of 40 m^3/h [2].

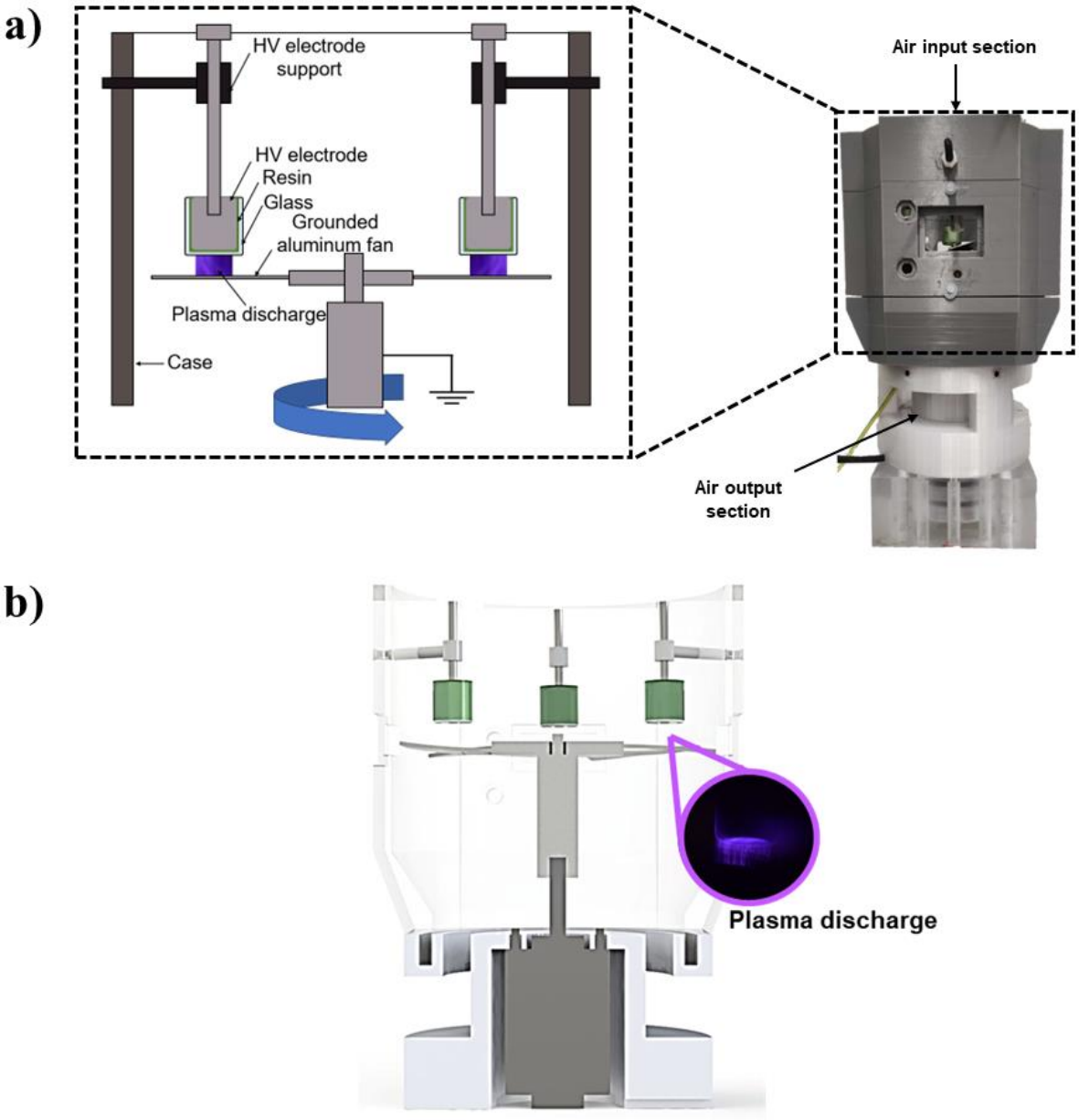

Figure 4.1 – a) *RDBD plasma source and its components; -* ***b)*** *Render of the inner section of RDBD plasma source and real picture of its plasma discharge.*

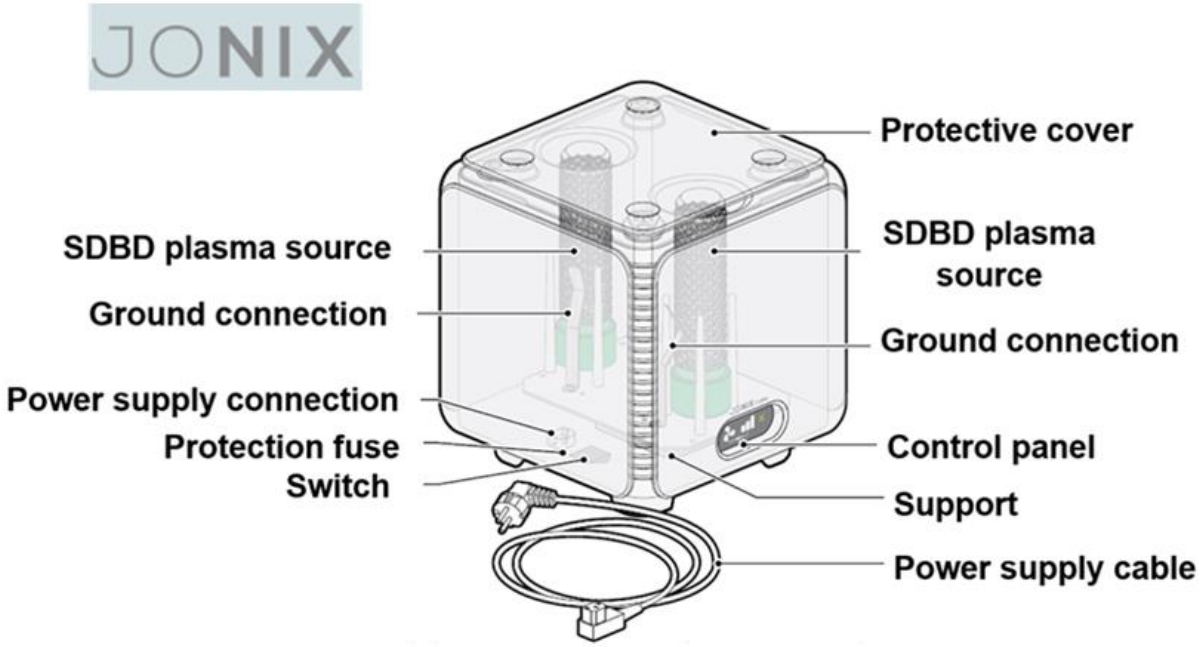

Figure 4.2 *– The commercial device for air decontamination: the Jonix Cube device (https://jonixair.com/en/products/cubeline). All rights to this image are owned by Jonix S.p.A (https://jonixair.com/).*

Finally, it is also possible to integrate the RDBD plasma source with commercial activated carbon filters to reduce ozone emissions into the environment (Figure 4.3-a). Specifically, a series of supports have been designed to insert activated carbon filters in both the inlet and outlet sections of the plasma source (Figure 4.3-b and 4.3-c). The filters have a thickness of 2 mm, and the supports are engineered to be easily removable, enabling quick operation of the device with or without filters and easy replacement in case of wear or damage (Figure 4.3-d and 4.3-f).

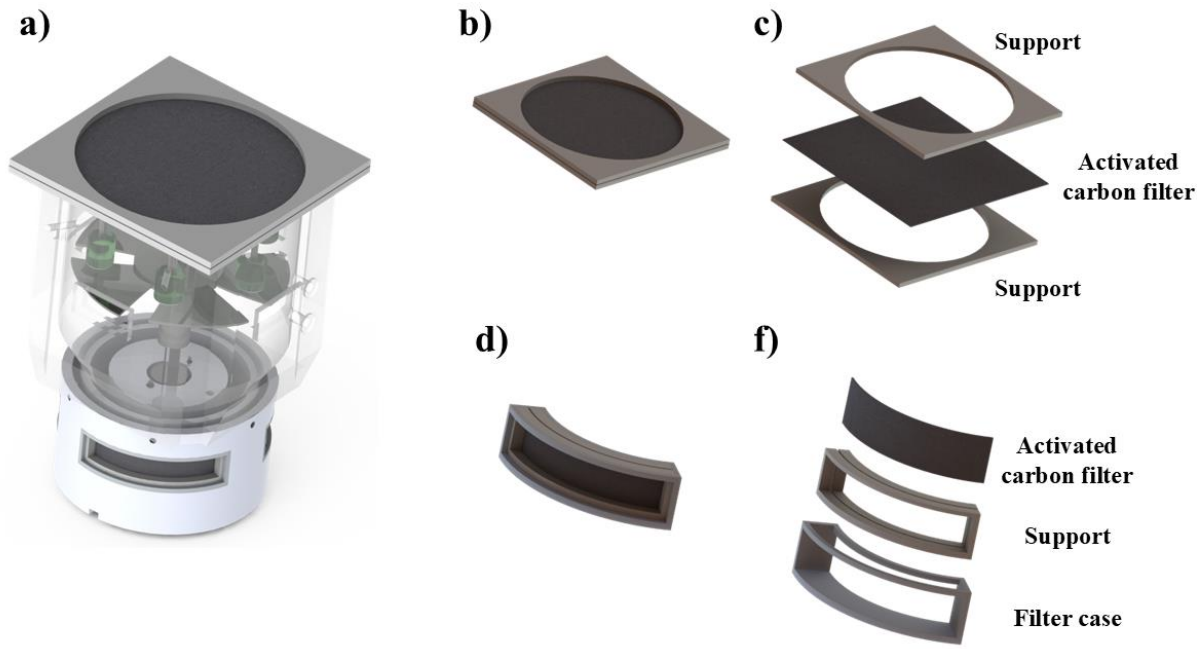

Figure 4.3 – a) *RDBD plasma source equipped with activated carbon filters in both inlet and outlet sections;* ***b)*** *activated carbon filter for inlet section;* ***c)*** *exploded view of filter components for inlet section;* ***d)*** *activated carbon filter for outlet sections;* ***f)*** *exploded view of filter components for outlet sections.*

4.2.2 Statistical analysis

All experiments were performed in three independent replications. The results are presented as the mean ± standard deviation (SD). Significant differences in the results were assessed using the Student's test and were specified with asterisks (* $p \leq 0.05$, ** $p \leq 0.001$).

4.2.3 RDBD electrical characterization

The RDBD plasma source was driven by a micropulsed high voltage generator (AlmaPULSE; Alma Plasma s.r.l., Bologna), allowing the application of a tuneable duty cycle (D.C.) (1-100%). Four operating conditions (O.C.) were identified to obtain three different average discharge powers. Specifically, two D.C. values were selected, resulting in two operating conditions (B and C) with statically different peak-to-peak voltage values but similar average discharge power values. The electrical characterization was performed for all four chosen O.C.s (Table 4.1).

O.C.	V_{p-p} (peak-to-peak voltage) [kV_{p-p}]	f (frequency) [kHz]	D.C. (duty cycle) [%]
A	29.4 ± 0.09	4	100 %
B	29.4 ± 0.09	4	60 %
C	26.6 ± 0.08	4	100 %
D	26.6 ± 0.08	4	60 %

***Table 4.1** –O.C.s applied for the RDBD plasma source.*

The applied voltage *v(t)* and the current *i(t)* were measured using a HV probe (Tektronix P6015A) and a current probe (Pearson 6585), both positioned on the HV cable (Figure 4.4). The corresponding waveforms were recorded using a digital oscilloscope (Tektronix MSO46) (Figure 4.4).

The average discharge power (P**)** dissipated over the applied voltage period (T) was determined using the formula given in formula (1).

$$P = \frac{D.C.}{T}\int_0^T V(t)I(t)dt \qquad (1)$$

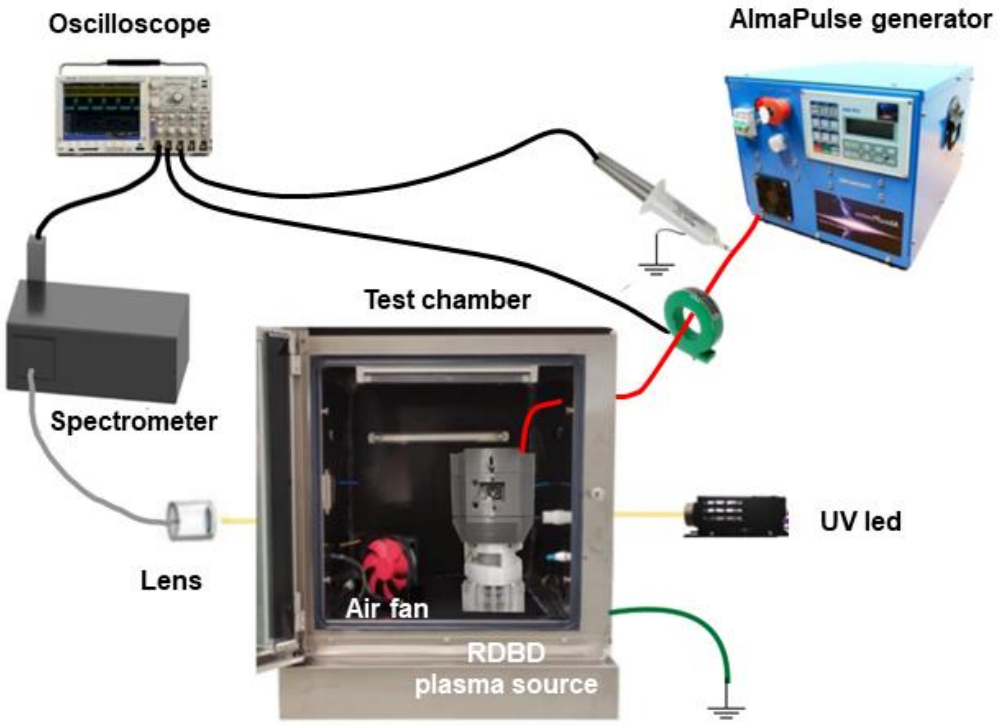

***Figure 4.4** - Experimental setup for the RDBD plasma source electrical characterization and evaluation of ozone and nitrogen dioxide concentration inside the test chamber.*

4.2.4 Evaluation of the gas phase

Ozone is one of the long-lived reactive oxygen species produced by CAP, with a strong ability to oxidize bacteria and viruses [3], [4]. OAS was used to evaluate the ozone and nitrogen dioxide concentration of the two devices inside a stainless-steel airtight test chamber (Figure 4.4). The test chamber (V=0,09 m^3) was designed to simulate an indoor environment potentially contaminated by airborne pathogens. It has two quartz optical windows and enables measurements without interference from the plasma discharge emission in the optical path (L = 410 mm), which was chosen near the air outlet section for both devices. A deep-UV LED module (Omicron Laserage Laserprodukte GmbH) served as a light source for the ozone concentration measurement. A commercially available LED with a specific emission wavelength of 400 nm was employed for the measurement of nitrogen dioxide (NO_2) concentration. The light beam was focused using optical fibers and fused silica lenses (50 mm of focus length) to achieve a parallel beam which passed through the test chamber and collected into a 500 mm spectrometer (Acton SP2500i; Princeton Instruments) to spectrally resolve the light beam in the UV, VIS, and near-infrared regions (Figure 4.4). The width of the inlet spectrometer slit was fixed as 10 μm for OAS acquisitions, and a grating with a resolution of 150 mm^{-1} was adopted. A photomultiplier tube (PMT Princeton Instruments PD439) connected to a fast oscilloscope (Tektronix MSO46) was operated as the detector. To ensure the same initial conditions, the test chamber was opened and flushed for 5 minutes with fresh air before every measurement. The Lambert-Beer law was considered following the same procedure reported in section 2.2.4 to evaluate the O_3 concentration from the absorption measurement using a wavelength value of 253 nm and the absorption cross-section of $(1.12 \pm 0.02)*10^{-17}$ cm^2. Similarly, for NO_2 measurement, a wavelength of 400 nm and an absorption cross-section of $(6.4 \pm 0.02)*10^{-19}$ cm^2 were used. The two species concentration inside the chamber were monitored for 500 s (480 s plasma discharge ON and 20 s plasma discharge OFF). The same experimental conditions used for microbial inactivation tests were reproduced for the OAS analysis.

Additionally, the ozone concentration in the test chamber was measured using the RDBD plasma source equipped with activated carbon filters. The filter efficiency (ε) was then evaluated using the Formula (2).

$$\varepsilon = \frac{C_0 - C_f}{C_0} \times 100 \qquad (2)$$

C_0 represents the maximum concentration measured in the test chamber using the plasma source without the filter, while C_f is the maximum concentration measured in the chamber with the filter in place.

4.2.5 Evaluation of bactericidal efficacy in bioaerosol

The microbial inactivation efficacy of the RDBD plasma source was evaluated by contaminating the air inside the test chamber with a bioaerosol containing *Staphylococcus epidermidis*, a Gram-positive bacteria commonly present on human skin and not ordinarily dangerous but often involved in HAIs [5]. For this, a culture of *S. epidermidis* (ATCC 12228) cells, kept at -20 °C, was incubated in brain heart infusion (BHI, Biolife, Italy) broth for ± 24 h (37 °C), after which a loopful of cells were transferred to tryptic soy agar (TSA, VWR, Belgium) plates by means of the four quadrants streak method. After incubation (± 24 h, 37 °C), a pure culture was picked and grown (± 24 h, 37 °C) on a TSA slant. Finally, the slants were kept in the fridge (4 °C) until further use. For every test, a subculture of *S. epidermidis* was taken from a slant, cultivated on TSA, and incubated at 37°C for ± 24 hr. Colonies were used to prepare a standardized suspension in DPBS (Corning, USA) at $OD_{600\ nm}$ = 0.2 (i.e., 7 – 8 Log_{10} CFU/mL).

The experimental setup for performing biological tests is illustrated in Figure 4.5. The same methods and procedures outlined in Chapter 2 (section 2.2.3) were employed for the generation of bioaerosols; a bacterial suspension flow rate of 0.852 mL/min and an airflow rate of 1.2 mL/min were delivered to a nebulizer (single-jet Blaustein Atomizer – BLAM; CH Technologies) using a syringe pump (Legato 100; kdScientific) and a digital flowmeter (EL-FLOW; Bronkhorst), respectively. The bioaerosol flowed inside the test chamber for 10 minutes up to a challenge concentration of approximately 5 Log_{10} CFU/m^3. After the nebulization period, the chamber air was sampled to assess the initial bacterial concentration (N_0) by using a biosampler (SKC-impinger; SKC INC.) containing 20 mL of DPBS. Subsequently, the RDBD prototype treated the bioaerosol-contaminated chamber air for 8 minutes. At the end of the treatment, sampling was carried out identically to evaluate the final bacterial concentration within the chamber (N_t). During the entire procedure, a fan was employed inside the chamber to move the air to avoid the accumulation of droplets on the chamber walls. The DPBS sampling liquid was plated using the standard spread plating technique on TSA, and the plates were incubated at 37°C for 24 h for viable colonies counting. The inactivation efficacy of the treatment was evaluated according to the formula given by Formula (3).

$$Log\ R = Log\ N_0 - Log\ N_t \qquad (3)$$

Control samples were collected using the same procedure, but the plasma discharge was not generated to assess the possible impact of fan rotation on bacterial bioaerosol and possible droplet deposition on the chamber walls. To ensure the same initial conditions, the test chamber was sterilized in between tests using UV lamps installed in the chamber. Furthermore, the chamber was opened and flushed with fresh air for 5 minutes before each measurement. The same experimental setup and biological protocol were used to evaluate the antimicrobial efficacy of the Jonix cube device.

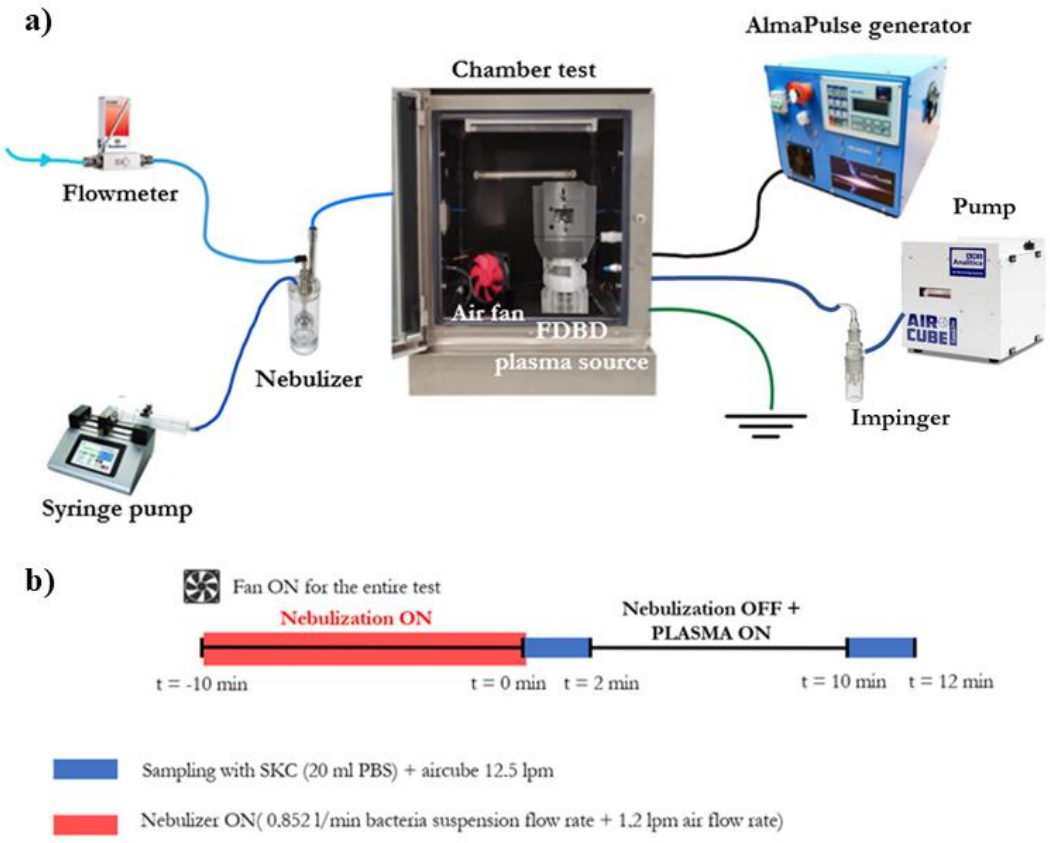

Figure 4.5 *– Experimental setup for microbial inactivation tests using the RDBD plasma source.*

4.3 Results and discussion

4.3.1 RDBD plasma source electrical characterization results

Figure 4.6-a shows an example of current and voltage waveforms at the operating condition of 29.4 ± 0.09 kVp-p with a fixed frequency of 4 kHz (O.C. A). During the applied voltage period (250 µs), multiple spikes can be observed on the current waveform (at around 54 and 176 µs),

corresponding to the active phase of filamentary discharge typical of DBDs operated in the air at atmospheric pressure. The behavior of waveforms at 26.6 ± 0.08 kV_{p-p} and 4 kHz (O.C. C) is similar apart from the reduced voltage measured (Figure 4.6-b). In Figure 4.7, the average discharge powers are evaluated using Formula (1); O.C. A corresponds to the highest average discharge power, while O.C. B and C have values not statistically different (Student's test, $p \geq 0.05$). Finally, O.C. D has the lowest average discharge power.

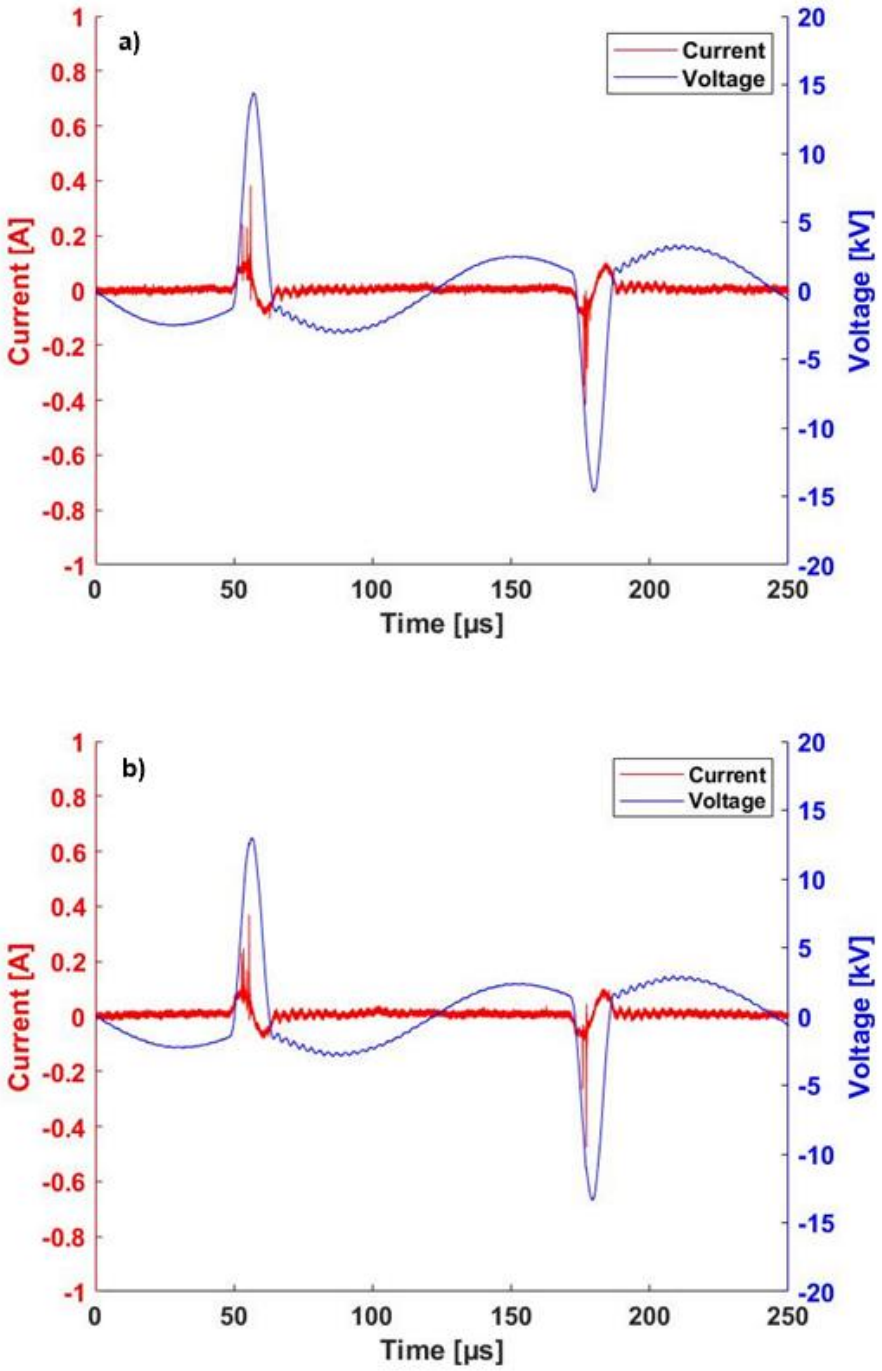

***Figure 4.6** – **a)** Current and applied voltage waveforms at O.C. A and **b)** O.C. C.*

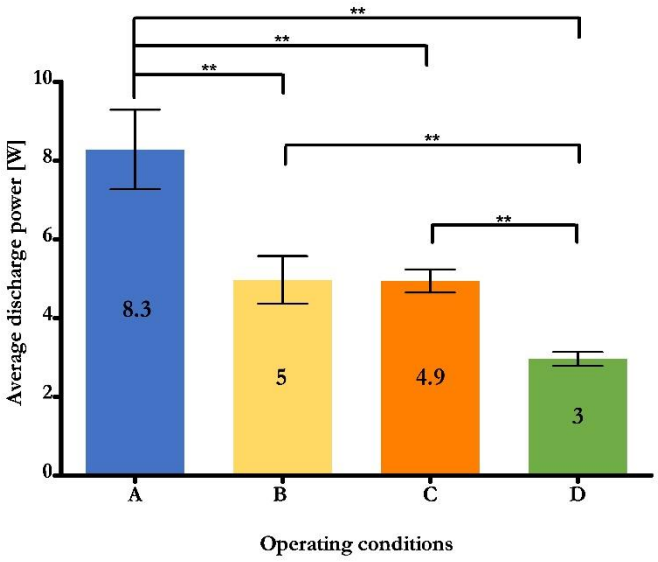

***Figure 4.7** - Average discharge powers for the four O.C.s applied for the RDBD plasma source.*

4.3.2 Ozone and nitrogen dioxide concentration inside the test chamber

Figure 4.8 shows the evolution of the ozone concentration inside the test chamber when operating the RDBD source under different O.C.s and when using the commercial device. The ozone concentration exhibits a consistent and incremental rise over the entire duration of the treatment. Notably, a decline in ozone concentration is evident in Figure 4.8 at 480 seconds, coinciding with the deactivation of the RDBD source. This is the result of ozone degradation, as this component is known to be unstable and decomposes in a few minutes at ambient temperatures [6]. The highest ozone concentration achieved within the chamber was attained by employing the RDBD source under O.C. A, yielding approximately 83 ppm. Conversely, a confined range of ozone concentrations (ranging from 23 to 27 ppm) was observed when operating the RDBD source under conditions B and C (which exhibited statically comparable average discharge power levels) as well as the Jonix device. O.C. D, with the lowest average discharge power, is associated with the lowest ozone concentration (~9 ppm).

The use of filters led to a significant reduction in ozone concentration for all operating conditions, as illustrated in Figure 4.9. The efficiency of filters ranged from 55% to 65%.

For all tested conditions, the concentration of NO_2 remained undetectable within the chamber.

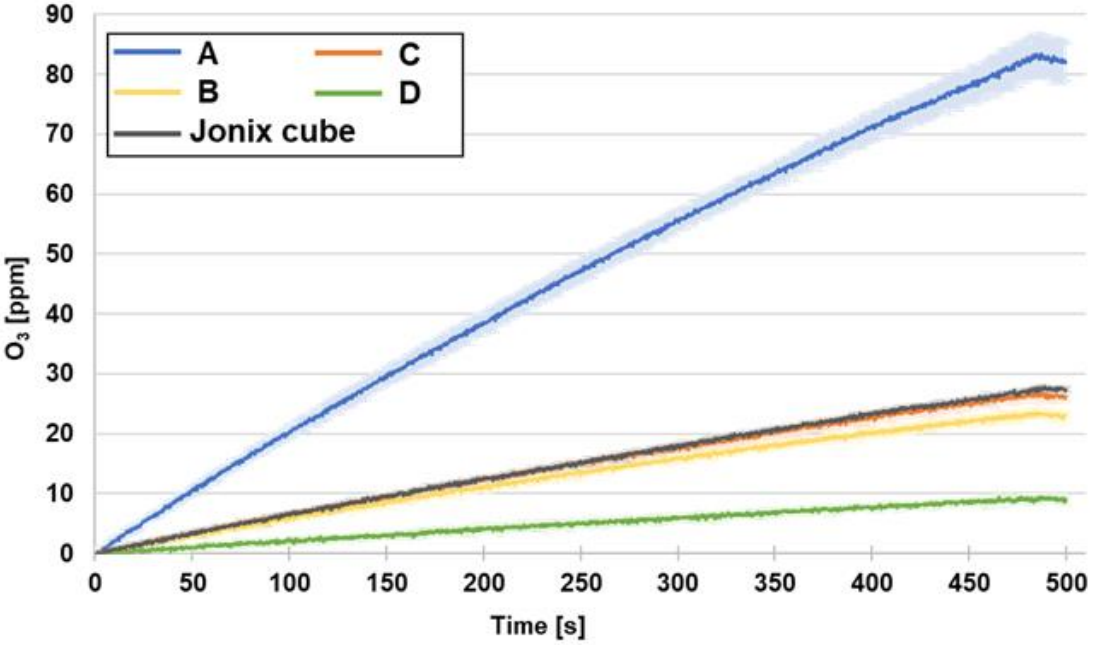

Figure 4.8 *- Ozone concentrations and respective standard deviations (SD) inside the test chamber produced by the RDBD plasma source using the four operating conditions and Jonix Cube device. The SD of the data is graphically displayed as the shaded colored band surrounding the mean line.*

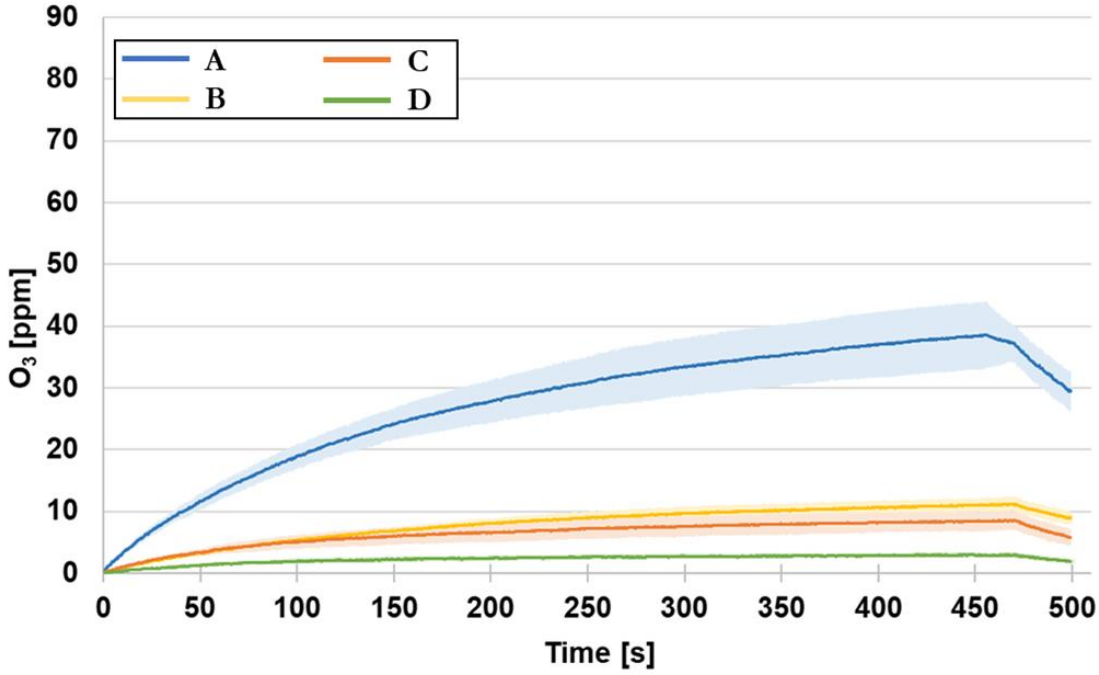

Figure 4.9 *- Ozone concentrations and respective standard deviations (SD) inside the test chamber produced by the RDBD plasma source equipped with activated carbon filters using the four operating conditions. The SD of the data is graphically displayed as the shaded colored band surrounding the mean line.*

4.3.3 Biological inactivation test on *S. epidermidis* bioaerosol

As summarized in Figure 4.10, the RDBD source exerts a comparable antimicrobial effect to the Jonix cube device (Log R = 4.1 ± 0.6), with Log R = 3.8 ± 0.3, 3.6 ± 0.5 and 3.9 ± 0.4 for o.c. A, B and C, respectively. Statistical analysis (Student's test $p \geq 0.05$) shows no statistical difference between these values of Log Reduction. On the other hand, there is a statistical difference (Student's test, $p \leq 0.05$) between the bacterial inactivation results obtained with the operating condition D (Log R = 2.3 ± 0.4) and the other conditions, as well as the commercial device, with O.C. D resulting in a reduced bacterial inactivation. Control tests assessing the impact of fan rotation and possible droplet deposition on chamber walls showed no significant Log R.

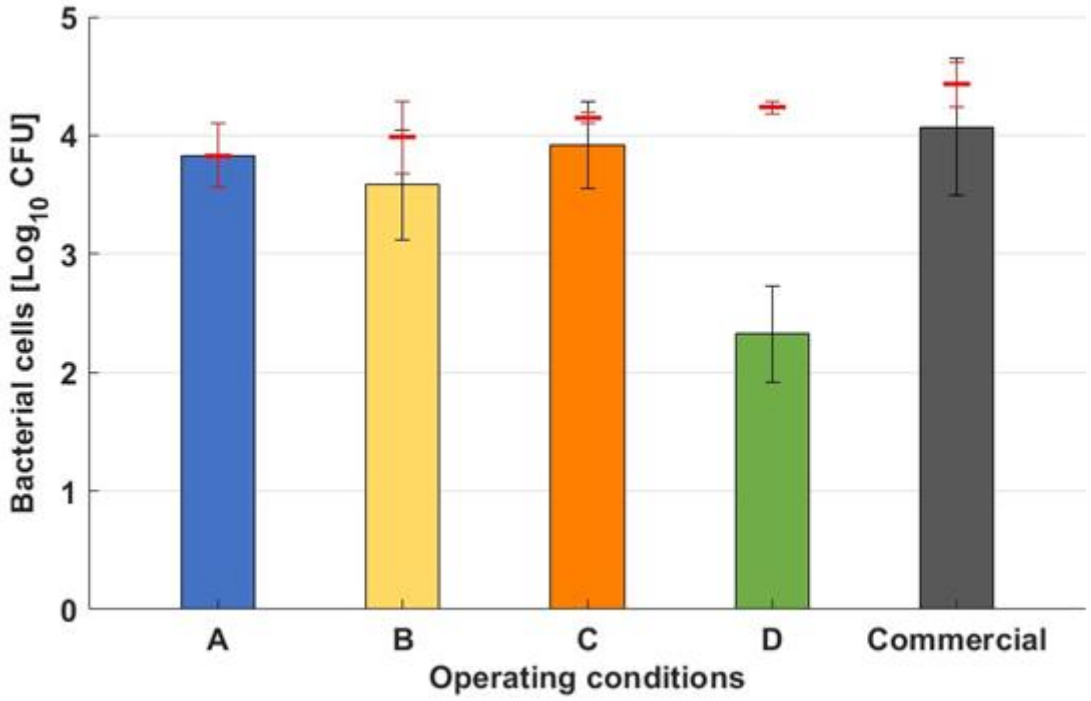

Figure 4.10 *- Average Log_{10} Reduction of S. epidermidis in the bioaerosol after RDBD plasma source treatment using different operating conditions (A-D, see Table 4.1) and the commercial device, shown as bars, with their respective standard deviations. UADL levels and respective standard deviations are indicated with red lines.*

It is essential to notice that the upper antimicrobial detection limit (UADL) was reached for at least one repeat of O.C.s A, B, C and, the commercial Jonix cube, due to the practical limitations of the current sampling system. There was no statistical difference between inactivation levels and the UADL (Student's test, $p \geq 0.05$) for these conditions. Therefore, the Log R values corresponding to these specified operating conditions signify that both systems

can achieve a satisfactory level of bioaerosol decontamination, close to complete inactivation, equivalent to or surpassing 4 Log_{10} CFU. Only for operating condition A, the UADL was reached for all repeats, which could indicate that the true bactericidal potential is the highest among all tested operating conditions. On the other hand, there was a significant difference between the inactivation level and its UADL for O.C. D (Student's test, $p \leq 0.05$).

It is reasonable to consider the average discharge power and consequent ozone production as pivotal factors when designing a novel air decontamination device based on CAP technology. Indeed, ozone is a strong antibacterial agent, acting on both cell membrane and cell content [7]–[9]. An increase in ozone concentration leads to higher efficiency in deactivating microorganisms. Among the various operating conditions (A, B, and C) examined, O.C. A stands out due to its superior average power value and ozone concentration, consistently reaching the UADL in all experimental repetitions. Comparatively, when scrutinizing the outcomes of O.C. A and B, it becomes apparent that satisfactory levels of microbial deactivation can also be achieved by reducing the average discharge power by implementing a duty cycle. Consequently, bacterial inactivation is not compromised during short periods when the plasma discharge is inactive. Although conditions B, C, and the Jonix device do not consistently reach the UADL, they demonstrate satisfactory levels of bacterial deactivation, approaching complete inactivation while exhibiting a significantly lower ozone concentration, approximately three times lower. This outcome is advantageous in terms of minimizing the emission of ozone into the surrounding environment. Furthermore, the lack of statistical difference (based on the Student's test, $p \geq 0.05$) between the Log R values for O.C. B and C highlights that the fluctuation in voltage within the studied plasma source does not seem to affect bacterial inactivation. Indeed, these two O.C.s have similar average discharge powers and ozone concentration but differ in their peak-to-peak voltage values. Conversely, an average discharge power of about 3 W (O.C. D) coupled with an ozone concentration lower than 10 ppm resulted in only partial bacterial inactivation. Thus, despite the potential for a higher antimicrobial efficacy under O.C. A, employing such a high ozone concentration is unnecessary for this specific application. Moreover, the RDBD source can achieve a comparable antimicrobial effect with reduced power compared to the Jonix device while providing a 3.5 times higher air flow rate.

4.4 Conclusions

This research study introduces a novel portable system for indoor air decontamination based on plasma technology. The primary objective of this device is to optimize the process of plasma-assisted air decontamination by utilizing the fan, which serves as both the functional element for air movement and the constituent part of the plasma source. For this reason, the fan is employed as the ground electrode for the dielectric barrier discharge plasma source. To design the new system, the average discharge power and ozone concentration were identified as crucial parameters to monitor. These parameters are considered key factors in the inactivation process of airborne microorganisms. Under various operating conditions, ozone production and antimicrobial efficacy were evaluated for the RDBD plasma source. The results were then compared with those obtained from the commercial Jonix device based on SDBD sources widely used for air decontamination. The RDBD source achieved a satisfactory microbial inactivation value, close to total inactivation, and similar to that achieved by the Jonix device, but with a lower average discharge power than the power consumption of the Jonix device (10 W) and a 3.5 higher air flow rate. This increased flow rate is particularly advantageous for decontaminating larger rooms. Furthermore, the possibility of equipping the RDBD plasma source with activated carbon filters enables a significant reduction in the output ozone concentration. Therefore, the RDBD source could represent a promising approach to air decontamination using plasma technology, a viable indoor air quality control solution.

4.5 References

[1] P. Isabelli, K. De Baerdemaeker, F. Devlieghere, M. Gherardi, and R. Laurita, 'Rotating Dielectric Barrier Discharge (RDBD) Plasma Source for effective bacterial decontamination of bioaerosols', *Plasma Med.*, vol. 14, no. 1, pp. 33–47, 2024, doi: 10.1615/plasmamed.2024053628.

[2] Https://jonixair.com/en/products/cubeline, 'jonixair'. .

[3] M. Martinelli, F. Giovannangeli, S. Rotunno, C. M. Trombetta, and E. Montomoli, 'Water and air ozone treatment as an alternative sanitizing technology', *J. Prev. Med. Hyg.*, vol. 58, no. 1, 2017, doi: 10.15167/2421-4248/jpmh2017.58.1.757.

[4] B. Bayarri, A. Cruz-Alcalde, N. López-Vinent, M. M. Micó, and C. Sans, 'Can ozone inactivate SARS-CoV-2? A review of mechanisms and performance on viruses', *J. Hazard. Mater.*, vol. 415, 2021, doi: 10.1016/j.jhazmat.2021.125658.

[5] F. Gomes, P. Teixeira, and R. Oliveira, 'Mini-review: Staphylococcus epidermidis as the most frequent cause of nosocomial infections: Old and new fighting strategies', *Biofouling*, vol. 30, no. 2, pp. 131–141, 2014, doi: 10.1080/08927014.2013.848858.

[6] N. N. Morgan, 'Atmospheric pressure dielectric barrier discharge chemical and biological applications', *Int. J. Phys. Sci.*, vol. 4, no. 13, pp. 885–892, 2009.

[7] A. K. Greene, Z. B. Güzel-Seydim, and A. C. Seydim, 'Chemical and Physical Properties of Ozone', *Ozone in Food Processing*, Oxford, UK: Wiley-Blackwell, 2012, doi: 10.1002/9781118307472.

[8] Z. B. Guzel-Seydim, A. K. Greene, and A. C. Seydim, 'Use of ozone in the food industry', *LWT - Food Sci. Technol.*, vol. 37, no. 4, pp. 453–460, Jun. 2004, doi: 10.1016/j.lwt.2003.10.014.

[9] K. Ishizaki, K. Sawadaishi, K. Miura, and N. Shinriki, 'Effect of ozone on plasmid DNA of Escherichia coli in situ', *Water Res.*, vol. 21, no. 7, pp. 823–827, 1987, doi: 10.1016/0043-1354(87)90158-8.

4.6 Appendix 3 - CAP prototypes and improvements

Section 4.2.1 shows the last version of the tabletop plasma source designed and developed for bioaerosol decontamination in order to contrast airborne transmission. Before achieving the final version and results presented in Chapter 4, several plasma source configurations were designed and developed, following the process described in Section 3.4. The objective for the design of this plasma-based device was to optimize its components, which led to the innovative idea of using the air-handling fan as an integral part of the plasma source, serving as the ground electrode. This approach aimed to employ all the antimicrobial agents produced by the plasma discharge in the air decontamination process.
However, incorporating the fan device as the ground electrode and interfacing the high-voltage electrodes posed significant constructional challenges.

4.6.1 First CAP prototypes for bioaerosol decontamination

The initial designs for the tabletop plasma source focused on corona architectures, aiming to use pointed ends to intensify the local electric field and generate plasma discharges between HV electrodes and a commercial plastic fan equipped with a metal coating. Three configurations were evaluated:

1. **Blade Plasma Source**: This configuration utilized blades as HV electrodes attached to the fan using specially designed supports (Figure 4.11-a). While this design generated plasma discharges between the blades and the coated fan blades, the plasma discharges were confined to the smallest gaps and the blade tips, severely limiting the discharge area.

2. **Multiple Pins Plasma Source**: Pins mounted on a ring serve as HV electrodes in this design. With appropriate supports, plasma discharges occurred between the pins and the fan (Figure 4.11-b). However, aligning the pins with the curved surfaces of the fan blades was complex, requiring each pin's height to be individually adjusted. This alignment issue also made it impossible to use different fan types. Furthermore, this configuration experienced high current spikes (above 3 A), rapidly degrading both the fan and the metal coating.

3. **Ring Plasma Source**: This design featured one or more sharpened concentric rings as HV electrodes (Figure 4.11-c). When opposed to the fan, they generated a circular plasma discharge around the ring’s perimeter. However, this setup caused unwanted

discharges in the fan's motor, located at its center in most commercial fans, leading to motor deterioration after extended use.

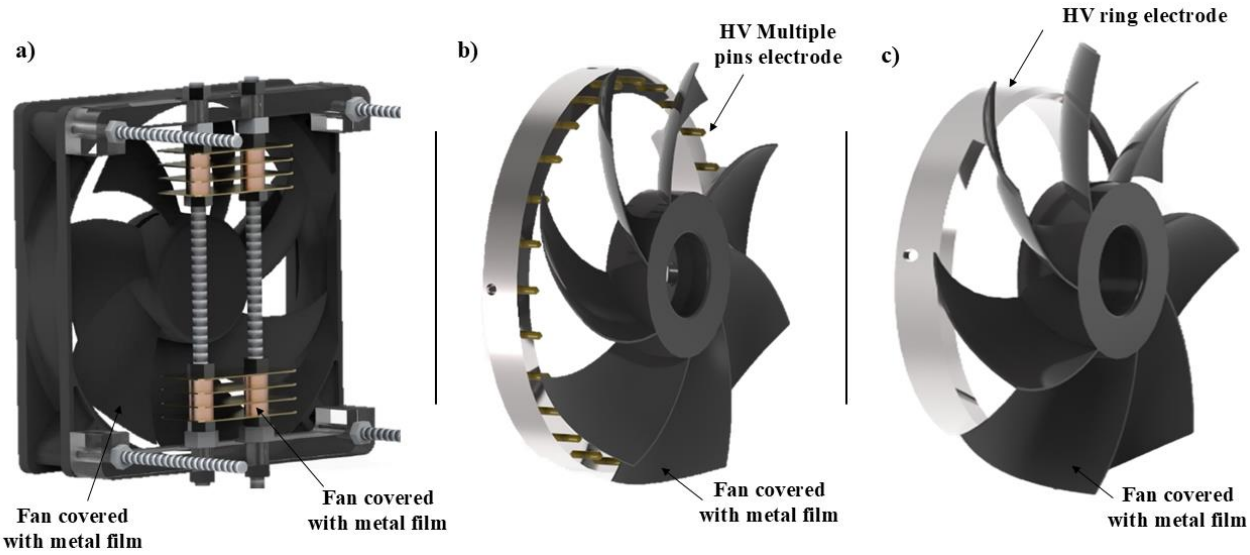

Figure 4.11 *– First prototypes for the tabletop device:* ***a)*** *Blade plasma source;* ***b)*** *Multiples pins plasma source;* ***c)*** *Ring plasma source.*

Each configuration faced significant challenges, including limited plasma generation zones, complex alignment requirements, or rapid wear on components, all of which guided further iterations.

4.6.2 Improvements in the RDBD plasma source

The issues encountered in previous configurations were addressed in the RDBD version through several design improvements. A DBD configuration was chosen to reduce current spikes, with high voltage rods fixed in glass dielectric tubes using epoxy resin, allowing the tubes to serve as dielectric barriers. To prevent fan deterioration, a metal fan was introduced and grounded through a creep connection. Additionally, the fan was decoupled from the motor by inserting a shaft, distancing the motor from the fan to eliminate unwanted plasma discharges and avoid motor damage (Figure 4.12).

To resolve alignment issues between the fan and electrodes, multiple independently supported electrodes were introduced. These supports allow for adjustment of both the distance and orientation of the electrodes relative to the fan blades (Figure 4.12 detail), facilitating quick alignment and easy replacement of electrodes in case of breakage or malfunction.

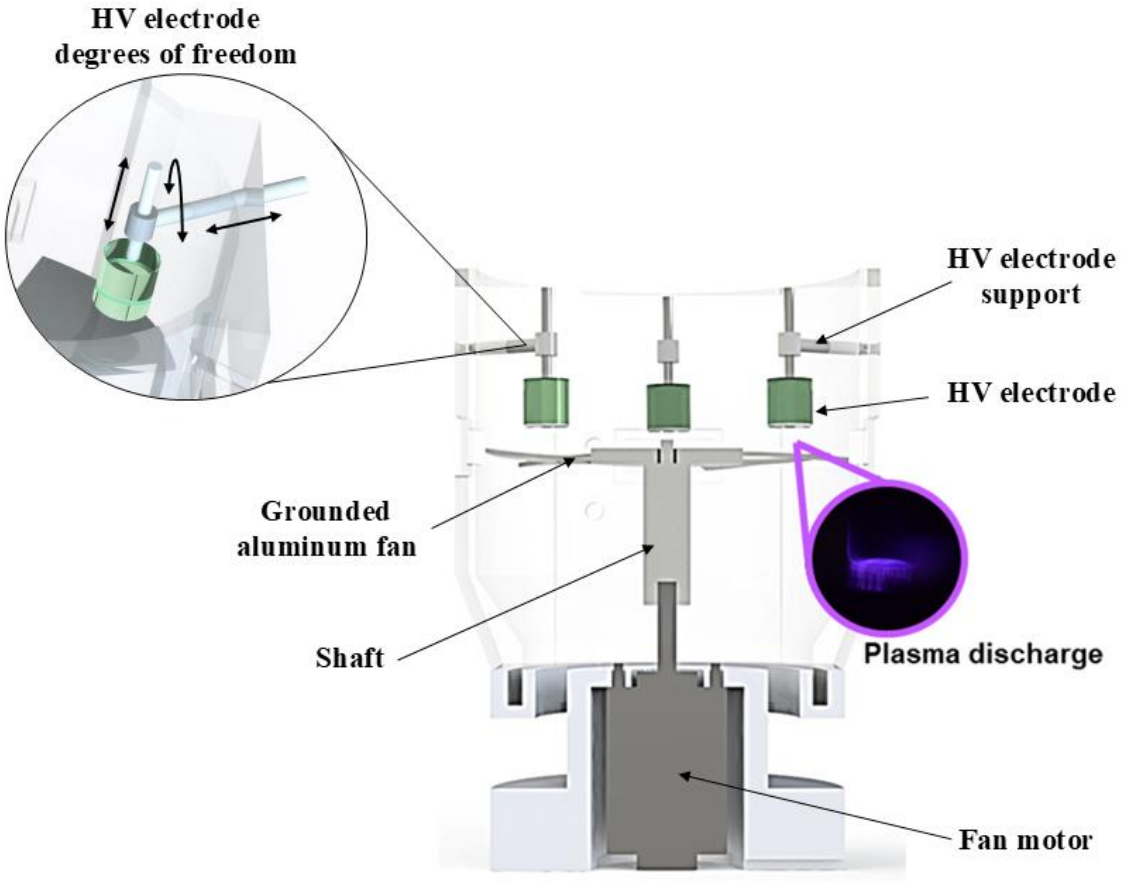

Figure 4.12 *- Enhancements in the RDBD plasma source version detail on the increased degrees of freedom for the electrodes provided by the support structure.*

Chapter 5

InDuct plasma source

5.1 Introduction

This chapter presents the design, development, and characterization of a plasma source to decontaminate air within ventilation ducts. The primary objective is to identify a suitable architecture that can be effectively integrated into indoor air ducts. To accomplish this, a device called InDuct Plasma Source was developed and installed in a laboratory-scale duct (Lab-scale duct) to test its antimicrobial efficacy. The efficacy of the device was assessed by evaluating its impact on bioaerosols containing *S. epidermidis* under two different operating conditions. Additionally, the efficacy of the InDuct plasma source was compared to that of an SDBD plasma source, where the bioaerosol interacts solely with long-lived reactive species, such as ozone, without direct contact with the plasma discharge. The chemical composition of the gas phase generated by the InDuct and SDBD plasma sources was analyzed using OAS. Moreover, the gas phase produced by the InDuct plasma source was investigated more deeply through optical emission spectroscopy (OES) and mass spectrometry (MS); this chemical characterization was carried out during a research period abroad.

5.1.1 Period abroad activity

During the period abroad (March 1 to May 31, 2024), a comprehensive investigation into the gas-phase chemical composition produced by the InDuct plasma source was performed in collaboration with the Elementary Processes in Gas Discharge (EPG) group at Eindhoven University of Technology (TU/e) in the Netherlands, under the supervision of Prof. G. Kroesen. Specifically, experimental setups were created and optimized to employ advanced diagnostic techniques such as MS and OES. This project was part of a short-term scientific mission (STSM) titled 'Diagnostic of cold atmospheric plasma systems for air decontamination' funded by PlasTher COST Action CA20114 - Therapeutical applications of Cold Plasma.

5.2 Materials and Methods

5.2.1 Plasma sources

5.2.1.1 Design of a CAP system for ducts: the InDuct Plasma source

The CAP source is designed to act as an 'active filter' by decontaminating microorganisms in the air as they pass through it. The InDuct plasma source (Figure 5.1), has two HV electrodes surrounded by 7 ground electrodes. Each HV electrode consists of an AISI

304 steel rod coaxially fixed inside a glass dielectric tube (with dielectric constant ε_r between 5 and 10) and filled with epoxy resin (Figure 5.2). The coaxial design is maintained by specially designed supports made by 3D resin printing (Anycubic Photon M3 Max). The ground electrodes, also made of AISI 304 steel rods, are spaced 3 mm from the HV electrodes. The gap between the HV and ground electrodes is ensured by specially designed and 3D-printed supports inside which the electrodes are fixed by epoxy resin. The InDuct plasma source was integrated within a lab-scale PVC duct to simulate a ventilation duct environment and validate its antimicrobial efficacy (Figure 5.3). The duct is equipped with a dual ball-bearing DC brushless fan, providing an airflow of 3.5 m^3/h directed toward the plasma source. Additionally, the duct includes a section for introducing bioaerosols containing bacteria and optical windows for performing OAS analyses.

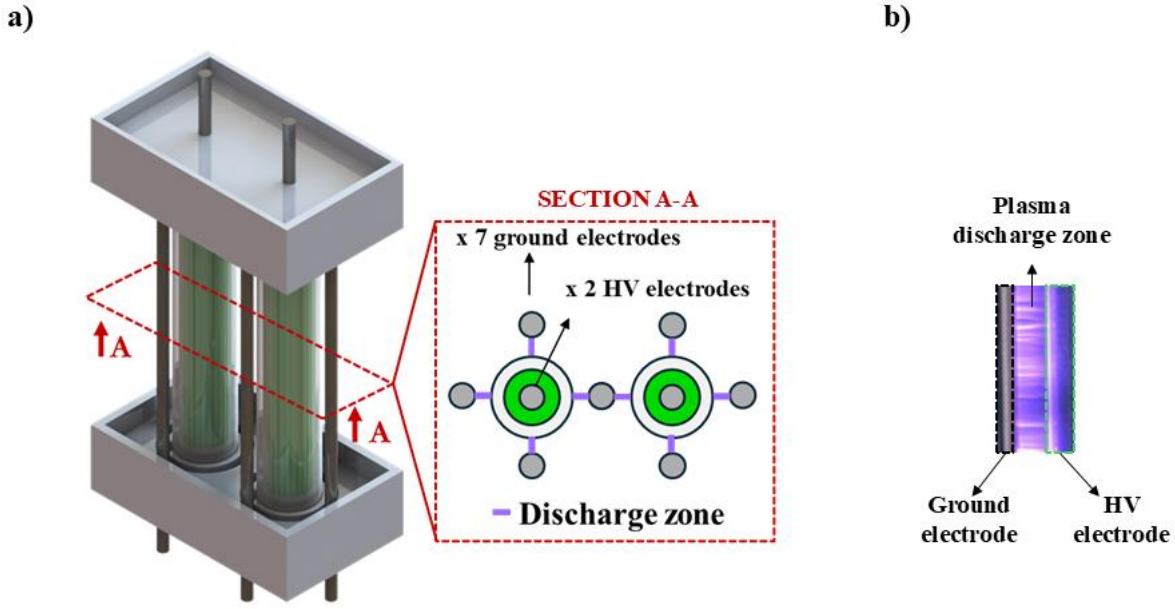

***Figure 5.1** – **a)** InDuct plasma source; **b)** Real picture of the plasma discharge.*

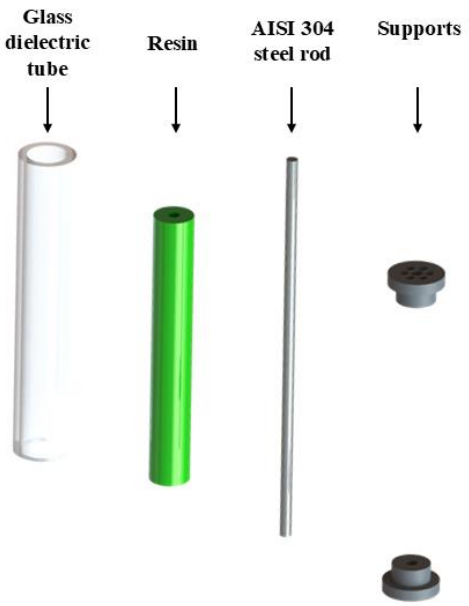

Figure 5.2 *– HV electrode exploded view.*

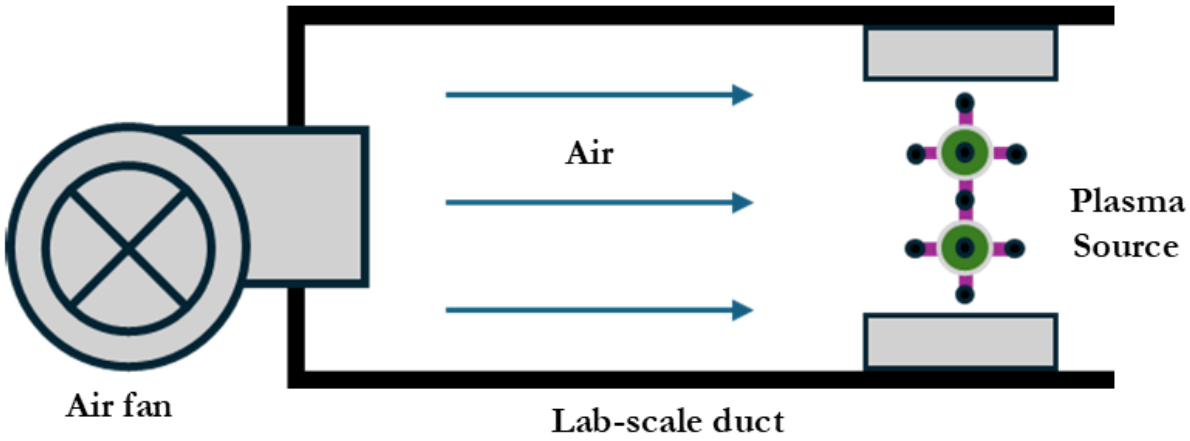

Figure 5.3 *– Sectional view schematic of the lab-scale duct simulating a ventilation duct environment, equipped with an air fan, optical windows, and a section for introducing bioaerosols into the airflow.*

5.2.1.2 SDBD plasma source for the lab-scale duct

The SDBD was designed to generate ozone concentrations statistically similar to those produced by the InDuct plasma source. However, unlike the InDuct source, the SDBD was specifically engineered so that the bacterial bioaerosol does not pass directly through the discharge. Instead, any antimicrobial efficacy is due solely to long-lived reactive species, such as ozone.

As shown in Figure 5.4, the SDBD source comprises an HV electrode mounted inside a support, with a 2 mm layer of MICA (ε_r = 6 - 8) as the dielectric material, fixed to the HV

electrode using epoxy resin. A grid is the ground electrode, with the plasma discharge localized at the grid mesh.

As shown in Figure 5.5, the SDBD source was installed in one of the walls of the lab-scale duct. In this setup, the air does not directly contact the plasma discharge generated at the grid mesh. To ensure consistent duct volume when assessing ozone production and antimicrobial efficacy of the SDBD, the InDuct source remained mounted inside the duct but was not activated.

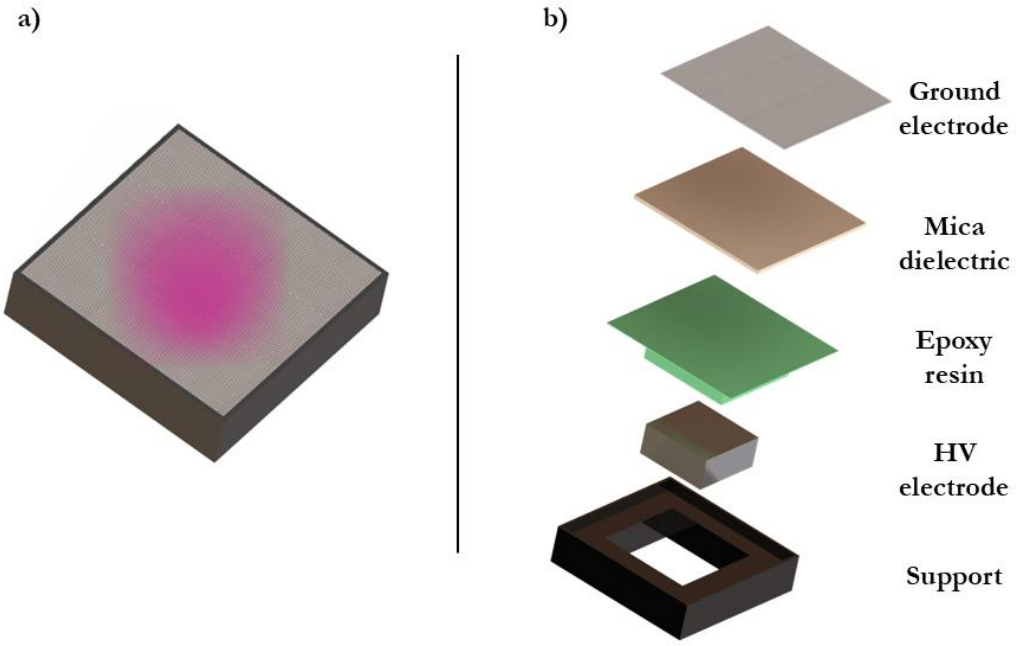

***Figure 5.4** – **a)** Render of the SDBD plasma source; **b)** Exploded view and main components of the SDBD plasma source.*

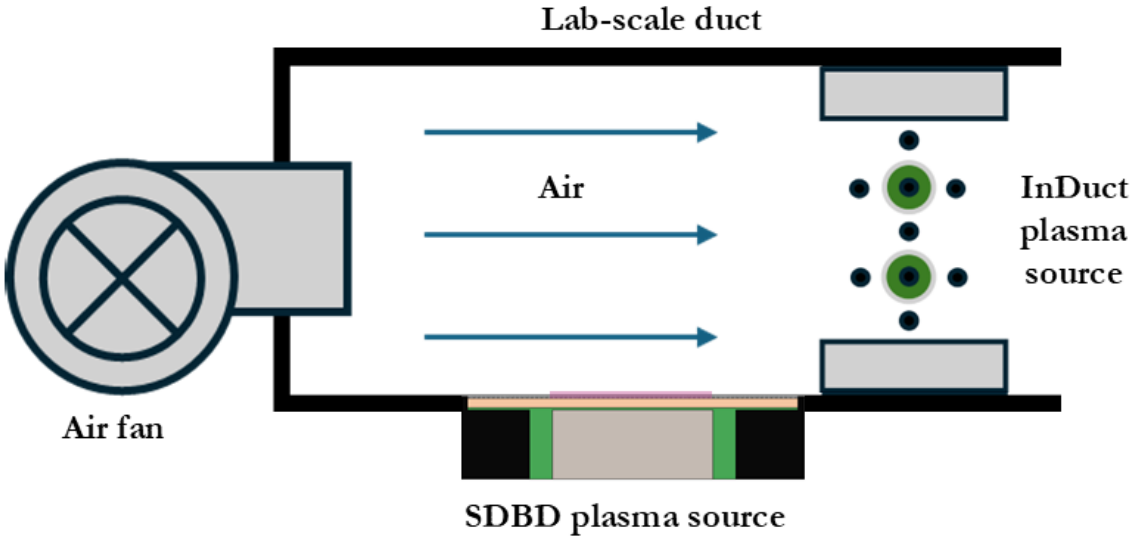

***Figure 5.5** – Sectional schematic view of the lab-scale duct equipped with the SDBD plasma source.*

5.2.2 Statistical Analysis

All experiments were performed in three independent replications. The results are presented as the mean ± standard deviation (SD). Significant differences in the results were assessed using the Student's test and were specified with asterisks (* p≤ 0.05, ** p≤0.001).

5.2.3 Plasma sources electrical characterization

The InDuct plasma source and the SDBD were driven by a micropulsed HV generator (AlmaPULSE; Alma Plasma s.r.l., Bologna), both applying two operating conditions (O.C.) (Table 5.1 and Table 5.2).

Operating condition (O.C.)	***Vp-p (peak-to-peak voltage) [kVp-p]***	***f (frequency) [kHz]***
A	32	5
B	34.6	5

Table 5.1 *– O.C.s applied for the InDuct plasma source.*

Operating condition (O.C.)	***Vp-p (peak-to-peak voltage) [kVp-p]***	***f (frequency) [kHz]***
C	32.4	4
D	31.6	10

Table 5.2 *– O.C.s applied for the SDBD plasma source.*

The applied voltage *v(t)* and the current *i(t)* were measured using an HV probe (Tektronix P6015A) connected to the HV cable and a current probe (Pearson 6585) positioned on the ground cable. The corresponding waveforms were recorded using a digital oscilloscope (Tektronix MSO46) (Figure 5.6). The same experimental setup was used for both plasma sources.

The average discharge power (P) dissipated over the applied voltage period (T) was determined using the formula (1).

$$P = \frac{1}{T}\int_0^T V(t)I(t)dt \qquad (1)$$

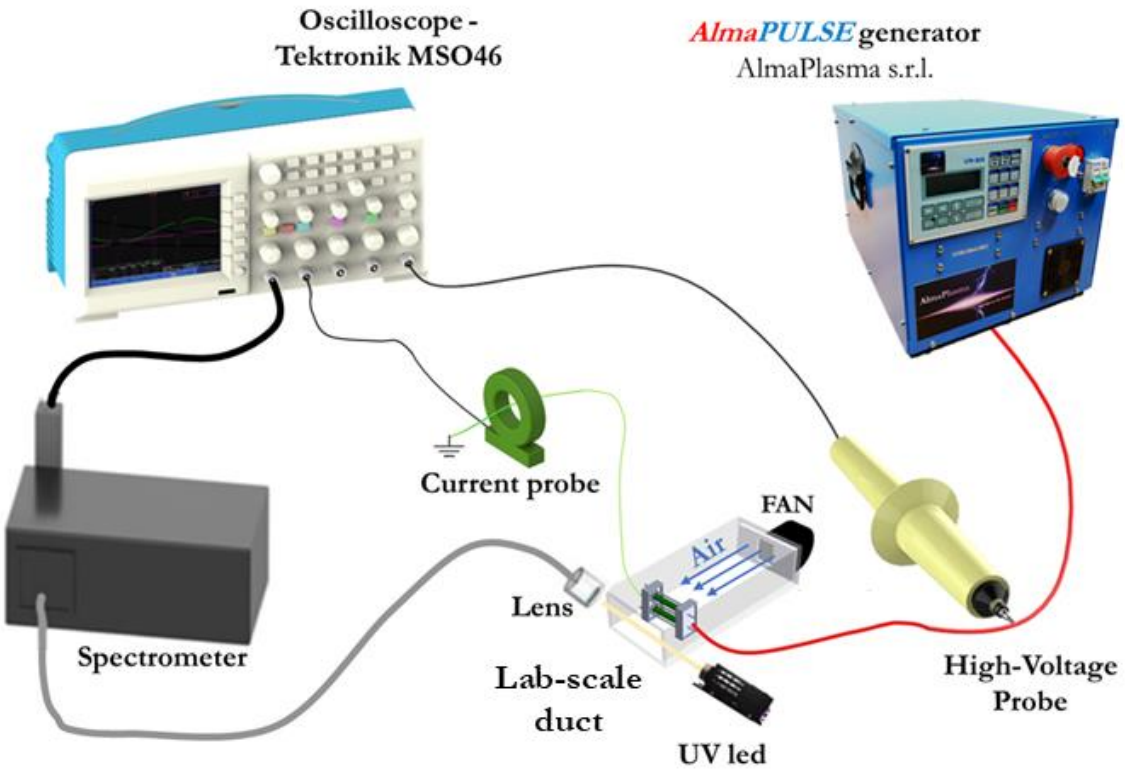

Figure 5.6 *- Experimental setup for the InDuct and SDBD plasma sources electrical characterization and evaluation of ozone and nitrogen dioxide concentration inside the lab-scale duct.*

5.2.4 Evaluation of the gas phase

5.2.4.1 InDuct and SDBD OAS analysis

OAS was used to evaluate the ozone and nitrogen dioxide concentration produced by the InDuct plasma source inside the lab-scale duct at five centimeters from the plasma discharge (Figure 5.6). The lab-scale duct featured two quartz optical windows, enabling measurements free from interference caused by the plasma discharge emission during the optical analysis. The materials and methods used for this analysis, briefly summarized below, are the same as those detailed in Chapter 4 (Section 4.2.5). Two light sources were used to emit an orthogonal beam to the airflow through a 70 mm optical path (L) within the duct at 5 cm of plasma discharge. The transmitted light was directed to a 500 mm spectrometer (Acton SP2500i; Princeton Instruments) for spectral resolution across UV, visible (VIS), and near-infrared regions. The data was captured by a photomultiplier tube (PMT, Princeton Instruments PD439) and a fast oscilloscope (Tektronix MSO46). A 235 nm deep-UV LED module (Omicron Laserage Laserprodukte GmbH) was used for ozone measurement, while a commercially available 400

nm LED measured nitrogen dioxide (NO_2) concentration. Optical fibers and fused silica lenses focused the light beam, which was analyzed by the spectrometer. The inlet slit was set to 10 µm, and a 150 mm^{-1} grating was used. O_3 and NO_2 concentrations were determined using the Lambert-Beer law and their respective absorption cross-sections, (σ_{O3_253nm} = (1.12 ± 0.02)*10^{-17} cm^2 and σ_{NO2_400nm} = (6.4 ± 0.02)*10^{-19} cm^2). The concentration of the two species inside the duct was monitored continuously for 80 seconds, with the plasma discharge active for 60 seconds. The same experimental setup and procedure were used to monitor the ozone concentration inside the duct produced by the SDBD plasma source.

5.2.4.2 InDuct mass spectrometry analysis

MS is an advanced diagnostic technique able to detect a wide range of species generated by plasma, including ions, neutral atoms, and molecules [1][2][3]. A molecular beam mass spectrometer (MBMS, SIM900N, Hiden Analytical Limited) was used to analyze gas-phase chemistry produced by the InDuct plasma source. Figure 5.7-a shows a simplified schematic representation of the experimental setup and the MBMS used in this study.

The MBMS differentiates ions based on their mass-to-charge ratio (*m/q*) by manipulating their trajectories using electromagnetic fields [3][4]. This process is achieved through a quadrupole mass filter (QMF) consisting of four parallel rods. Two opposing rods are supplied with a combination of direct current (DC) and radio frequency (RF) voltages, allowing precise modulation of ion paths for accurate mass selection. To measure neutral species, both neutral and radical species must first be ionized before entering the QMF. The ionizer generates electrons by passing an emission current through a filament. The applied potential (electron energy, V) creates an electric field that accelerates these electrons toward the molecular beam, where they ionize neutral molecules. After ionization, they pass through the QMF, which selects the desired mass-to-charge ratios, and finally, the ions are detected by the detector. The ionizer is a filament that generates electrons at specific energy and emission current. Additionally, the MBMS is equipped with a Bessel box energy analyzer (BBEA) positioned before the QMF. The BBEA separates electrons from ions and ensures that no photons reach the MBMS detector, which is an ion-counting secondary electron multiplier (SEM). The SEM counts the number of ions striking it per second (c/s).

The MBMS operates at low pressure to minimize ion collisions, while the plasma source functions at atmospheric pressure. Therefore, a transition from atmospheric pressure to vacuum is necessary. Plasma is sampled through a 25 µm metal orifice connected to a three-stage pressure reduction system. The pressure reduction system is continuously pumped down by

turbopumps (Pfeiffer HiPace 300) and pre-pumps (Boc Edwards XDS 10). In the first stage (P_1), the pressure is approximately 10^{-3} mbar and monitored using a Pirani gauge (Edwards APG-L-NW 16). The second (P_2) and third (P_3) stages operate at around 10^{-6} mbar and 10^{-7} mbar, respectively, with pressures measured by cold cathode gauges (Edwards AIM-S-NW 25, Edwards AIM-X-M/SEAL DN40CF). This configuration facilitates a fast pressure drop from the atmospheric pressure of the plasma source down to the high-vacuum environment required by the mass analyzer. To achieve this, the system utilizes a free-jet expansion originating from the atmospheric pressure into the initial low-pressure stage. A skimmer efficiently extracts a molecular beam from the resulting supersonic expansion, subsequently directed toward the QMF for analysis. Species created within the atmospheric plasma discharge are thus introduced into the analyzer for detection and identification.

In this study, the mass spectrometer was operated in residual gas analyzer (RGA) mode, enabling the sampling of stable particles[1]. During the RGA mode, the molecules are ionized by the ion source via electron impact ionization. When electrons have sufficient energy, they can ionize an atom or molecule, resulting in the formation of a positively charged ion through the collision (2) [1][3].

$$M + e^- \rightarrow M^+ + 2e^- \qquad (2)$$

An electron may carry significantly more energy than required for a single ionization event, potentially leading to the formation of multiple ionized ions (3) or dissociative ionization (4) [1][3].

$$M + e^- \rightarrow M^{z+} + (z+1)e^- \qquad (3)$$

$$AB + e^- \rightarrow A^+ + B + 2e^- \qquad (4)$$

Stable species such as O_3 (48 amu) and NO_2 (46 amu) can be detected by setting the ionizer to a standard electron energy of 70 eV, facilitating all three ionization processes. Moreover, this study employed an emission current of 100 µA. The monitored masses were recorded over a total acquisition period of 300 seconds. During this time, the plasma alternated between on (PS ON – plasma source ON phase) and off (PS OFF – plasma source OFF phase) states in 5-second intervals (Figure 5.7-b). The distance between the sampling hole and the plasma discharge is 5 cm. To analyze mass spectrometer data, a phase averaging technique was employed to enhance the signal-to-noise ratio and ensure the accurate extraction of the periodic components of the signal [5][6][7]. This method consists of three main steps:

- Segmentation: the continuous signal is divided into segments, each corresponding to one signal period of the signal.

- Alignment: each segment is aligned in phase so that corresponding points within each period are matched across all segments.

- Averaging: where the aligned segments are then averaged point by point. This means that for each point in the period, values from all segments are summed and then divided by the number of periods. The resulting averaged signal $\overline{S}$ (t) is obtained using Formula (5), where *S(t)* is a periodical signal with N cycles, denoted as $S_1(t)$, $S_2(t)$,..., $S_N(t)$.

$$\overline{S}(t) = \frac{1}{N}\sum_{i=1}^{N} S_i(t) \qquad (5)$$

This technique led to a more accurate analysis of the periodic features of the signal.

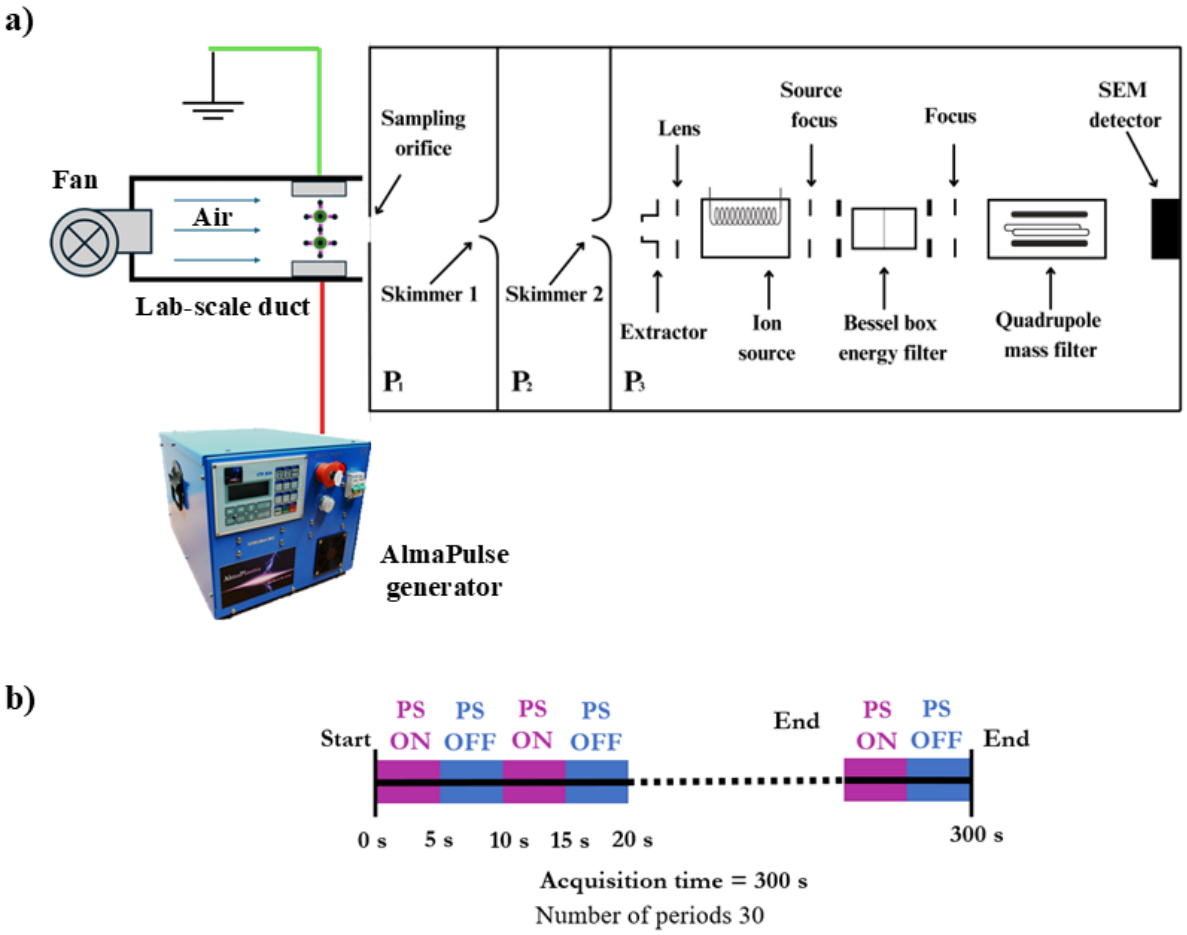

Figure 5.7 – a) *Experimental setup for mass spectrometry analysis using the InDuct plasma source and main SIM900 N MBMS components;* ***b)*** *acquisition mode and sample scan time using MS.*

5.2.4.3 InDuct OES analysis

OES, like OAS, is a non-intrusive technique used to analyze plasma characteristics through its natural emission [8]. This technique measures the light emitted by excited atoms, ions, and molecules within the plasma, providing information such as the gas composition [8][9].

This study adopted the OES technique to determine the active species in the InDuct plasma source in the wavelength range of 300 – 435 nm. A Maya 2000 PRO fiber optic spectrometer (Ocean Optics, USA) with a spectral resolution of 0.17 nm and a fiber optical cable (FC-UVIR200-2, Avantes), were used to collect spectroscopy data (Figure 5.8). The fiber optical probe was positioned 5 cm from the plasma discharge. The OceanOptics Spectra Suite software subtracted the background light from the spectra. The recorded spectra were then analyzed to determine the rotational temperature (T_r) of molecules in the electronically excited $N_2(C)$ state [8]. The T_r was calculated using a MATLAB script developed by the EPG group at Eindhoven University of Technology (TU/e), which fitted a mathematical model (Voigt profile) to the observed spectral lines. Theoretical spectra with T_r as a fitting parameter were fitted with the experimental spectra to obtain the rotational temperature.

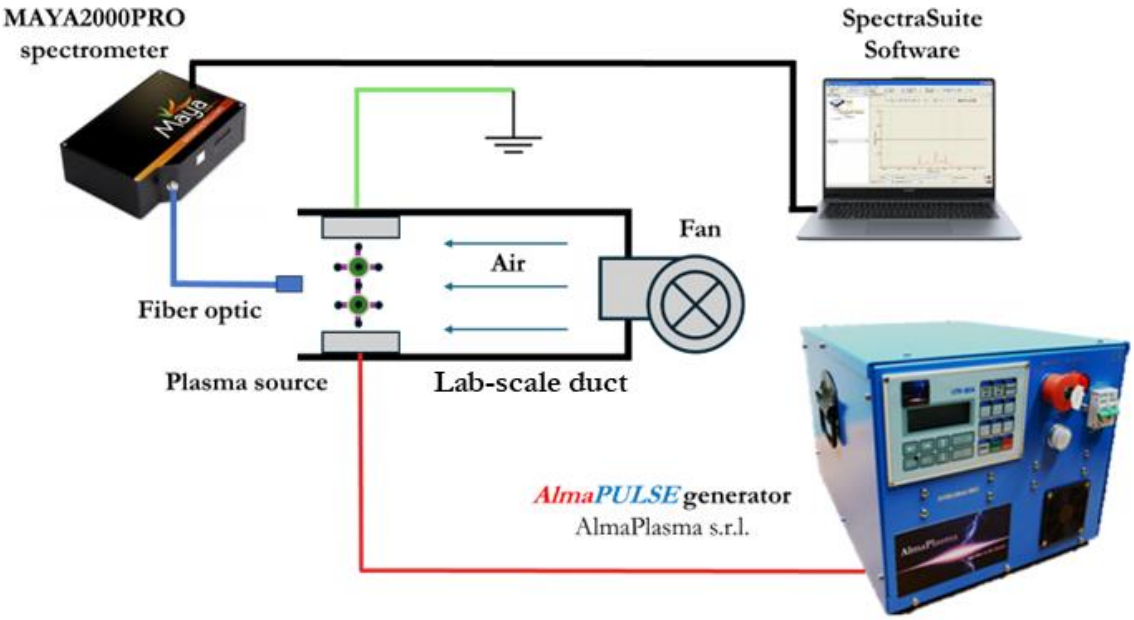

Figure 5.8 *– Experimental setup for OES analysis using the InDuct plasma source.*

5.2.5 Evaluation of bactericidal efficacy in bioaerosol

The efficacy of the InDuct and SDBD plasma sources was evaluated using a bioaerosol containing *S. epidermidis* (ATCC 12228). The bacteria were cultured and prepared as a standardized suspension (10^7–10^8 CFU/mL), which was then nebulized into the same test chamber described in Section 4.2.4, for 10 minutes, resulting in a concentration of approximately 5 Log_{10} CFU/m^3. The experimental setup is depicted in Figure 5.9. The bioaerosols were generated using the same methods described in Chapter 2 (Section 2.2.3), with a bacterial suspension flow rate of 0.852 mL/min and an airflow rate of 1.2 mL/min supplied to a nebulizer (BLAM; CH Technologies) via a syringe pump (Legato 100; kdScientific) and a digital flowmeter (EL-FLOW; Bronkhorst). After the nebulization step, the contaminated air in the chamber was fluxed through the duct using the duct fan (with the plasma source OFF) and sampled for 2 minutes to determine the initial bacterial concentration (N_0) using a biosampler (SKC-impinger; SKC INC.) containing 20 mL of DPBS. The plasma sources were then switched ON to treat the bioaerosol for 2 minutes. During the two-minute CAP treatment, the air was sampled by the biosampler to measure the bacterial concentration after the bioaerosol had passed just once through the plasma discharge (N_t). The DPBS sampling liquid was plated using the standard spread plating technique on tryptic soy agar (TSA), and the plates were incubated at 37°C for 24 hours to count viable colonies. The inactivation efficacy of the treatment was calculated using the formula (6):

$$Log\ R = Log\ N_0 - Log\ N_t \qquad (6).$$

Control samples were collected following the same procedure without generating plasma discharge to evaluate the effects of fan rotation and droplet deposition on the duct walls. The test chamber and the duct were cleaned between tests using UV lamps and ethanol. Moreover, the chamber was opened and flushed with fresh air for 5 minutes before each measurement to maintain consistent initial conditions.

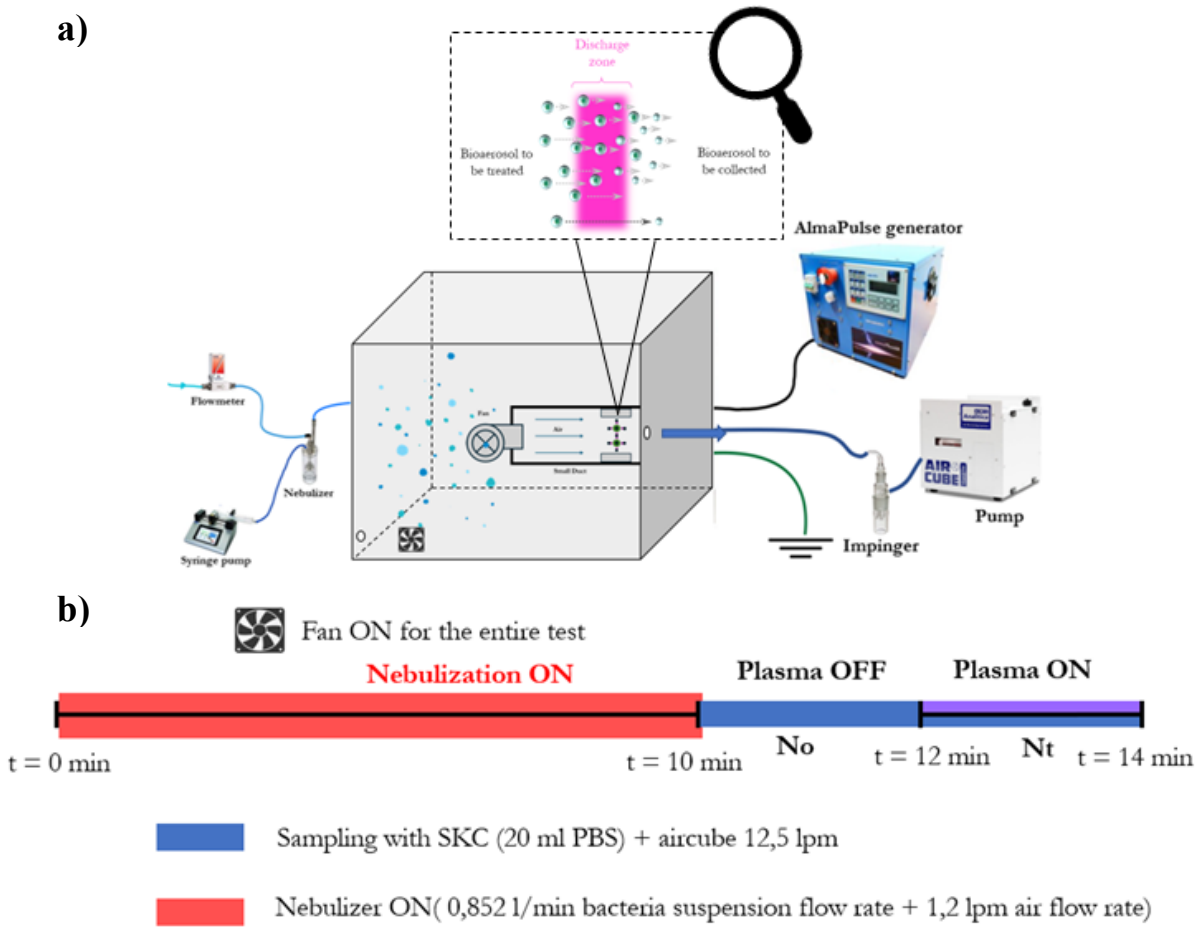

***Figure 5.9** – **a)** Experimental setup for microbial inactivation tests using the InDuct and the SDBD plasma sources; **b)** acquisition mode and sample scan time.*

5.3 Results and discussion

5.3.1 Plasma source electrical characterization results

The InDuct plasma source operates at two distinct levels of average discharge power (Figure 5.10). O.C. B represents the highest power level at approximately 12.6 ± 0,98 W. In contrast, O.C. A operates at a statistically lower power level of approximately 8.1 ± 0,96 W (Student's t-test, $p \leq 0.001$). Two distinct levels of average discharge power (Student's t-test, $p \leq 0.001$) were also identified for the SDBD. O.C.D, characterized by a higher frequency, achieved the highest power at 33.47 ± 1.4 W, while O.C. C had an average discharge power of 15.65 ± 0.4 W.

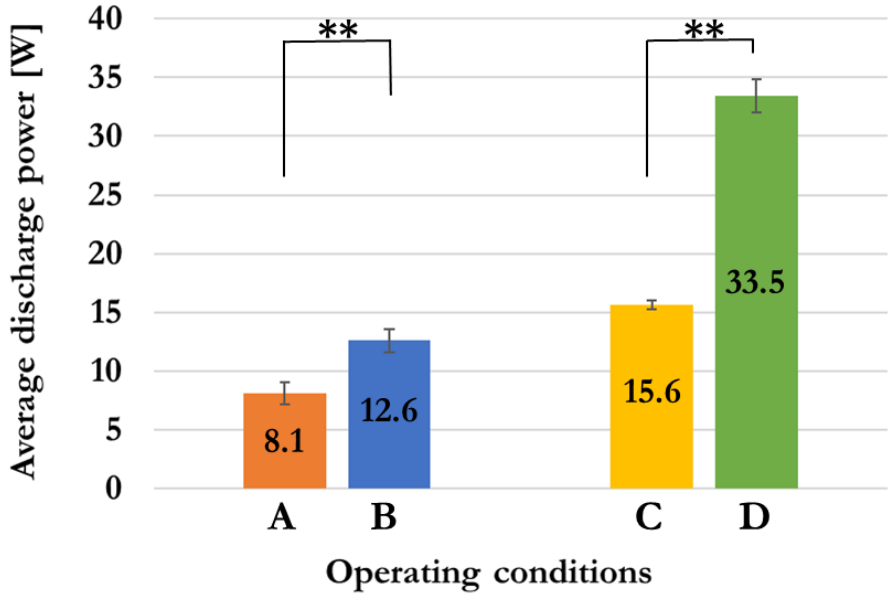

Figure 5.10 *– Average discharge powers of the two plasma sources (O.C. A and B for the InDuct plasma source and O.C. C and D for the SDBD plasma source) (Student's test, * $p \leq 0.05$, ** $p \leq 0.001$).*

Moreover, Figures 5.11 and 5.12 show an example of current and voltage waveforms for the O.C.s investigated with the two plasma sources. During the different applied voltage periods, it is possible to observe multiple spikes corresponding to the active phase of the plasma discharge on the current waveforms.

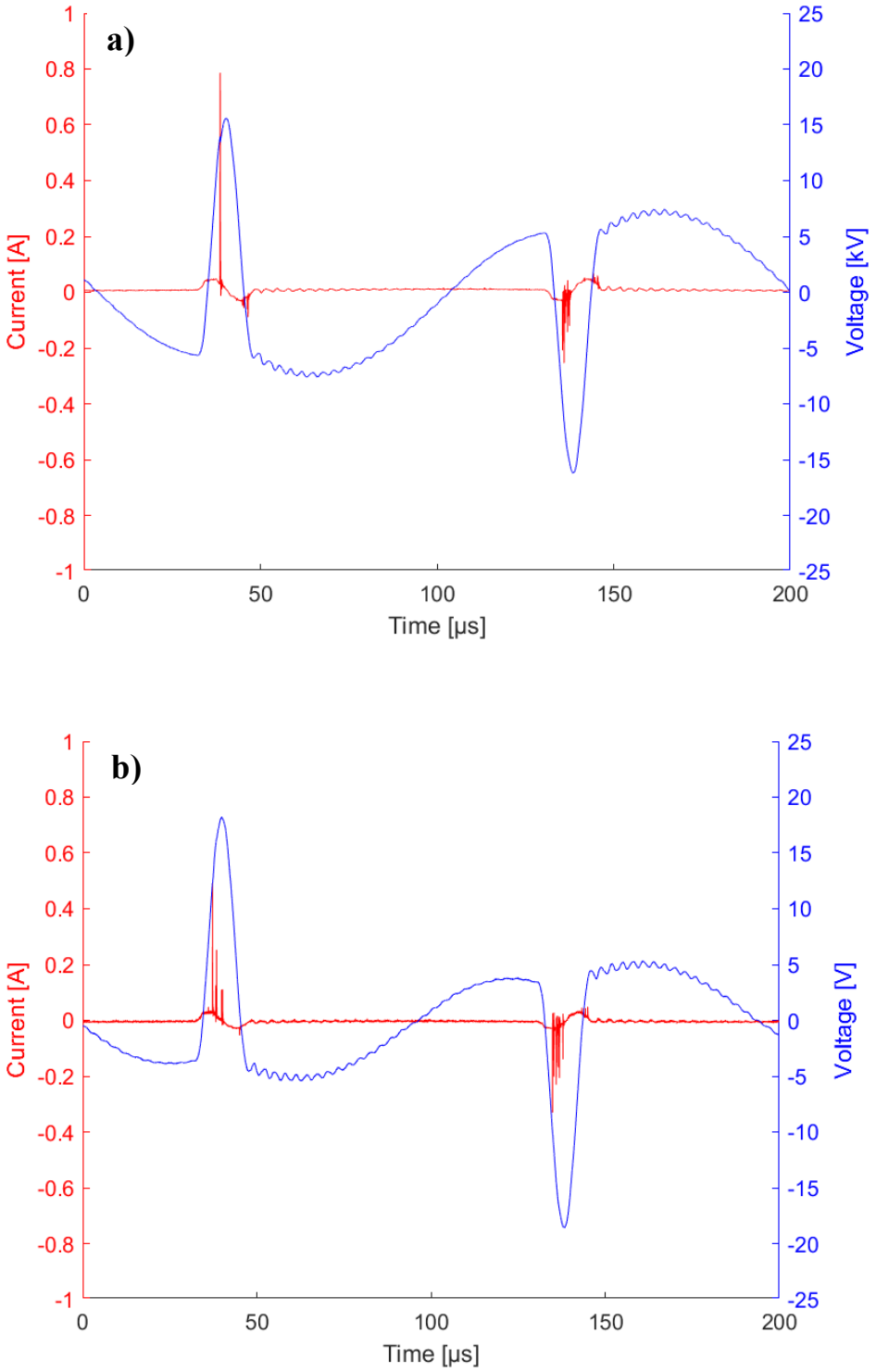

Figure 5.11– a) Current and applied voltage waveforms at O.C. A and **b)** O.C. B for the InDuct plasma source.

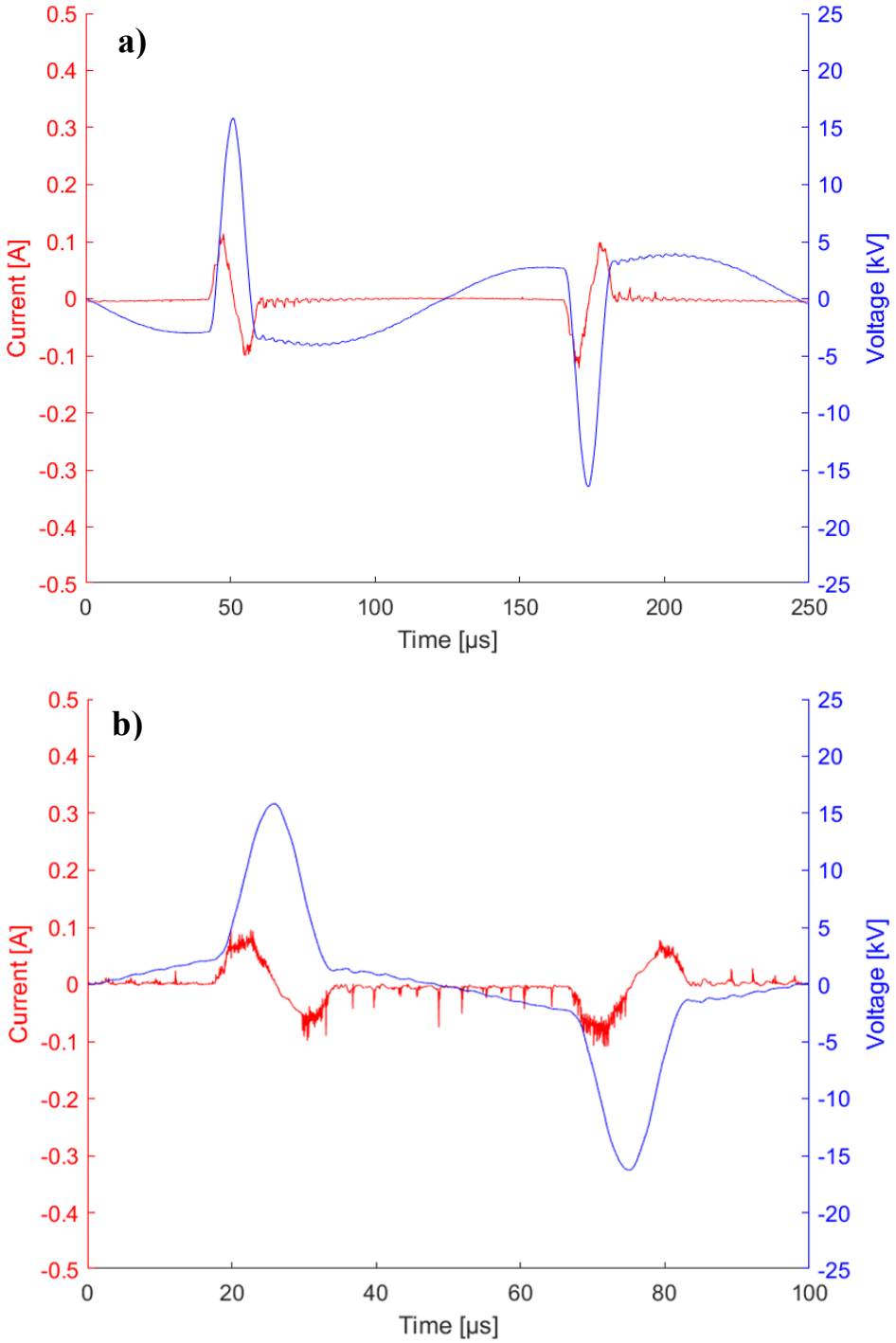

Figure 5.12– a) Current and applied voltage waveforms at O.C. C and **b)** O.C. D for the SDBD plasma source.

5.3.2 Evaluation of the gas phase results

5.3.2.1 OAS results

Regarding the OAS results, the InDuct plasma source remains OFF for the first ten seconds in both operating conditions. Upon activation, there is a rapid increase in ozone concentration, which then quickly decreases when the plasma source is switched off after 60 seconds (Figure 5.13). For both tested conditions, the concentration of NO_2 remained undetectable within the lab-scale duct.

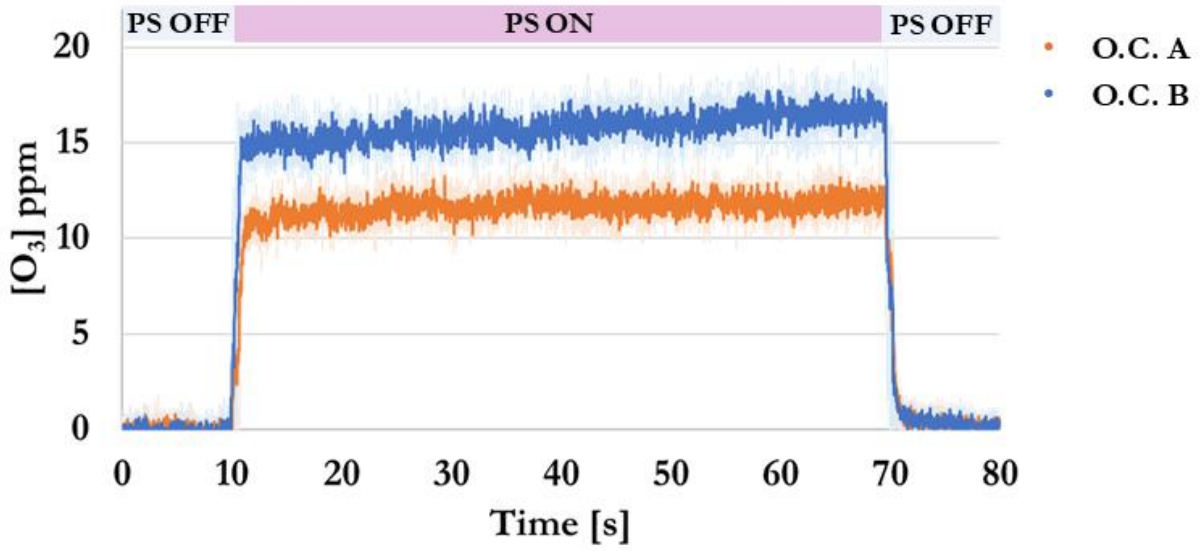

***Figure 5.13** – InDuct ozone concentrations and respective standard deviations inside the duct produced by the InDuct plasma source. The SD of the data is graphically displayed as the shaded colored band surrounding the mean line. PS ON = plasma source ON and PS OFF = plasma source OFF.*

Quantitatively, the InDuct average ozone concentration during the PS ON phase is around 15.8 ± 0.68 ppm for O.C. B and 11.6 ± 0.5 ppm for O.C. A (Figure 5.14), indicating that ozone concentration increases with higher discharge power. The results shown in Figure 5.14 indicate similar behavior for the SDBD plasma source. Additionally, the two O.C.s of the SDBD generate average ozone concentrations inside the duct during the PS ON phase that are comparable to those produced by the InDuct plasma source. Specifically, O.C. C of the SDBD yields an ozone concentration of 11.1 ± 0.62 ppm, which aligns with that produced using O.C. A of the InDuct plasma source. In comparison, O.C. D achieves a concentration of 15.8 ± 1.24 ppm, comparable to O.C. B of the InDuct plasma source.

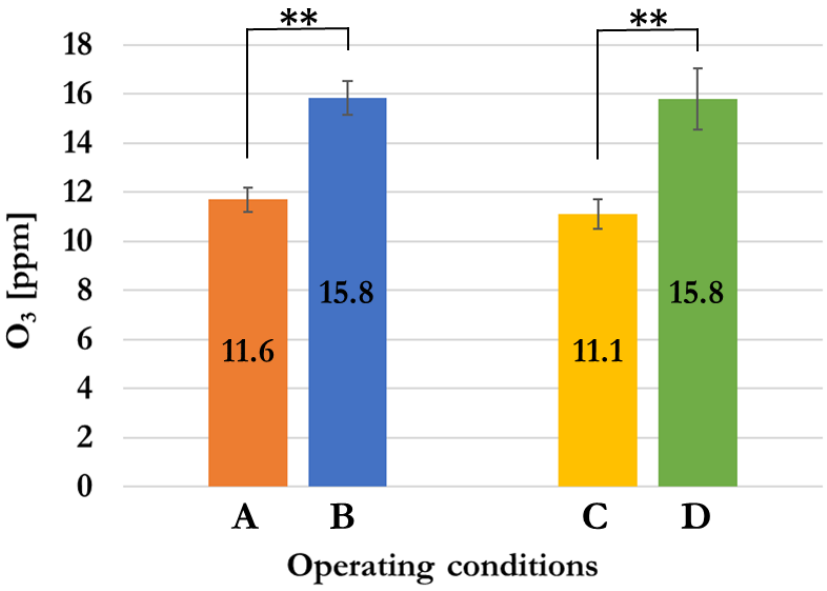

Figure 5.14 – *Average ozone concentrations produced by the InDuct plasma source (O.C. A and B) and the SDBD plasma source (O.C. C and D).*

5.3.2.2 InDuct mass spectrometry results

Figure 5.15 shows the InDuct results from MS sampling of 48 amu associated with the ozone under two operating conditions, while the MS detected no significant signal related to 46 (nitrogen dioxide) during the acquisition period. To capture potential changes in counts per second (c/s) and verify the presence of the analyzed masses, the InDuct plasma source was alternated ON and OFF every 5 seconds. A phase-averaging technique was applied to enhance signal analysis accuracy, especially when weak signals indicate low analyte concentrations. This approach presents the data as a single period of 5 seconds with the plasma ON and 5 seconds with the plasma OFF. The results show a behavior similar to those obtained from the OAS analysis, showing a rapid increase in signal when the plasma source is activated, a steady signal during the ON phase, and a quick decrease upon deactivation. Notably, an increase in c/s is observed during the ON phase when the highest power O.C. is used.

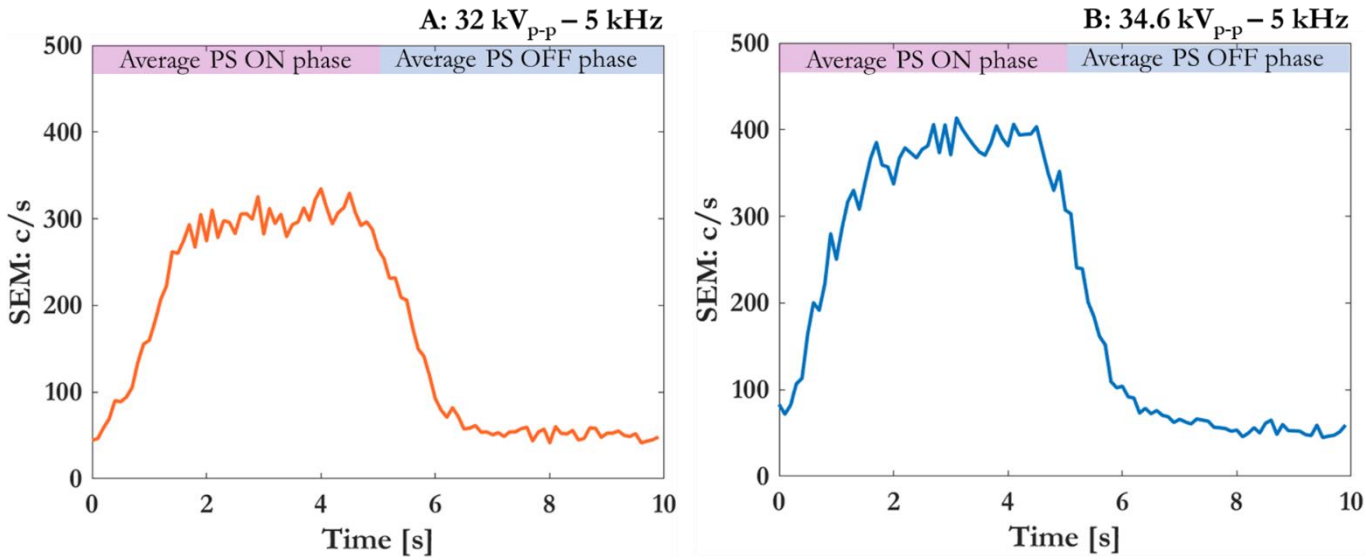

Figure 5.15 *– Phase averaging results of the time-resolved measurements of ozone mass (48 amu) obtained from the MS using* ***a)*** *O.C A and* ***b)*** *O.C. B.*

5.3.2.3 InDuct OES results

The OES analysis revealed that the most prominent spectral bands correspond to the N_2 second positive system, arising from the radiative de-excitation of N_2 molecules from the $C^3\Pi u$ to $B^3\Pi g$ states (Figure 5.16). Table 5.3 summarizes the plasma excited species observed in the emission spectra. No changes in plasma species were observed in the spectra acquired under the two operating conditions.

According to Soler-Arango *et al.* [10], only N_2 bands, without nitrogen-excited atoms, indicate that the discharge energy primarily excites nitrogen molecules rather than causing nitrogen dissociation. Additionally, O_2 influences the electron energy distribution, as its dissociation by electron impact requires less energy (5.2 eV) than N_2 (9.7 eV). O_2 also acts as an electron scavenger due to its electronegative nature, efficiently forming O^- ions via dissociative attachment, thereby reducing the electron density in the plasma.

Ozone generation in the plasma involves a series of reactions starting with the dissociation of O_2 molecules [11], which requires 5.2 eV of energy. This dissociation produces oxygen atoms (O) through electron collisions that excite O_2 from its ground state to the excited state.

$$O_2 + e^- \rightarrow O_2^+ + e^- \rightarrow O + O + e^- \qquad (7)$$

These oxygen atoms then combine with O_2 in three-body reactions to form ozone (O_3) [12].

$$O + O_2 + M \rightarrow O_3 + M \qquad (8)$$

where M, in the case of air plasma, could be O, O_2, O_3 or N_2 [11].

Indeed, in air-based plasmas, there is also the contribution of N_2, mostly due to atomic nitrogen and electronically excited nitrogen molecules [12]. Reactions involving nitrogen atoms and excited N_2 states can generate extra oxygen atoms, further contributing to ozone formation. Atomic nitrogen contributes to ozone formation through the intermediate production of oxygen atoms. However, this process is limited, generating only about 10% additional atomic oxygen relative to the total amount produced [12]. Instead, the production of atomic oxygen and ozone is significantly enhanced by reactions involving electrically excited nitrogen molecules [10],[12].

$$N_2(A^3\Sigma_u^+) + O_2 \rightarrow N_2O + O \qquad (9)$$

$$N_2(A^3\Sigma_u^+,\ B^3\Pi_3) + O_2 \rightarrow N_2 + 2O \qquad (10)$$

Approximately 50% of the O_3 generated in CAP air discharges is attributed to indirect processes involving nitrogen [11],[12]. The observation of relative N_2 second positive bands exclusively in the OES spectra aligns with findings from OAS and MS, which detected only ozone at a 5 cm distance from the discharge. Therefore, more excited nitrogen molecules in the discharge increase ozone production, enhancing the plasma source's effectiveness in bacterial inactivation.

Finally, the rotational temperatures for both operating conditions resulted to be between 318 K and 322 K (45 °C to 49 °C). In scientific literature, the T_r obtained from the fitting of the spectra related to the 2nd positive nitrogen system is used at atmospheric pressure as an approximation of gas temperature, at least slightly overestimated [9],[10],[13],[14]. In this study, the T_r of both O.C.s are close to the room temperature, indicating that temperature does not significantly contribute to bacterial inactivation.

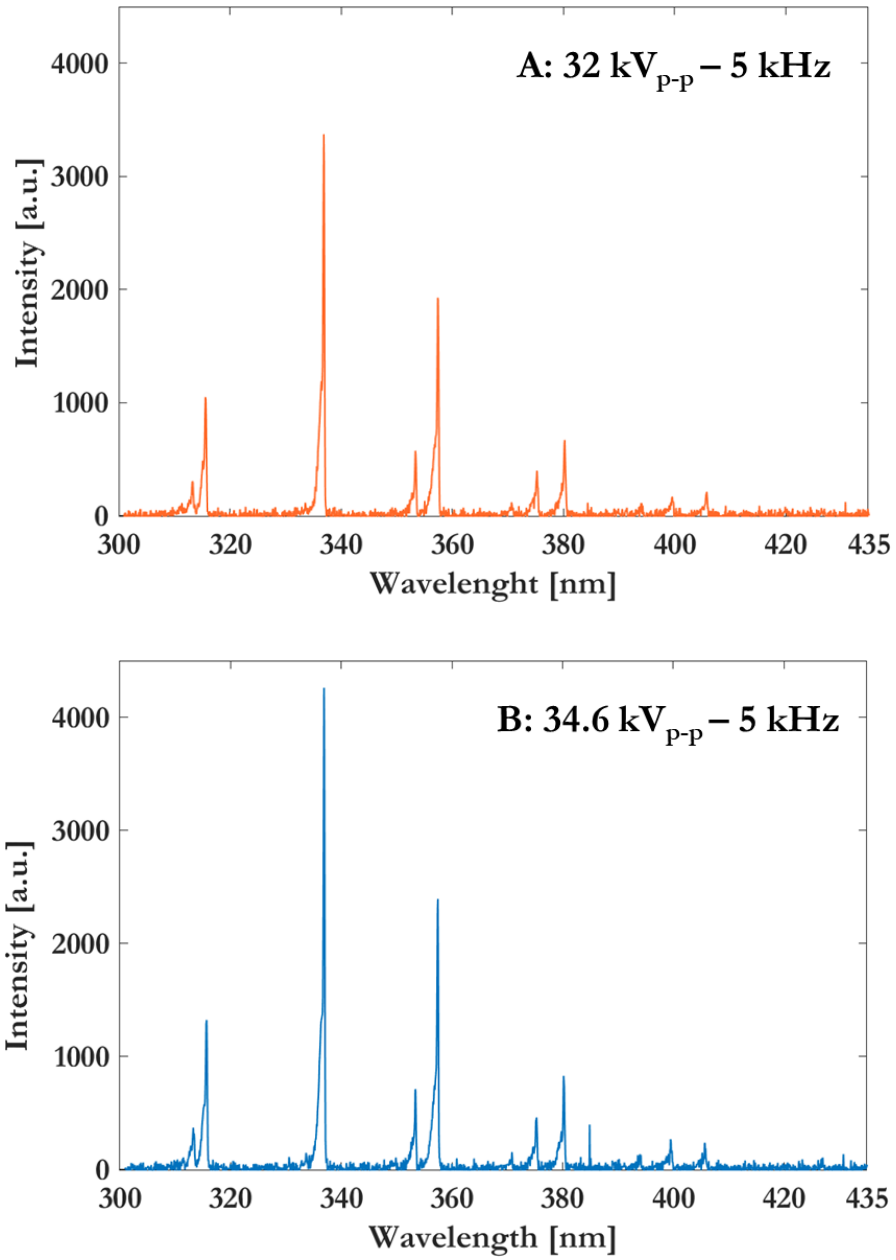

Figure 5.16 *– Emission spectra for the InDuct Plasma source between 300 and 435nm.*

Species	***Wavelength (nm)***	*Transition system band (v', v")*	***Species***	***Wavelength (nm)***	*Transition system band (v', v")*
N_2	**313.6**	C $^3\Pi u \rightarrow$ B $^3\Pi g$ (2,1)	**N_2**	**375.5**	C $^3\Pi u \rightarrow$ B $^3\Pi g$ (1,3)
N_2	**315.9**	C $^3\Pi u \rightarrow$ B $^3\Pi g$ (1,0)	**N_2**	**380.5**	C $^3\Pi u \rightarrow$ B $^3\Pi g$ (0,2)
N_2	**337.1**	C $^3\Pi u \rightarrow$ B $^3\Pi g$ (0,0)	**N_2**	**394.3**	C $^3\Pi u \rightarrow$ B $^3\Pi g$ (2,5)
N_2	**353.7**	C $^3\Pi u \rightarrow$ B $^3\Pi g$ (1,2)	**N_2**	**399.8**	C $^3\Pi u \rightarrow$ B $^3\Pi g$ (1,4)
N_2	**357.7**	C $^3\Pi u \rightarrow$ B $^3\Pi g$ (0,1)	**N_2**	**405.9**	C $^3\Pi u \rightarrow$ B $^3\Pi g$ (0,3)
N_2	**371.1**	C $^3\Pi u \rightarrow$ B $^3\Pi g$ (2,4)			

Table 5.3 – Species identified from Figure 5.16 present in both spectra.

5.3.3 Biological inactivation test on *S. epidermidis* bioaerosol

The InDuct source demonstrated significant antimicrobial efficacy under O.C. A, achieving a Log R greater than 3.8, corresponding to over 99.9% bacterial inactivation (Figure 5.17). This result is especially promising, given that the bioaerosol containing the bacteria passes through the discharge only once. By contrast, O.C. B achieved a lower bacterial reduction, with a Log R above 2.8, equivalent to 99% inactivation. As discussed in Chapter 4, ozone concentration appears to play a key role in microbial inactivation. To further explore the contribution of ozone to bacterial inactivation, an SDBD source was designed to produce two ozone concentrations in the duct, statistically similar to those produced by the InDuct plasma source (O.C. A from InDuct matches O.C. C from SDBD, and O.C. B from InDuct matches O.C. D from SDBD). The SDBD source generates antimicrobial effects primarily through long-lived reactive species like ozone without direct contact between the bioaerosol and plasma discharge. Therefore, following the same methodology used for the InDuct plasma source, the antimicrobial efficacy of the SDBD source was evaluated and compared with the results from the InDuct source. As summarized in Figure 5.17, results showed that O.C. A and C (with ozone levels between 11.1 and 11.6 ppm) achieved statistically similar Log R values (Student's test, $p \geq 0.05$). However, O.C. B and D, with an ozone concentration of about 15.8 ppm, had statistically different Log R values (Student's test, $p \leq 0.05$). While preliminary, these results suggest that increasing ozone concentration from around 11 ppm to nearly 16 ppm in the SDBD source does not enhance microbial efficacy as it does in the InDuct source. The enhanced antimicrobial effectiveness observed with the InDuct source is likely attributable to the additional presence of short-lived reactive species. In the InDuct configuration, contaminated air passes directly through the plasma discharge, exposing the bacterial bioaerosol to the full spectrum of biocidal components associated with the plasma, including short-lived reactive species.

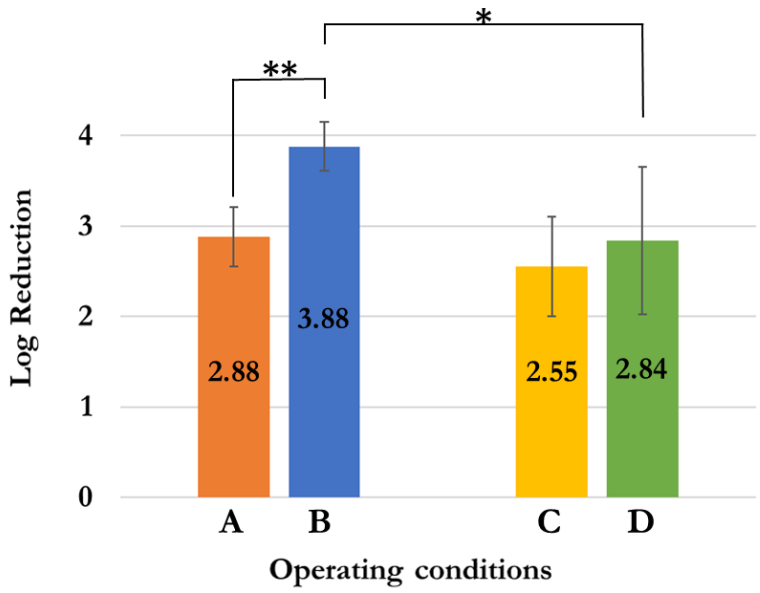

Figure 5.17 *– Average Log Reduction achieved by the InDuct plasma source (O.C. A and B) and the SDBD plasma source (O.C. C and D).*

5.4 Conclusions

This chapter introduces a novel system based on CAP technology, specifically designed for integration within ventilation ducts to treat air before release into indoor environments, thereby enhancing indoor air quality. The primary objective of this design was to develop a system compatible with duct installations that effectively exploits the full biocidal potential of plasma-generated reactive species for air decontamination. A volumetric DBD plasma source, the InDuct plasma source, was designed, realized, and characterized to achieve these goals. The design focuses on creating a large plasma generation zone to ensure all passing air contacts the full blend of reactive species produced by the plasma discharge.

The InDuct source was characterized under two operating conditions (O.C.s) with power levels of approximately 8 W and 12.5 W. Analysis of the gas phase generated by the InDuct source was conducted using OAS, MS, and OES. Results revealed that ozone is the dominant reactive species detected at 5 cm from the discharge, with both OAS and MS showing only an ozone signal. OES findings, highlighting the exclusive presence of N_2 2^{nd} positive system bands, support the conclusion that ozone generation occurs at the expense of other reactive species, such as NO_2. Additionally, the ratios between the powers, ozone concentrations, and MS signals obtained with the two O.C.s range from 1.4 to 1.5, indicating a proportional relationship that may be essential for scaling up the prototype.

Biological tests demonstrated that the InDuct plasma source operating under O.C. A achieved a Log R greater than 3.8, indicating over 99.9% bacterial inactivation with a single

bioaerosol pass through the plasma discharge. Comparative testing with an SDBD source designed to yield statistically similar ozone concentrations to those of the InDuct source revealed a statistically significant difference in Log R for the higher ozone condition, with the InDuct source achieving a higher Log R. This enhanced efficacy may be attributed to the direct passage of bioaerosols through the plasma discharge, where they interact with the full spectrum of reactive species, including short-lived species and with the electric field, both not quantified in this study. Nevertheless, these comparative results are preliminary and need further investigation.

In conclusion, the InDuct source has shown effectiveness in decontaminating bacterial bioaerosols and offers a possible alternative or complementary approach to traditional air decontamination methods in ventilation ducts. The findings from this chapter have informed the initial scale-up of this prototype, targeting higher airflow rates of up to 600 m^3/h, as outlined in Appendix 4.

5.5 References

[1] J. Benedikt *et al.*, 'Quadrupole mass spectrometry of reactive plasmas', *Journal of Physics D: Applied Physics*, vol.45, no. 40, 2017, doi: 10.1088/0022-3727/45/40/403001.

[2] E. Stoffels, *et al.* 'Mass spectrometric detection of short-living radicals produced by a plasma needle', *Plasma Sources Science and Technology*, vol. 16, no. 3, 2007, doi: 10.1088/0963-0252/16/3/014.

[3] J. Jiang et *al.*, 'Absolute spatially and time-resolved O, O3, and air densities in the effluent of a modulated RF-driven atmospheric pressure plasma jet obtained by molecular beam mass spectrometry', *Plasma Process. Polym.*, vol. 17, no. 6, pp. 1–14, 2020, doi: 10.1002/ppap.201900163.

[4] J. H. Batey, 'The physics and technology of quadrupole mass spectrometers', *Vaccum*, vol. 101, pp. 410–415, 2014, doi: 10.1016/j.vacuum.2013.05.005.

[5] E. B. Halim *et al.*, 'Time domain averaging across all scales : A novel method for detection of gearbox faults', *Mechanical Systems and Signal Processing*, vol. 22, pp. 261–278, 2008, doi: 10.1016/j.ymssp.2007.08.006.

[6] S. Braun, 'The synchronous (time domain) average revisited', *Mech. Syst. Signal Process.*, vol. 25, no. 4, pp. 1087–1102, 2011, doi: 10.1016/j.ymssp.2010.07.016.

[7] L. Wang *et al.* , 'Time Synchronous Averaging Based on Cross - power Spectrum', *Chinese Journal of Mechanical Engineering*, vol.38, no.1, pp.51, 2023, doi: 10.1186/s10033-023-00867-9.

[8] M. I. Boulos, P. L. Fauchais, and E. Pfender, *Handbook of Thermal Plasmas*, 2023.

[9] G. P. and A. V. Rok Zaplotnik, 'Optical Emission Spectroscopy as a Diagnostic Tool for Characterization of Atmospheric Plasma Jets', *Applied Sciences*, vol. 11, no. 2275, 2021, doi: 10.3390/app11052275.

[10] J. Soler-Arango *et al.*, 'Characterization of an Air-Based Coaxial Dielectric Barrier Discharge Plasma Source for Biofilm Eradication', *Plasma Chem. Plasma Process.*, vol. 38, no. 3, pp. 535–556, 2018, doi: 10.1007/s11090-018-9877-3.

[11] U. Kogelschatz, 'Dielectric-barrier Discharges: Their History, Discharge Physics, and Industrial Applications', *Plasma Chem. Plasma Process.*, vol. 23, no. 1, pp. 1–46, 2003, doi: 10.1023/A:1022470901385.

[12] A. Fridman, *Plasma chemistry*. Cambridge University Press, 2008.

[13] F. Barletta *et al.*, 'Insights into plasma-assisted polymerization at atmospheric pressure by spectroscopic diagnostics', *Plasma Process. Polym.*, vol. 17, no. 6, pp. 1–15, 2020, doi: 10.1002/ppap.201900174.

[14] P. J. Bruggeman *et al.*, 'Gas temperature determination from rotational lines in non-equilibrium plasmas: A review', *Plasma Sources Sci. Technol.*, vol. 23, no. 2, 2014.

5.6 Appendix 4 – Scale-up of the InDuct plasma source

Chapter 5 demonstrated that the InDuct plasma source geometry is well-suited for duct installation and effectively decontaminates bacterial bioaerosols. Building on the findings in Chapter 5, efforts have been initiated to scale-up the InDuct source to significantly increase its airflow capacity beyond the previous 3.5 m³/h. This scale-up process involved increasing the plasma source size, specifically tripling the length of the electrodes from 45 mm (Figure 5.18-a) to 135 mm (Figure 15.8-b).

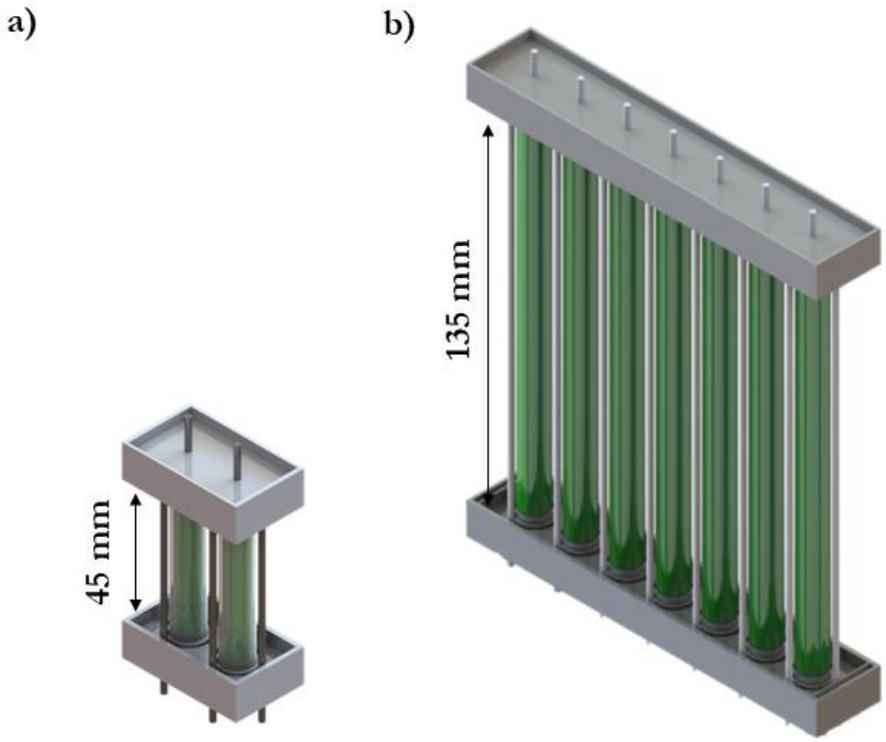

Figure 15.8 a) *InDuct plasma source presented in Chapter 5;* ***b)*** *scaled-up InDuct plasma source.*

Additionally, the number of HV electrodes increased from 2 to 7, and the number of ground electrodes from 7 to 22 (Figure 5.19), leading to a substantial increase in the plasma discharge region.

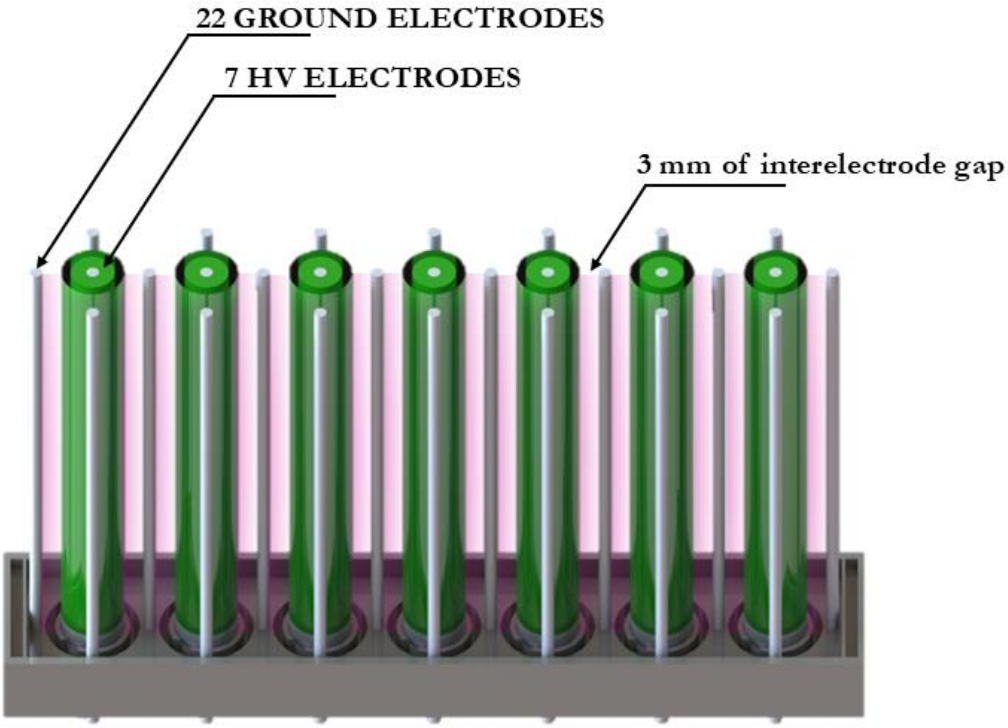

Figure 5.19 *– Section view of the scaled-up InDuct plasma source.*

Consequently, the average discharge power levels also increased. Indeed, as noted in Chapter 3, Section 3.2, one major challenge in scaling up CAP devices is ensuring a uniform plasma discharge distribution to prevent "dead zones" that may reduce the antimicrobial effectiveness of the device. Using the same experimental setup and procedure detailed in Section 5.2.3, preliminary tests were conducted to map the operating conditions of the scaled-up source. This initial mapping identified the conditions necessary to achieve a uniform discharge with the scaled-up InDuct source, and they correspond to an average discharge power range between 40 and 150 W. Furthermore, the source was installed inside a duct equipped with a variable-speed fan capable of delivering air flow rates up to 600 m^3/h.

Future investigation will focus on analyzing the gas phase and determining how reactive species concentrations vary with changes in air flow rate. These results will correlate with microbial inactivation tests to assess the device's effectiveness. This final phase presents the additional challenge of designing an experimental setup capable of safely managing high-contaminated air flows.

Chapter 6

Conclusions and future perspectives

This Ph.D. thesis investigates CAP systems as a novel strategy to improve indoor air quality, contrasting the airborne transmission of pathogens involved in spreading diseases such as COVID-19 and HAIs.

The Ph.D. project began with a comprehensive analysis of the state of the art concerning the interaction between CAPs and microorganisms. This analysis led to a systematic review in Chapter 1, which examines current knowledge of CAP applications in virology. Data extraction focused on publication year, last author's country affiliation, CAP source type, targeted applications, and investigated viral species. The findings revealed a significant increase in publications in this field since 2019, coinciding with the emergence of COVID-19. The United States was identified as the leading contributor, accounting for 24.5% of the total publications. Among the reviewed articles, 27.3% were classified as reviews, while the remaining 72.7% comprised original research studies. Fundamental research represented the largest category of articles (28.2%), followed by studies on surface decontamination using CAP technology (21.8%). DBDs were the most commonly used CAP source, making up 27.2% of the studies. The review identified investigations encompassing 41 distinct viral species, with single-stranded positive RNA (ssRNA+) viruses being the most extensively studied group, representing 75.6% of the research focus. The findings of the systematic review underscored the efficacy of CAP in viral inactivation across various applications. CAPs have demonstrated promising results in decontaminating inanimate surfaces through direct exposure to plasma discharges or RONS-rich atmospheres, which could help combat contact-based infections. CAP treatments have been shown to be especially effective in decontaminating wet surfaces, as the presence of liquids can enhance the formation of RONS. Additionally, CAPs may effectively address foodborne diseases by treating the surfaces of food products. Promising results have also been observed in mitigating airborne virus transmission, as also shown in Chapter 2. Furthermore, CAPs offer a potential solution for enhancing water safety by inactivating viruses.

The efficacy of CAPs was evaluated against both enveloped and non-enveloped viruses, as well as DNA and RNA viruses affecting humans, animals, and plants. CAP viral inactivation is primarily linked to the RONS produced, which operate through multiple mechanisms, including direct damage to viral particles, viral replication disruption, and host immune response modulation.

Chapter 2 introduces a direct DBD source developed as the proof of concept for the Ph.D. project. This prototype was designed and realized to demonstrate the capability of decontaminating bioaerosols with a size distribution comparable to droplet nuclei involved in airborne bacterial and viral transmission. Specifically, the proof of concept was tested on

bioaerosols containing *S. epidermidis* and SARS-CoV-2, achieving a Log Reduction of approximately 3.7 for the bacteria and completely inactivating SARS-CoV-2 with a residence time of the particles into the plasma discharge less than 0.1 seconds. Notably, low power operating condition (around 5 W) was more effective for viral inactivation, likely due to structural differences between *S. epidermidis* and SARS-CoV-2. As a Gram-positive bacterium, *S. epidermidis* possesses a thick peptidoglycan layer, providing resistance to RONS and, in general, to oxidative treatments, such as CAP. RT-PCR analysis showed that CAP treatment disrupted the structural integrity of viral RNA, a finding further confirmed by inoculating plasma-treated viral suspensions into highly permissive cell lines. After three days of incubation, no viral replication was observed in the cells.

The knowledge and expertise acquired from designing and characterizing the proof of concept were employed for the scale-up of the prototype. This scale-up resulted in developing two distinct CAP devices through an iterative CAP device design and characterization process. These devices are presented in Chapters 4 and 5 after an overview in Chapter 3 on the concept of CAP device scale-up.

The RDBD source introduced in Chapter 4 is a novel tabletop system for air decontamination. This design optimizes the air decontamination process by incorporating the fan as an active component of the plasma source, with the fan functioning as the ground electrode. The RDBD source effectively decontaminated the air of a chamber test containing *S. epidermidis* bioaerosol (Log R around 3.9). Its microbial inactivation results were comparable to those achieved by the commercial Jonix device, which uses SDBD plasma sources; however, the RDBD required lower power consumption and operated at a flow rate 3.5 times higher. The RDBD source was also characterized under various operating conditions, highlighting the importance of average discharge power and ozone concentration as key parameters to consider when designing new CAP systems for air decontamination. Finally, the RDBD antimicrobial results showed that voltage differences under operating conditions with statistically similar average discharge powers did not affect bacterial inactivation.

Chapter 5 presented the second prototype developed from the proof of concept's scale-up: the InDuct plasma source. This design aimed to create a configuration suitable for integration within ventilation ducts, allowing contaminated air to be treated in a single pass through the plasma discharge and utilizing the complete blend of reactive species generated by CAP. Installed in a lab-scale duct, the InDuct plasma source was tested on an airflow contaminated with *S. epidermidis* bioaerosol. The results showed promising microbial inactivation, especially considering only a single pass through the plasma discharge. Gas-phase

characterization using OAS, MS, and OES indicated that ozone is the predominant reactive species in the duct. However, a preliminary comparison of the InDuct source with an SDBD plasma source suggests a possible contribution to microbial inactivation from short-lived reactive species and electric fields. However, these factors were not explored in depth within this thesis.

To conclude, the primary goal of decontamination is to decrease the number of pathogenic microorganisms significantly. Specific standards may vary depending on the context (hospital, food industry, home, etc.), the type of contaminant, and the regulations in the country. However, the WHO identified different levels of decontamination:

- cleaning (the physical removal of body materials, dust, or foreign material);
- disinfection (the destruction or removal of microorganisms at a level that is not harmful to health and safe to handle, not necessarily including the destruction of bacterial spores);
- sterilization (the complete destruction or removal of microorganisms, including bacterial spores).

Considering the levels of viral inactivation revealed in the systematic review and the results obtained with the devices presented in this thesis, it can be deduced that CAP technology is promising in disinfection. However, further research is needed to deepen understanding of its interactions with microorganisms. CAP generates a complex mix of biocidal components, and their synergistic effects make identifying the exact microbial inactivation challenging. RONS, in particular, play a central role in these inactivation mechanisms. However, assessing the individual contributions of each reactive species remains difficult, especially for short-lived species with rapid reaction times (1–3 µs). From an industrial perspective, managing indoor ozone levels is critical. While ozone possesses strong antimicrobial properties, as discussed in Chapter 3, high indoor concentrations and prolonged exposure can pose risks to human health. Therefore, ongoing efforts must ensure ozone levels remain within safe limits.